EXPLORATION OF KINASE-REGULATED CELLULAR SIGNALING IN CHLAMYDOMONAS REINHARDTII

Emily G. Werth

A dissertation submitted to the faculty at the University of North Carolina at Chapel Hill in partial fulfillment of the requirements for the degree of Doctor of Philosophy in the Department of Chemistry in the School of Arts and Sciences.

Chapel Hill
2018

Approved by:

Leslie M. Hicks

James W. Jorgenson

Gary L. Glish

Lee M. Graves

Brandie M. Ehrmann

ABSTRACT

Emily G. Werth: Exploration of kinase-regulated cellular signaling in *Chlamydomonas reinhardtii*
(Under the direction of Leslie M. Hicks)

Post-translational modifications (PTMs) on proteins to form functional protein products are a key level of cellular signaling regulation. Because of this, there has been an immense effort in the proteomics community to improve quantitative enrichment, acquisition, and bioinformatics strategies for the analysis of PTMs to probe metabolic pathways. The identification of dynamic protein phosphorylation events, a vital PTM, is especially important for understanding kinase/ phosphatase-regulated signaling pathways, and is the focus of this dissertation. The aim of this dissertation is to develop and apply phosphoproteomic strategies in the alga *Chlamydomonas reinhardtii* to characterize the role of protein phosphorylation on cellular regulation in a diverse array of signaling networks.

Techniques for algal cell culturing, protein extraction, quantitative enrichment, acquisition and bioinformatics processing developed and adapted for Chlamydomonas are discussed (Chapter 2). Using these techniques, a quantitative workflow for a dual enrichment strategy to target intact protein kinases via capture on immobilized multiplexed inhibitor beads with subsequent proteolytic digestion of unbound proteins and peptide-based phosphorylation enrichment was developed (Chapter 3). This workflow obtained quantitative coverage on 115 protein kinases and 2,304 phosphopeptides. Application of the quantitative phosphoproteomic pipeline was employed to study the effect of Target of Rapamycin (TOR) kinase inhibition on the Chlamydomonas phosphoproteome in wild-type (Chapter 4) and extension into a rapamycin

hypersensitive mutant line (Chapter 5). From the wild-type study, three TOR inhibitors with varying mechanisms of inhibition were used to obtain quantitative coverage on 2,547 unique phosphosites with 258 phosphosites differentially changing following inhibition. This approach identified Chlamydomonas homologs of TOR signaling-related proteins such as RPS6 and LARP1 that had decreased phosphorylation upon TORC1 inhibition. Additionally, this led to follow-up experiments guided by our phosphoproteomic findings showing that carotenoid levels are affected by TORC1 inhibition, the first evidence that carotenoid production is under TOR control. From the rapamycin hypersensitive mutant study, the workflow obtained quantitative coverage on 2,699 phosphosites with 316 sites changing following rapamycin treatment. This study showed similarities with the sites modulated in the wild-type study described in Chapter 4 while also providing another distinct group of phosphosites not previously interrogated.

ACKNOWLEDGEMENTS

I would like to thank my advisor, Leslie M. Hicks, for her mentorship and research guidance. Leslie gave me the freedom to be curious and to take ownership over my project while always giving insightful ideas and feedback to move the work forward. Her leadership and passion has made the Hicks group a special place to work and I look back at my time at UNC fondly because of it. Thank you to the members of the Hicks group that I've spent every day (and some nights) working alongside, I am grateful for your edits, advice, coffee breaks, and the laughter. Christine, I don't think I would have made it through if you weren't there alongside. Seriously, I question if I would have missed a final admin deadline and been kicked out if it weren't for you. Evan, I think we've talked through more problems and come up with more ideas on walks to lunch than I can count, so thank you for being my PTM person. Megan and Anthony, I am excited to see where you take your projects from here and how you will move the TOR work along. Nicole and Tessa, I appreciate your friendship and getting to know you.

This experience wouldn't be nearly as much fun or possible without the friendships I've made during my time at Carolina. I want to thank my classmates and peers, especially Christine, Rima, Alex, Micah, Nate, Jake, Jenn, Matt Campbell, and Matt Boyce for the memories. Whether it was the beach trips, game nights, or potlucks, I always looked forward to the conversations.

To my family, I am endlessly grateful for your support and encouragement. To my mom and dad, you never let myself or others set limits on who I can become. Thank you. To my sister,

I could not have imagined how close we would become as adults when we were younger. I'm glad four years doesn't seem so different now and you, Jason, Benjamin, and Addison mean the world to me. I would also like to thank my grandma, Regina Flood Callahan, for being the original chemist in the family. I have always been in awe of your experience as a female chemist in the 1940's, you inspire me. And of course, I want to end with the canine members of my family, Ella and Fitz. Their ability to brighten my day, without fail, is the best way to brush off bad results and try again.

TABLE OF CONTENTS

LIST OF TABLES

LIST OF FIGURES

LIST OF ABBREVIATIONS

AMPK	AMP-activated protein kinases
AUC	area under the curve
CDKs	cyclin-dependent protein kinases
CID	CTC-interacting domain
CV	coefficient of variation
DDA	data-dependent acquisition
DIA	data-independent acquisition
DTT	dithiothreitol
EEF2	elongation factor 2
EEF2K	elongation factor 2 kinase
FA	formic acid
FDR	false discovery rates
GO	gene ontology
HPLC	high-pressure liquid chromatography
IAM	iodoacetamide
IMAC	Immobilized metal affinity chromatography
InsPs	inositol polyphosphate
iTRAQ	Isobaric Tags for Relative and Absolute Quantification
KO	KEGG ontology
LARP1	LA RNA-binding protein
LFQ	label-free quantification
LOD	limit of detection

LST8	lethal with sec-13 protein 8
MAPK	mitogen-activated protein kinase
MCM	minichromosome maintenance
MeCN	acetonitrile
MGF	mascot generic file
MIBs	multiplexed inhibitor beads
MOAC	metal oxide affinity chromatography
MS/MS	tandem mass spectrometry
MT	mating type
NEM	N-Ethylmaleimide
OD	Optical density
PAGE	polyacrylamine gel electrophoresis
PBS	phosphate-buffered saline
PI3K	phosphatidylinositol 3-kinase
PPM	parts per million
PTMs	Post-translational modifications
Q-TOF	quadrupole time-of-flight
RAPTOR	regulatory associate protein target of rapamycin
SCX	strong cation exchange
SDS	sodium dodecyl sulfate
Ser	Serine
SILAC	Stable Isotope Labeling by Amino Acids in Cell Culture
SOPs	standard operating procedures

SWATH	Sequential Windowed Acquisition of All Theoretical Fragment Ion Mass Spectra
TAG	triacylglycerol
TAP	Tris-Acetate-Phosphate
TCEP	Tris(2-carboxyethyl)phosphine hydrochloride
TFA	trifluoroacetic acid
Thr	Threonine
TiO_2	titanium dioxide
TMT	Tandem Mass Tags
TOP	Terminal Oligopyrimidine
TOR	Target of Rapamycin
TORC1	TOR complex 1
TORC2	TOR complex 2
Tyr	Tyrosine
UPLC	ultra-high pressure liquid chromatography

CHAPTER 1: *Chlamydomonas reinhardtii* Phosphoproteomics

1.1 Phosphoproteomics

Post-translational modifications (PTMs) such as phosphorylation, acetylation and ubiquitination are crucial aspects of regulating protein expression. Occurring after protein products are translated, the addition or removal of PTM functional groups regulates protein folding and converts the primary sequence of proteins into functional protein products, or proteoforms[1], with diverse structure and function within the cell. Proteoforms can exist with multiple PTMs that work in tandem regulating cellular signaling and contributing to the complexity of possible protein products involved in a cell.

Protein phosphorylation is a prevalent PTM responsible for regulating a myriad of cellular processes from cell cycle to programmed cell death[2-4]. The addition or removal of a phosphate moiety onto the hydroxyl group of either serine (Ser), threonine (Thr), or tyrosine (Tyr) amino acid residues by a kinase or phosphatase is responsible for conformational changes on direct substrates which affect downstream signaling networks. The significant and ubiquitous role protein phosphorylation has within cellular processes such as cell survival, proliferation, metabolism, and cellular signaling emphasizes the need for an efficient and selective method for enrichment capable of identifying phosphorylation sites to understand the biological significance of the modification. The effects of perturbing phosphorylation events and subsequently studying them *in vivo* is of significance because it allows for identification of key proteins and, specifically, the phosphosites on those proteins that are involved in signaling pathways.

To assess the changes in phosphorylation events at the systems-level as a result of abiotic or biotic stress, a quantitative label-free platform with a reproducible phosphopeptide enrichment is necessary to address the substoichiometric levels of phosphorylation in cellular proteins. Currently, characterization of protein phosphorylation events remains an analytical challenge due to numerous contributions toward phosphopeptide losses such as reduced ionization efficiency over unphosphorylated peptides and losses during chromatography[5]. Phosphorylation enrichment strategies to combat these challenges have allowed for robust detection and quantitation of phosphorylation events. For phosphopeptide studies, affinity purification techniques such as immobilized metal affinity chromatography[6] (IMAC) and titanium dioxide[7] (TiO_2) enrichment schemes are two of the most frequently used approaches. These techniques permit qualitative and quantitative evaluation on thousands of phosphorylation events in a single analysis however, careful sample preparation at the protein and peptide level are essential for success in both[8]. In IMAC and TiO_2 enrichment strategies, binding of carboxyl groups to the IMAC or TiO_2 material can result in co-purification of acidic peptides and phosphopeptides limiting specificity and requires method development such as pH modulation for IMAC[9] and addition of organic acids to binding solvents in TiO_2 based enrichments[10]. Both require extensive method optimization and reproducibility in sample preparation to gain a meaningful understanding of the phosphoproteome. When comparing the two affinity purification techniques, IMAC has been shown to be less selective than TiO_2[7] but identifies more multiply phosphorylated peptides[10]. Additionally, TiO_2 chromatography has been shown to be less sensitive to interfering compounds such as salts and detergents[9, 11] than IMAC and all of these characteristics should be evaluated when determining the enrichment strategy best for the experimental design.

1.2 Label-Free Quantitation

Over the past two decades, the use of "gel-free" or mass-spectrometry-based techniques for quantification of differential proteomics in biological systems has gained popularity. Offering a powerful analytical technique for studying large-scale protein expression and characterization over gel-based methods, LC-MS/MS proteomic platforms offer highly reproducible and accurate systems-level quantification. This allows for the investigation of the global effect a diseased state or cellular stress would have on the proteome by comparing healthy cells to diseased or stressed cells and identifying key proteins that are changing between conditions. This is known as differential proteomics. From these experiments, protein targets affected by the disease or stress are identified by their significant change to that in healthy cells. One of the quantitation approaches used to identify these protein targets is label-free quantitative proteomics.

1.2.1 Label-Free Quantitative Proteomics

When considering the quantitation method most suitable for a biological question, both labeled and label-free methods have benefits and limitations to consider before moving forward. LFQ proteomic strategies are an especially useful analytical approach for differential experiments because they can accommodate a wide range of experimental designs and are unlimited in experimental complexity as long as reproducible chromatography and mass accuracy can be achieved and maintained[12-13]. This is an advantage over stable isotope labeling approaches such as Stable Isotope Labeling by Amino Acids in Cell Culture (SILAC)[14], Tandem Mass Tags (TMT)[15], and Isobaric Tags for Relative and Absolute Quantification (iTRAQ)[16], which are limited in experimental complexity and replicates to the number of labels available.

A main advantage of labeling strategies is reduced acquisition time from pooling sample mixtures prior to acquisition and requiring a single LC-MS/MS run[13]. These multiplexing

capabilities allow for shorter acquisition time however labeling techniques, such as iTRAQ, have shown underestimations of ratios in quantitation, limited dynamic range, and instrument-specific requirements for use[17]. Multiple studies have compared labeling and label-free techniques in complex biological samples[17-19], including a comparison in *Chlamydomonas reinhardtii*[17], highlighting the benefits and limitations of each approach. To become a viable alternative to current labeling techniques, quantitative label-free proteomics must have highly reproducible sample processing and chromatography capable of accurately measuring changes in ion intensity amongst biological conditions or treatments across LC-MS/MS runs. Additionally, a comprehensive bioinformatics pipeline for accurate peak picking and processing -omics data into tangible quantitative information for biological inference is required[20-21].

This demand for high reproducibility both from chromatographic peaks across replicates and in the post-acquisition data analysis gave rise to a wide array of LFQ software suites available for peak picking, retention time alignment and statistical analysis. This includes commercial products such as Progenesis QI for proteomics (Nonlinear Dynamics), Scaffold[22] and academic softwares such as MAXQUANT[23] and Skyline[24], among others[13, 25]. While the specific technical details are unique for each bioinformatic pipeline, the two most common methods for relative quantification using a label-free approach are peak intensity-based and spectral counting[26]. Peak intensity-based strategies rely on measuring and comparing MS signal intensity of peptide precursor ions belonging to a particular protein, (Figure 1.1) while spectral counting strategies count and compare the number of fragment spectra identifying peptides of a given proteins[27]. The fundamental steps of sample preparation (reduction, alkylation, digestion), separation and analysis by LC-MS/MS are common throughout.

For years, the predominant acquisition strategy for LFQ proteomics involves data-dependent acquisition (DDA) followed by searching of MS^2 spectra against a database for protein inference. While this acquisition method is prevalent throughout current proteomic analyses, it can result in irreproducible precursor ion selection due to the stochastic nature of ion selection[28], undersampling[29], and a required minimal signal for ions to trigger MS^2 analysis within a finite duty cycle[30]. Data-independent acquisition (DIA) strategies, which perform unbiased fragmentation of all peptide precursors to theoretically record all fragment ion signals above the instrument's limit of detection (LOD)[31], have gained in popularity in recent years. A hurdle to overcome is fragment ion identification since standard bottom-up (DDA) proteomic approaches such as searching an *in silico* digested library database are not possible and protein inference instead relies on preparing a spectral library for matching prior to performing an experiment[32]. While this technique requires additional front-end work to gain a comprehensive library of possible fragment ions for searching, the strategy can allow for a more complete look at the proteome.

In addition to utilizing multiple acquisition strategies to improve proteome coverage and relative quantitation using an LFQ proteomic approach, experiments focused on subsets of the proteome can also require alterations to the LFQ pipeline discussed above. When focusing the analysis on PTMs, specifically phosphorylation on proteins, a reproducible enrichment strategy is required to remove background unphosphorylated species from interfering in the analysis. The study of protein phosphorylation events at the systems-level using this approach is called label-free quantitative phosphoproteomics and is discussed further in the following section.

1.2.2 Label-Free Quantitative Phosphoproteomics

Dynamic protein phosphorylation plays a central regulatory role in the living cell but studying these events remains an analytical challenge. Low phosphorylation stoichiometry and overall low abundance relative to unmodified proteins contribute to this and require an enrichment strategy prior to acquisition for reproducible detection and quantitation of phosphorylation events at the systems-level[33-35]. Enrichment can occur at the phosphoprotein level using pSer, pThr, pTyr antibodies and/or at the phosphopeptide level using mediums such as IMAC or metal oxide affinity chromatography (MOAC)[34]. For insight into the global phosphoproteome, peptide-based enrichment approaches in line with traditional LFQ sample processing have shown promise in maintaining high reproducibility among replicates allowing for label-free quantitation on phosphorylation sites that play significant roles in cellular pathways[36]. Similarly to differential proteomic experiments, the global effect a diseased state or cellular stress would have on the *phospho*proteome can be determined by comparing healthy cells to diseased or stressed cells and identifying key phosphosites changing between conditions.

While this uses many of the same software tools available for other LFQ experiments, the quantitative data in phosphoproteomic studies reflects both changes in phosphorylation status and change in expression of substrate proteins. Because of this, both factors must be considered when performing phosphosite quantification. While simultaneous quantification of protein expression and phosphorylation would allow true differential phosphorylation to be distinguished from protein expression, there are several technical challenges making this solution difficult to enact. Literature has shown a low overlap in quantitative coverage between unenriched whole-cell proteins identified and phosphoproteins identified following enrichment with a significant portion of every phosphoproteome profile “invisible” without enrichment[37]. This is due to

limitations in instrument dynamic range and a bias toward high abundance proteins being selected for fragmentation, which is a driving force behind using a phosphopeptide enrichment strategy to remove unmodified proteins prior to analysis[5] therefore making it possible in a single LC-MS/MS run to analyze the global protein expression or phosphorylation, but not both[37].

To address this, data normalization between global and phosphoproteome experiments to account for changes in protein expression when investigating changes in phosphorylation status are possible. This requires quantitative comparison of overlapping proteins in both whole-cell and phospho-enriched experiments to account for abundance differences not due to phosphorylation changes. But, normalization is only relevant for differential experiments that result in protein abundance levels changing during the time frame of the phosphoproteomic experiment. For experimental designs that investigate the phosphoproteome after short treatments such as 15 min. after target of rapamycin (TOR) inhibition[38] to 24 hours following nitrogen stress[39-40] in Chlamydomonas, no significant differences in protein abundances were identified. Therefore, phosphopeptide ratios in general were not considered affected by normalization to protein levels.

1.3 Phosphoproteomics for Studying Cellular Signaling in *Chlamydomonas reinhardtii*

The photosynthetic organism *Chlamydomonas reinhardtii* is an intensively-studied model for microalgal processes such as triacylglycerol (TAG) accumulation[41-43] and cell cycle control[44]. With considerable efforts focused on genomic, transcriptomic and proteomic analyses[42, 45-49], there have been significant advancements in understanding the molecular infrastructure and metabolic signaling in Chlamydomonas over the past decade since the genome was first sequenced[45]. From such analyses, interest in global studies on protein phosphorylation's role in regulating cellular signaling arose with early studies detecting 83 phosphopeptides in the

Chlamydomonas eyespot[50] and several hundred phosphoproteins in the flagella[51-53]. More recently, the phosphoproteome was extensively characterized with a conservative estimate of 4,588 phosphoproteins corresponding to 15,862 unique phosphosites with numerous phosphoproteins in key biological pathways indicating the significance of protein phosphorylation and kinase-regulated signaling networks in Chlamydomonas[54].

Following these comprehensive studies, quantitative work in Chlamydomonas has been applied to investigate the effects of nutrient deprivation on the phosphoproteome. Nutrient deprivation has been shown to result in TAG and starch accumulation[41-43] but fundamental research into algal metabolism regulation, specifically knowledge into Chlamydomonas signaling and regulatory processes to improve biofuel production, is needed. Recently, we have reported a quantitative phosphoproteomic strategy with coverage on 2,250 phosphopeptides[32] and similar reports have quantified 1,227 phosphopeptides where 470 phosphopeptides were significantly changing following nitrogen deprivation[55].

1.4 Target of Rapamycin Signaling in *Chlamydomonas reinhardtii*

The Target of Rapamycin kinase is a conserved regulator of cell growth whose activity is modulated in response to nutrients, energy and stress[56-60]. TOR signaling coordinates a balance between protein synthesis and protein degradation as a response to the cell's nutrient quality and quantity[61]. Because of the high potential behind microalgal biofuel production, significant attention has been focused on proteins regulating cell growth, such as the TOR kinase, in Chlamydomonas. As such, we have applied our LFQ phosphoproteomic work to probe the effects of TOR inhibition on the phosphoproteome quantifying 2,559 phosphopeptides with 219 phosphopeptides significantly changing following TOR inhibition[38]. Homology among TOR targets in a diverse set of organisms suggests TOR-associated proteins are broadly conserved[56];

and while the role of TOR in mammalian cell metabolism has been extensively investigated[62], its role in photosynthetic organisms is less well established[63-64]. Since inhibition of the TOR kinase by rapamycin has shown TAG and lipid droplet formation similarly to other nutrient deprivation studies[65], understanding its signaling and regulatory processes regulated by TOR is important. Key TORC1 complex proteins encoded by single-copy genes including TOR (Cre09.g400553.t1.1), regulatory associate protein target of rapamycin (RAPTOR) (Cre08.g371957.t1.1), and lethal with sec-13 protein 8 (LST8) (Cre17.g713900.t1.2) are conserved in Chlamydomonas[66-67] but the substrates of TOR kinase and downstream signaling network have not been elucidated. In Chlamydomonas, TOR inhibition induces autophagy-like processes similar to those induced by nitrogen starvation[59, 65, 68-69] and research into the regulatory processes is necessary to understand dynamic phosphorylation events involved in TAG accumulation and autophagy.

1.5 Scope of Dissertation

The focus of this dissertation is to improve the framework for studying protein phosphorylation quantitatively on a global scale in Chlamydomonas. For the work described herein, a peak intensity-based label-free quantitative approach has been optimized for studying the kinome and phosphoproteome in Chlamydomonas. First, I will introduce you to the standard operating procedures (SOPs) developed and optimized throughout the experimental chapters described herein (Chapter 2). SOPs have been established specifically for Chlamydomonas and detail optimized conditions from cell culture to biological inference via pathway analysis. Second, I will discuss the quantitative coverage obtained with this platform both from the kinome and the phosphoproteome (Chapter 3). This chapter focuses on employing the methods developed in Chapter 2 on studying the kinome and phosphoproteome in tandem in

Chlamydomonas with both DDA and DIA acquisition strategies (Figure 1.2). Next, I will build off the quantitative coverage that we have achieved in the phosphoproteome by using the quantitative phosphoproteomic workflow from Chapter 3 (Figure 1.3) to probe the effects of TOR inhibition in Chlamydomonas (Chapter 4). Following the investigation of TOR-modulated phosphosites in wild-type cells, I show the effects of studying this system using a rapamycin-hypersensitive strain in Chapter 5 to glean more insight into the effects of TOR inhibition on the phosphoproteome. Lastly, I will highlight the expansion of this project through the investigation of other kinase-regulated cellular processes in Chlamydomonas in addition to other photosynthetic organisms such as *Arabidopsis thaliana* that would require minimal change to the optimized workflows developed in this work.

1.6 Figures

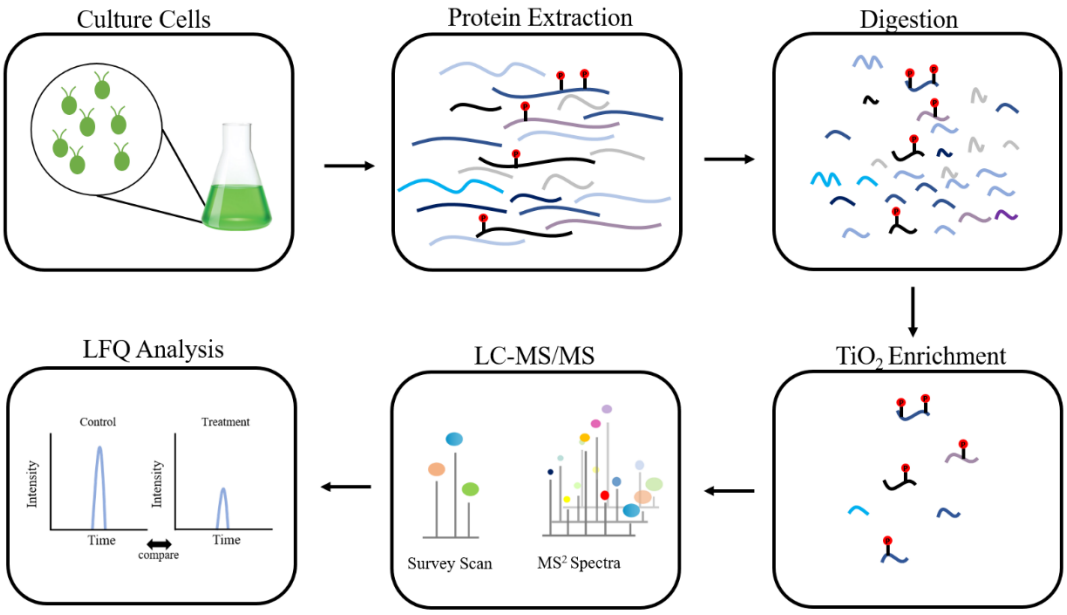

Figure 1.1 Schematic of a label-free quantitative workflow showing n=5 replicates per condition. Chlamydomonas cells were cultured photoheterotrophically with subsequent protein extraction, digestion, and LC-MS/MS acquisition. Following acquisition, relative quantification using area under the curve (AUC) abundance at the MS^1 level occurs between control and treatment samples to determine differentially changing proteins and protein identification is done through database searching using MS^2 spectra.

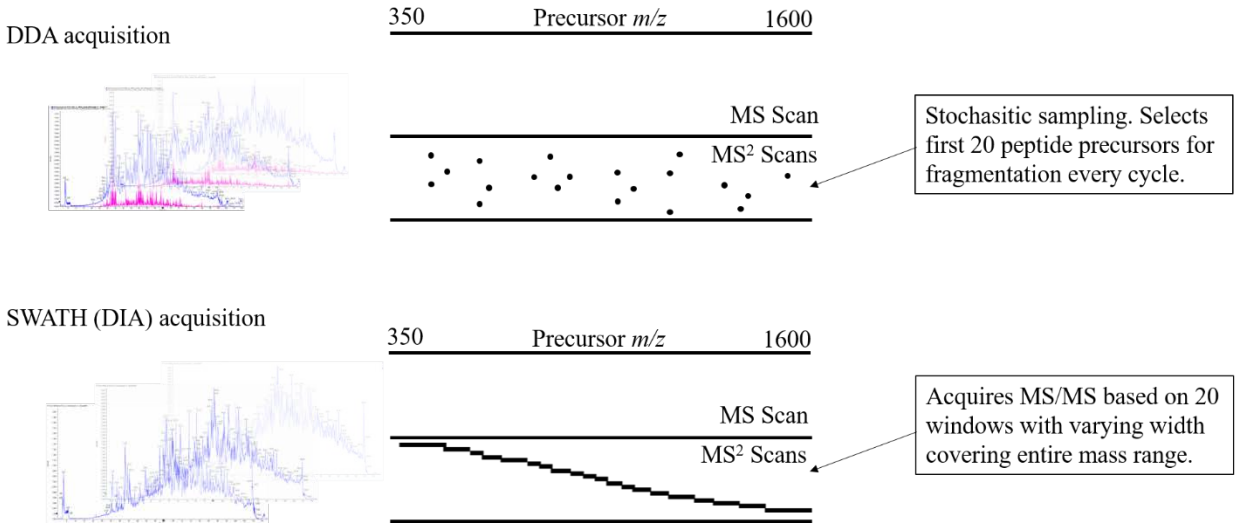

Figure 1.2 DDA and DIA acquisition workflows for AB Sciex TripleTOF 5600 instrument platform. For DDA, first 20 peptide precursors are selected for fragmentation every 2 second cycle based on optimized proteomic parameters[70]. For DIA, 20 MS/MS are selected for fragmentation based on windows of varying widths optimized to effectively cover the entire mass range while concurrently focusing on dense m/z regions with smaller Q1 windows and larger Q1 windows on less dense m/z regions.

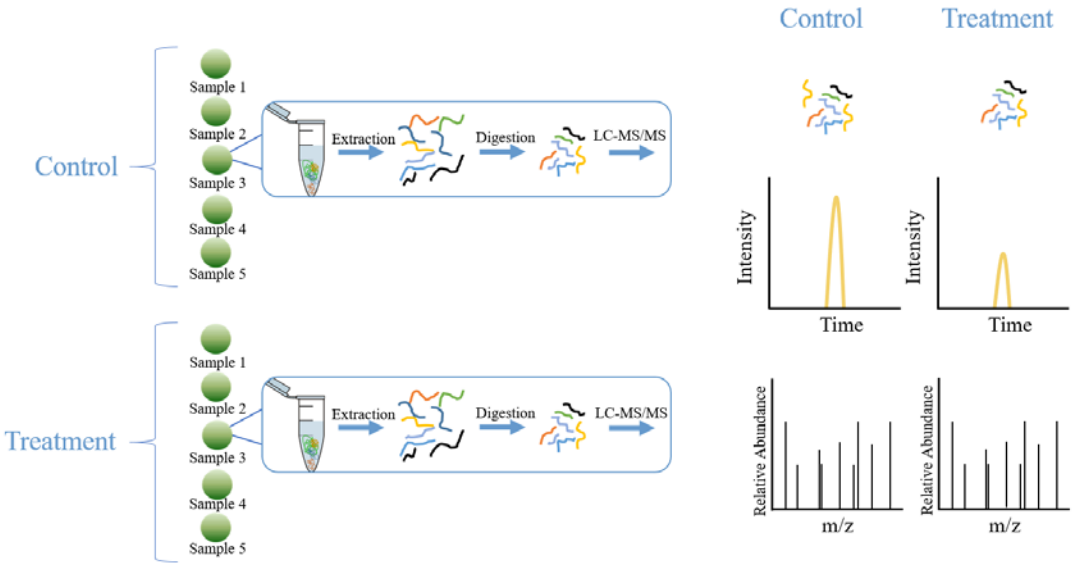

Figure 1.3 Standard bottom-up phosphoproteomic workflow including cell culturing, protein extraction, protein digestion, TiO_2 phosphopeptide enrichment, LC-MS/MS acquisition, and label free quantitative analysis.

REFERENCES

1. Smith, L. M.; Kelleher, N. L.; Linial, M.; Goodlett, D.; Langridge-Smith, P.; Goo, Y. A.; Safford, G.; Bonilla, L.; Kruppa, G.; Zubarev, R., Proteoform: a single term describing protein complexity. *Nature methods* **2013,** *10* (3), 186-187.

2. Hunter, T., Protein kinases and phosphatases: the yin and yang of protein phosphorylation and signaling. *Cell* **1995,** *80* (2), 225-236.

3. Allen, J. F., Protein phosphorylation in regulation of photosynthesis. *Biochimica et Biophysica Acta (BBA)-Bioenergetics* **1992,** *1098* (3), 275-335.

4. Hubbard, M. J.; Cohen, P., On target with a new mechanism for the regulation of protein phosphorylation. *Trends in biochemical sciences* **1993,** *18* (5), 172-177.

5. Solari, F. A.; Dell'Aica, M.; Sickmann, A.; Zahedi, R. P., Why phosphoproteomics is still a challenge. *Mol Biosyst* **2015,** *11* (6), 1487-1493.

6. Neville, D. C.; Townsend, R. R.; Rozanas, C. R.; Verkman, A.; Price, E. M.; Gruis, D. B., Evidence for phosphorylation of serine 753 in CFTR using a novel metal-ion affinity resin and matrix-assisted laser desorption mass spectrometry. *Protein Science* **1997,** *6* (11), 2436-2445.

7. Larsen, M. R.; Thingholm, T. E.; Jensen, O. N.; Roepstorff, P.; Jørgensen, T. J., Highly selective enrichment of phosphorylated peptides from peptide mixtures using titanium dioxide microcolumns. *Molecular & cellular proteomics* **2005,** *4* (7), 873-886.

8. Beltran, L.; Cutillas, P. R., Advances in phosphopeptide enrichment techniques for phosphoproteomics. *Amino acids* **2012,** *43* (3), 1009-1024.

9. Tsai, C.-F.; Wang, Y.-T.; Chen, Y.-R.; Lai, C.-Y.; Lin, P.-Y.; Pan, K.-T.; Chen, J.-Y.; Khoo, K.-H.; Chen, Y.-J., Immobilized metal affinity chromatography revisited: pH/acid control toward high selectivity in phosphoproteomics. *Journal of proteome research* **2008,** *7* (9), 4058-4069.

10. Aryal, U. K.; Ross, A. R., Enrichment and analysis of phosphopeptides under different experimental conditions using titanium dioxide affinity chromatography and mass spectrometry. *Rapid Communications in Mass Spectrometry* **2010,** *24* (2), 219-231.

11. Ye, J.; Zhang, X.; Young, C.; Zhao, X.; Hao, Q.; Cheng, L.; Jensen, O. N., Optimized IMAC− IMAC protocol for phosphopeptide recovery from complex biological samples. *Journal of proteome research* **2010,** *9* (7), 3561-3573.

12. Neilson, K. A.; Ali, N. A.; Muralidharan, S.; Mirzaei, M.; Mariani, M.; Assadourian, G.; Lee, A.; Van Sluyter, S. C.; Haynes, P. A., Less label, more free: approaches in label-free quantitative mass spectrometry. *Proteomics* **2011,** *11* (4), 535-553.

13. Zhu, W.; Smith, J. W.; Huang, C.-M., Mass spectrometry-based label-free quantitative proteomics. *BioMed Research International* **2009,** *2010*.

14. Ong, S.-E.; Blagoev, B.; Kratchmarova, I.; Kristensen, D. B.; Steen, H.; Pandey, A.; Mann, M., Stable isotope labeling by amino acids in cell culture, SILAC, as a simple and accurate approach to expression proteomics. *Molecular & cellular proteomics* **2002,** *1* (5), 376-386.

15. Thompson, A.; Schäfer, J.; Kuhn, K.; Kienle, S.; Schwarz, J.; Schmidt, G.; Neumann, T.; Hamon, C., Tandem mass tags: a novel quantification strategy for comparative analysis of complex protein mixtures by MS/MS. *Analytical chemistry* **2003,** *75* (8), 1895-1904.

16. Wiese, S.; Reidegeld, K. A.; Meyer, H. E.; Warscheid, B., Protein labeling by iTRAQ: a new tool for quantitative mass spectrometry in proteome research. *Proteomics* **2007,** *7* (3), 340-350.

17. Wang, H.; Alvarez, S.; Hicks, L. M., Comprehensive comparison of iTRAQ and label-free LC-based quantitative proteomics approaches using two Chlamydomonas reinhardtii strains of interest for biofuels engineering. *Journal of proteome research* **2011,** *11* (1), 487-501.

18. Merl, J.; Ueffing, M.; Hauck, S. M.; von Toerne, C., Direct comparison of MS-based label-free and SILAC quantitative proteome profiling strategies in primary retinal Müller cells. *Proteomics* **2012,** *12* (12), 1902-1911.

19. Megger, D. A.; Bracht, T.; Meyer, H. E.; Sitek, B., Label-free quantification in clinical proteomics. *Biochimica et Biophysica Acta (BBA)-Proteins and Proteomics* **2013,** *1834* (8), 1581-1590.

20. Patel, V. J.; Thalassinos, K.; Slade, S. E.; Connolly, J. B.; Crombie, A.; Murrell, J. C.; Scrivens, J. H., A comparison of labeling and label-free mass spectrometry-based proteomics approaches. *Journal of proteome research* **2009,** *8* (7), 3752-3759.

21. Old, W. M.; Meyer-Arendt, K.; Aveline-Wolf, L.; Pierce, K. G.; Mendoza, A.; Sevinsky, J. R.; Resing, K. A.; Ahn, N. G., Comparison of label-free methods for quantifying human proteins by shotgun proteomics. *Molecular & cellular proteomics* **2005,** *4* (10), 1487-1502.

22. Searle, B. C., Scaffold: a bioinformatic tool for validating MS/MS-based proteomic studies. *Proteomics* **2010,** *10* (6), 1265-1269.

23. Cox, J.; Mann, M., MaxQuant enables high peptide identification rates, individualized ppb-range mass accuracies and proteome-wide protein quantification. *Nature biotechnology* **2008,** *26* (12), 1367-1372.

24. Schilling, B.; Rardin, M. J.; MacLean, B. X.; Zawadzka, A. M.; Frewen, B. E.; Cusack, M. P.; Sorensen, D. J.; Bereman, M. S.; Jing, E.; Wu, C. C., Platform-independent and label-free quantitation of proteomic data using MS1 extracted ion chromatograms in

Skyline application to protein acetylation and phosphorylation. *Molecular & Cellular Proteomics* **2012,** *11* (5), 202-214.

25. Nahnsen, S.; Bielow, C.; Reinert, K.; Kohlbacher, O., Tools for label-free peptide quantification. *Mol Cell Proteomics* **2013,** *12* (3), 549-556.

26. Bantscheff, M.; Schirle, M.; Sweetman, G.; Rick, J.; Kuster, B., Quantitative mass spectrometry in proteomics: a critical review. *Analytical and bioanalytical chemistry* **2007,** *389* (4), 1017-1031.

27. Bantscheff, M.; Schirle, M.; Sweetman, G.; Rick, J.; Kuster, B., Quantitative mass spectrometry in proteomics: a critical review. *Anal Bioanal Chem* **2007,** *389* (4), 1017-1031.

28. Liu, H.; Sadygov, R. G.; Yates, J. R., A model for random sampling and estimation of relative protein abundance in shotgun proteomics. *Analytical chemistry* **2004,** *76* (14), 4193-4201.

29. Michalski, A.; Cox, J.; Mann, M., More than 100,000 detectable peptide species elute in single shotgun proteomics runs but the majority is inaccessible to data-dependent LC−MS/MS. *Journal of proteome research* **2011,** *10* (4), 1785-1793.

30. Oppermann, F. S.; Gnad, F.; Olsen, J. V.; Hornberger, R.; Greff, Z.; Kéri, G.; Mann, M.; Daub, H., Large-scale proteomics analysis of the human kinome. *Molecular & Cellular Proteomics* **2009,** *8* (7), 1751-1764.

31. Kuharev, J.; Navarro, P.; Distler, U.; Jahn, O.; Tenzer, S., In-depth evaluation of software tools for data-independent acquisition based label-free quantification. *Proteomics* **2015,** *15* (18), 3140-3151.

32. Werth, E. G.; McConnell, E. W.; Gilbert, T. S. K.; Couso Lianez, I.; Perez, C. A.; Manley, C. K.; Graves, L. M.; Umen, J. G.; Hicks, L. M., Probing the global kinome and phosphoproteome in Chlamydomonas reinhardtii via sequential enrichment and quantitative proteomics. *The Plant Journal* **2017,** *89* (2), 416-426.

33. Macek, B.; Mann, M.; Olsen, J. V., Global and site-specific quantitative phosphoproteomics: principles and applications. *Annual review of pharmacology and toxicology* **2009,** *49*, 199-221.

34. Thingholm, T. E.; Jensen, O. N.; Larsen, M. R., Analytical strategies for phosphoproteomics. *Proteomics* **2009,** *9* (6), 1451-1468.

35. Kosako, H.; Nagano, K., Quantitative phosphoproteomics strategies for understanding protein kinase-mediated signal transduction pathways. *Expert review of proteomics* **2011,** *8* (1), 81-94.

36. Sharma, K.; D'Souza, R. C.; Tyanova, S.; Schaab, C.; Wiśniewski, J. R.; Cox, J.; Mann, M., Ultradeep human phosphoproteome reveals a distinct regulatory nature of Tyr and Ser/Thr-based signaling. *Cell reports* **2014,** *8* (5), 1583-1594.

37. Wu, R.; Dephoure, N.; Haas, W.; Huttlin, E. L.; Zhai, B.; Sowa, M. E.; Gygi, S. P., Correct interpretation of comprehensive phosphorylation dynamics requires normalization by protein expression changes. *Molecular & cellular proteomics* **2011,** *10* (8), M111. 009654.

38. Werth, E. G.; McConnell, E. W.; Couso, I.; Perrine, Z.; Crespo, J. L.; Umen, J. G.; Hicks, L. M., Investigating the effect of Target of Rapamycin kinase inhibition on the Chlamydomonas reinhardtii phosphoproteome: from known homologs to new targets. *Submitted.* **2018**.

39. Valledor, L.; Furuhashi, T.; Recuenco-Muñoz, L.; Wienkoop, S.; Weckwerth, W., System-level network analysis of nitrogen starvation and recovery in Chlamydomonas reinhardtii reveals potential new targets for increased lipid accumulation. *Biotechnology for biofuels* **2014,** *7* (1), 171.

40. Cunningham Jr, F.; Gantt, E., Genes and enzymes of carotenoid biosynthesis in plants. *Annual review of plant biology* **1998,** *49* (1), 557-583.

41. Siaut, M.; Cuiné, S.; Cagnon, C.; Fessler, B.; Nguyen, M.; Carrier, P.; Beyly, A.; Beisson, F.; Triantaphylidès, C.; Li-Beisson, Y., Oil accumulation in the model green alga Chlamydomonas reinhardtii: characterization, variability between common laboratory strains and relationship with starch reserves. *BMC biotechnology* **2011,** *11* (1), 7.

42. Park, J. J.; Wang, H.; Gargouri, M.; Deshpande, R. R.; Skepper, J. N.; Holguin, F. O.; Juergens, M. T.; Shachar-Hill, Y.; Hicks, L. M.; Gang, D. R., The response of Chlamydomonas reinhardtii to nitrogen deprivation: a systems biology analysis. *The Plant Journal* **2015,** *81* (4), 611-624.

43. Merchant, S. S.; Kropat, J.; Liu, B.; Shaw, J.; Warakanont, J., TAG, you're it! Chlamydomonas as a reference organism for understanding algal triacylglycerol accumulation. *Curr Opin Biotechnol* **2012,** *23* (3), 352-363.

44. Cross, F. R.; Umen, J. G., The Chlamydomonas cell cycle. *Plant J* **2015,** *82* (3), 370-392.

45. Merchant, S. S.; Prochnik, S. E.; Vallon, O.; Harris, E. H.; Karpowicz, S. J.; Witman, G. B.; Terry, A.; Salamov, A.; Fritz-Laylin, L. K.; Maréchal-Drouard, L., The Chlamydomonas genome reveals the evolution of key animal and plant functions. *Science* **2007,** *318* (5848), 245-250.

46. Zones, J. M.; Blaby, I. K.; Merchant, S. S.; Umen, J. G., High-Resolution Profiling of a Synchronized Diurnal Transcriptome from Chlamydomonas reinhardtii Reveals Continuous Cell and Metabolic Differentiation. *Plant Cell* **2015,** *27* (10), 2743-2769.

47. Miller, R.; Wu, G.; Deshpande, R. R.; Vieler, A.; Gärtner, K.; Li, X.; Moellering, E. R.; Zauner, S.; Cornish, A.; Liu, B., Changes in transcript abundance in Chlamydomonas reinhardtii following nitrogen-deprivation predict diversion of metabolism. *Plant physiology* **2010**, pp. 110.165159.

48. Förster, B.; Mathesius, U.; Pogson, B. J., Comparative proteomics of high light stress in the model alga Chlamydomonas reinhardtii. *Proteomics* **2006,** *6* (15), 4309-4320.

49. Atteia, A.; Adrait, A.; Brugière, S.; Tardif, M.; Van Lis, R.; Deusch, O.; Dagan, T.; Kuhn, L.; Gontero, B.; Martin, W., A proteomic survey of Chlamydomonas reinhardtii mitochondria sheds new light on the metabolic plasticity of the organelle and on the nature of the α-proteobacterial mitochondrial ancestor. *Molecular Biology and Evolution* **2009,** *26* (7), 1533-1548.

50. Wagner, V.; Ullmann, K.; Mollwo, A.; Kaminski, M.; Mittag, M.; Kreimer, G., The phosphoproteome of a Chlamydomonas reinhardtii eyespot fraction includes key proteins of the light signaling pathway. *Plant physiology* **2008,** *146* (2), 772-788.

51. Boesger, J.; Wagner, V.; Weisheit, W.; Mittag, M., Analysis of flagellar phosphoproteins from Chlamydomonas reinhardtii. *Eukaryotic cell* **2009,** *8* (7), 922-932.

52. Pan, J.; Naumann-Busch, B.; Wang, L.; Specht, M.; Scholz, M.; Trompelt, K.; Hippler, M., Protein phosphorylation is a key event of flagellar disassembly revealed by analysis of flagellar phosphoproteins during flagellar shortening in Chlamydomonas. *Journal of proteome research* **2011,** *10* (8), 3830-3839.

53. Wagner, V.; Geßner, G.; Heiland, I.; Kaminski, M.; Hawat, S.; Scheffler, K.; Mittag, M., Analysis of the phosphoproteome of Chlamydomonas reinhardtii provides new insights into various cellular pathways. *Eukaryotic Cell* **2006,** *5* (3), 457-468.

54. Wang, H.; Gau, B.; Slade, W. O.; Juergens, M.; Li, P.; Hicks, L. M., The global phosphoproteome of Chlamydomonas reinhardtii reveals complex organellar phosphorylation in the flagella and thylakoid membrane. *Molecular & Cellular Proteomics* **2014,** *13* (9), 2337-2353.

55. Roustan, V.; Bakhtiari, S.; Roustan, P.-J.; Weckwerth, W., Quantitative in vivo phosphoproteomics reveals reversible signaling processes during nitrogen starvation and recovery in the biofuel model organism Chlamydomonas reinhardtii. *Biotechnology for biofuels* **2017,** *10* (1), 280.

56. Loewith, R.; Hall, M. N., Target of rapamycin (TOR) in nutrient signaling and growth control. *Genetics* **2011,** *189* (4), 1177-1201.

57. Wullschleger, S.; Loewith, R.; Hall, M. N., TOR signaling in growth and metabolism. *Cell* **2006,** *124* (3), 471-484.

58. Dobrenel, T.; Caldana, C.; Hanson, J.; Robaglia, C.; Vincentz, M.; Veit, B.; Meyer, C., TOR Signaling and Nutrient Sensing. *Annual review of plant biology* **2016,** *67*, 261-285.

59. Pérez-Pérez, M. E.; Couso, I.; Crespo, J. L., The TOR Signaling Network in the Model Unicellular Green Alga Chlamydomonas reinhardtii. *Biomolecules* **2017,** *7* (3), 54.

60. González, A.; Hall, M. N., Nutrient sensing and TOR signaling in yeast and mammals. *The EMBO journal* **2017**, e201696010.

61. Raught, B.; Gingras, A. C.; Sonenberg, N., The target of rapamycin (TOR) proteins. *Proc Natl Acad Sci U S A* **2001,** *98* (13), 7037-7044.

62. Dibble, C. C.; Manning, B. D., Signal integration by mTORC1 coordinates nutrient input with biosynthetic output. *Nature cell biology* **2013,** *15* (6), 555-564.

63. Zhang, Y.; Persson, S.; Giavalisco, P., Differential regulation of carbon partitioning by the central growth regulator target of rapamycin (TOR). *Molecular plant* **2013,** *6* (6), 1731-1733.

64. Xiong, Y.; Sheen, J., The role of target of rapamycin signaling networks in plant growth and metabolism. *Plant physiology* **2014,** *164* (2), 499-512.

65. Rodrigues, S. P.; Alvarez, S.; Werth, E. G.; Slade, W. O.; Gau, B.; Cahoon, E. B.; Hicks, L. M., Multiplexing strategy for simultaneous detection of redox-, phospho- and total proteome – understanding TOR regulating pathways in Chlamydomonas reinhardtii. *Anal. Methods* **2015,** *7* (17), 7336-7344.

66. van Dam, T. J.; Zwartkruis, F. J.; Bos, J. L.; Snel, B., Evolution of the TOR pathway. *J Mol Evol* **2011,** *73* (3-4), 209-220.

67. Diaz-Troya, S.; Florencio, F. J.; Crespo, J. L., Target of rapamycin and LST8 proteins associate with membranes from the endoplasmic reticulum in the unicellular green alga Chlamydomonas reinhardtii. *Eukaryot Cell* **2008,** *7* (2), 212-222.

68. Perez-Perez, M. E.; Florencio, F. J.; Crespo, J. L., Inhibition of target of rapamycin signaling and stress activate autophagy in Chlamydomonas reinhardtii. *Plant Physiol* **2010,** *152* (4), 1874-1888.

69. Pérez-Pérez, M. E.; Couso, I.; Heredia-Martínez, L. G.; Crespo, J. L., Monitoring Autophagy in the Model Green Microalga Chlamydomonas reinhardtii. *Cells* **2017,** *6* (4), 36.

70. Andrews, G. L.; Simons, B. L.; Young, J. B.; Hawkridge, A. M.; Muddiman, D. C., Performance characteristics of a new hybrid quadrupole time-of-flight tandem mass spectrometer (TripleTOF 5600). *Analytical chemistry* **2011,** *83* (13), 5442-5446.

CHAPTER 2: SOPs for Culturing, Extraction, Digestion, Enrichment, Data Analysis Techniques for Algal-based Phosphoproteomics

2.1 Introduction

Phosphoproteomic studies in plant and algal species are unique in a variety of ways when compared to mammalian-based studies from sample culturing to bioinformatic resources available for biological inference. While there are steps common throughout all bottom-up proteomic experiments, optimization specifically for algae at every step of the pipeline is required to achieve ideal results such as specialized culturing conditions and extraction techniques for effective lysis of cell-wall containing organisms. Because of this and other requirements, the following chapter describes the standard operating procedures optimized and utilized throughout the subsequent research chapters.

2.2 Strain Selection and Algal Culturing

Algal culturing can be performed under photoautotrophic conditions requiring light for growth or photoheteroautotrophically, which includes a carbon source in the media and allows for growth in the absence of light. For cell synchronization to occur in Chlamydomonas, cells grown photoautotrophically require minimal media and a consistent light period such as diurnal cycles (12 h light, 12 h dark) driving photosynthetic cell growth and the cell division cycle[1]. For the experiments described throughout this dissertation, photoheteroautotrophic growth was employed using Tris-Acetate-Phosphate (TAP) solid and liquid media[2] from protocols made available through the Chlamydomonas Resource Center (https://www.chlamycollection.org).

Photohetereoautotrophic growth that does not involve cell synchronization was employed due to the dense cell cultures required for the large amount of cellular starting material needed for this phosphoproteomic workflow, a requirement not feasible with reproducible growth in light driven photoautotrophic cultures.

The strains used in the experimental chapters are all cell-walled strains with much of the method development work done in the wild-type strain CC-2895 6145c mt-. While it requires an optimized extraction method for effective cell lysis, using a cell-walled wild-type strain for differential phosphoproteomic studies was chosen to not extraneously stress the cell prior to investigating the effect of exogenous stresses on the phosphoproteome, which is a concern if using a cell wall-less mutant. For work on the rapamycin-hypersensitive mutant, vip1-1, the cell-walled strain CC-1690 mt+ was used as the parental strain to generate vip1-1 (Chapter 5).

After strain selection, algal culturing conditions require uniform growth across replicates. To measure log-phase growth and ensure harvesting at early-log phase, growth conditions were assessed using a Beckman Coulter cell counter with corresponding optical density (OD_{750}) measurements to evaluate during each experiment using UV-Vis. Cells were harvested at approximately $5x10^7$ cells/mL (OD_{750} ~ 0.4). For differential phosphoproteomic experiments discussed in Chapters 4 and 5, replicates of drug treatments were harvested to avoid variability amongst drug treatments through performing drug incubations for each replicate together. For example, in chapter 4, replicate 1 for Torin1, AZD8055, Rapamycin, and control drug treatments were harvested together and the process was continued until the fifth replicate for each treatment. The following protocol outlines the cell culturing and harvesting process used throughout the subsequent research chapters.

Cell Culturing, Day 1:

1. Prepare 350 mL starting liquid culture from strains grown on solid TAP media. Use a 1 L flask for 350 mL of culture to provide sufficient room for consistent mixing.
    a. Perform mixing at 120 RPM with 100 μmol m–2 s–1 white light at room temperature.
2. Grow overnight; typical doubling time is approximately 6 hr.

Day 2:

3. Measure cell count using Beckman Coulter cell counter, perform dilutions into new liquid TAP media cultures splitting cells into the number of flasks required for each replicate of the final experiment. Cells will be harvested at approximately $5x10^7$ cells/mL therefore dilute cultures of approximately 3.0 $x10^6$ cells/mL should be prepared 24 hours prior to harvesting.
    a. To reduce batch effects between replicates, dilutions for each set of replicates should be prepared so they are staggered growth. For example, if it requires approximately 1 hr to perform drug treatment and harvesting for each replicate, stagger dilutions of each replicate by one hour so each will grow to approximately $5x10^7$ cells/mL at the appropriate time.
4. Grow overnight
5. While cells are growing, prepare stock solutions of chemical inhibitors used. For Chapters 4 and 5, this requires a final concentration for AZD8055, Torin1, and Rapamycin of 700 μM, 500 μM, and 500 μM, respectively.
    a. Prepare 1 mM stock solutions in DMSO and store at -20°C to use the next day.

Day 3:

6. For each replicate, perform drug incubation to actively growing cultures at approximately $5x10^7$ cells/mL concentration.
7. Following drug incubation, quench cell cultures in a final concentration of 40% methanol. Prepare pre-chilled 80% methanol and pour equal volumes of cell culture prior to centrifugation for a final concentration of 40% methanol. This requires 350 mL 80% methanol for each replicate.
8. Centrifuge each culture for 5 min at 6,000 x g at 4°C
9. Decant supernatant with special attention to not disturb dark green cell pellet in centrifuge bottle.
10. Resuspend pellet in 10 mL of fresh TAP media, transfer solution to 15-mL conical centrifuge tube.
11. Centrifuge each culture for 2 min at 3,200 x g, maximum speed for Eppendorf 5810 centrifuge, at 4°C
12. Decant supernatant with special attention to not disturb dark green cell pellet in conical centrifuge tube.
13. Place conical centrifuge tube containing cell pellet in liquid nitrogen, once fully frozen store at -80°C until performing plant-based protein extraction.

2.3 Plant-based Extraction Techniques

Similar to other protein extractions, the objective of this step is to lyse the cells and gain access to proteins for downstream analysis. Because Chlamydomonas cells contain a cell-wall, efficient protein extraction requires both physical and reagent-based methods for cell lysis such as the use of a sonication step and the addition of detergents. For this, both native and denaturing

protein extractions have been adapted for efficient protein extraction in Chlamydomonas and are described below.

2.3.1 Native Extraction

Some enrichment techniques require native protein conformations to properly function. This consideration limits the detergents available for use during protein extraction and can require additional steps to effectively lyse cells, especially those that contain a cell wall. For the kinome enrichment employed in Chapter 3, the multiplexed inhibitor beads (MIBs) designed to preferentially bind to kinases over other proteins in the cell lysate required native kinase conformation for effective binding thus a native protein extraction was adapted from Daub et. al.[3] for algal cells. This protocol uses cell lysis via adaptive focused acoustics as an alternative to traditional sonication methods to reduce protein degradation and aggregation during cell disruption by avoiding sample overheating[4]. This is necessary to assist in lysing cells in a native environment absent from detergents. Compared to denaturing extraction procedures, this method yielded approximately 7.8 mg of protein per gram of wet cell pellet[5], only slightly reduced from the 8.0-9.5 mg g^{-1} extracted under denaturing conditions[6-7].

Native Protein Extraction:

1. Algal culturing is performed as described above in section 2.2 with minor changes to accommodate a native protein extraction. Specifically, cells are not quenched in methanol and protein extraction is performed directly following centrifugation instead of storage at -80°C.
2. Following algal culturing, cells are resuspended in non-denaturing lysis buffer and kept on ice. Cells are resuspended in 4 mL for every 1 gram of cell pellet.

a. Non-denaturing lysis buffer contains: 50 mM HEPES, pH 7.5, 0.5% Triton X-100, 150 mM NaCl, 1mM EDTA, 1mM EGTA, 10 mM NaF, 2.5 mM $NaVO_4$, and EDTA-free cOmplete protease inhibitor cocktail (Roche) and phosphatase inhibitor cocktails 2 and 3 (Sigma).

3. Cells in lysis buffer are then subjected to acoustic sonication for 3 min at 200 cycles/burst, 100 W power, and 13% duty cycle using an E220 focused ultra-sonicator (Covaris, Woburn, MA, USA).
4. Samples are transferred from glass Covaris tubes to Eppendorf centrifuge tubes. While transferring, the remaining samples are kept on ice.
5. Cell lysates are centrifuged at 16,000 x g for 10 min and the supernatant is collected.
6. While on ice, a small amount of each replicate is used for protein quantification using CB-X Protein Assay using manufacturer guidelines (G-Biosciences).
7. Following protein quantification, each replicate is normalized to the same concentration of 5.5mg/3mL for subsequent kinome and phosphoproteome enrichments (Section 2.5) using fresh lysis buffer, requiring at least 5 mg of lysate for kinome enrichment.

2.3.2 Denaturing Extraction

For peptide-based enrichment techniques that did not require a native protein lysate, such as the enrichments employed in Chapters 4 and 5, a Tris-based protein extraction with ionic, and denaturing, detergents was utilized to reproducibly extract a large subset of the proteome in Chlamydomonas. While the native protein extraction was optimized to yield similar amounts of mg g^{-1},[5] the addition of denaturing detergents to more effectively lyse cells was used when native conformation was not necessary.

Denaturing protein extraction:

1. Algal culturing is performed as described in Section 2.2
2. Following algal culturing, cells are resuspended in lysis buffer and kept on ice. Cells are resuspended in 4 mL for every 1 gram of cell pellet.
    a. Lysis buffer contains: 100 mM Tris, pH 8.0, 1% SDS, 1x cOmplete protease inhibitor and phosSTOP phosphatase inhibitor cocktails (Roche).
3. Cells in lysis buffer are then subjected to acoustic sonication in a 4°C water bath for 3 min at 200 cycles/burst, 100 W power, and 12% duty cycle using an E220 focused ultra-sonicator (Covaris, Woburn, MA, USA).
4. Samples are transferred from glass Covaris tubes to Eppendorf centrifuge tubes. While transferring, the remaining samples are kept on ice.
5. Cell lysates are centrifuged at 16,000 x g for 10 min and the supernatant is collected.
6. Back extraction from remaining pellet is performed by adding fresh lysis buffer and vortexing.
7. The samples are centrifuge at 16,000 x g for 10 min and the supernatant is collected and recombined with the first extraction.
8. Proteins are precipitated using 5 volumes of cold 100 mM ammonium acetate in methanol.
9. Samples are incubated for 3hr at -80°C.
10. After centrifugation for 5 min at 2,000 x g, the supernatant is decanted without disturbing the protein pellet.
11. Two washes are performed with fresh 100 mM ammonium acetate in methanol and a final wash with 70% ethanol, each followed with another centrifugation as described in step 10.

a. Protein pellets are vortexed with wash solution before spinning down.

12. Pellets are allowed to dry for approximately 5 min in hood followed by resolubilization in minimal resuspension buffer. Each 350 mL culture of starting material is resuspended in 1-2 mL of resuspension buffer for each replicate.
    a. Resuspension buffer contains: 8M urea in 100 mM Tris
13. Resuspended protein is incubated at room temperature for 1 hr.
14. A small amount of each replicate is aliquoted for protein quantification using CB-X Protein Assay using manufacturer guidelines (G-Biosciences).
15. Each replicate is normalized to the same concentration using fresh resuspension buffer before moving forward.
16. Resuspended protein lysates are stored at -80°C until continuing to protein-level enrichment or reduction, alkylation, and digestion.

2.4 Kinome Enrichment

To effectively enrich for the kinome of Chlamydomonas over other proteins in the cell lysate, a kinome enrichment strategy known as multiplexed inhibitor beads, MIBs, was performed prior to digestion on protein lysate samples that underwent native extraction. The MIBs columns were adapted for algal samples from a workflow previously described[8] and are composed of a 6 bead mix containing the following inhibitors: CTX0294885, VI16832, Purvalanol B, Shokat, PP58 and UNC21474 in the ratio of 1.5:1 (CTX0294885, VI16832): (Purvalanol B, Shokat, PP58 and UNC21474). This protocol was utilized in Chapter 3 to quantitatively characterize the kinome in tandem with the phosphoproteome using an LFQ proteomics-based approach.

Kinome enrichment:

1. Following native extraction, 5.5 mg/ 3 mL samples of protein lysate are loaded onto MIBs column.
2. 350 µL of bead slurry are used per replicate.
3. The MIBs mixture is vortexed to homogenize slurry and 350 µL are pipetted onto each column.
4. Prior to loading sample, the MIBs column is washed with 2 mL of “high salt” buffer.
    a. High salt buffer contains: 50 mM HEPES, pH = 7.5, 1 M NaCl, 0.5% Triton X-100, 1 mM EDTA, 1 mM EGTA.
5. 3 mL of protein lysate is pipetted onto the MIBs columns. The flow-through is reloaded one time.
6. The column is washed with 5 mL “high salt” buffer followed by 5 mL of “low salt” buffer.
    a. Low salt buffer contains: 50 mM HEPES, pH = 7.5, 50 mM NaCl, 0.5% Triton X-100, 1 mM EDTA, 1 mM EGTA.
7. The column is wash with 500 µL of low salt buffer containing 0.1% SDS.
8. The column is incubated with 500 µL of MIBs elution buffer at 95°C for 15 min.
    a. MIBs elution buffer contains: 0.5% SDS, 1% β-mercaptoethanol, 0.1% Tris, pH = 6.8
9. The elution is collected following incubation
10. The elution (steps 8 and 9) is repeated one time.
11. Following protein-level enrichment, protein precipitation is performed (Section 2.3.2, step 5) followed by reduction, alkylation, and digestion as discussed in the following section.

2.5 Digestion and C18 Clean-Up Techniques

While reduction, alkylation, and protein digestion are common steps throughout all bottom-up proteomic experiments, numerous reducing and alkylating agents in addition to experimental parameters during protein digestion have been tested to determine the best conditions. In Chlamydomonas, reducing agents such as dithiothreitol (DTT)[7] and Tris(2-carboxyethyl)phosphine hydrochloride (TCEP)[9-10] have been used to study protein thiols and the effectiveness of alkylation between iodoacetamide (IAM) and N-Ethylmaleimide (NEM) has been studied[7]. Additionally, to limit overheating of phosphopeptides leading to sample degradation, digestion was performed at 25°C instead of the traditional 37°C overnight. The following protocol was used to perform the reduction, alkylation, and digestion followed by desalting using a C-18 column.

Reduction, Alkylation, and Digestion:

1. Samples stored at -80°C are allowed to thaw to room temperature.
2. Samples are reduced using 10 mM dithiothreitol for 30 min at room temperature.
    a. Prepare 1 mL of 500 mM DTT solution and add 20 µL for each 1 mL of protein lysate.
3. Alkylation is done using 40 mM iodoacetamide for 45 min in darkness at room temperature.
    a. Prepare 2 mL of 500 mM IAM solution and add 80 uL for each 1 mL of protein lysate.
4. Following alkylation, samples are diluted 5-fold in 100 mM Tris so the concentration of urea is <2M, which is a requirement for effective protein digestion.

5. Overnight digestion is performed using Trypsin Gold (Promega) at a protease:protein ratio of 1:50 for 16 hr. at 25°C. For phosphopeptide enrichment experiments, this requires 40 µg of Trypsin Gold for every 2 mg of protein lysate.
6. Following the 16 hr incubation, digestion is quenched using a stock of 5% TFA to pH<3.0
7. Samples are frozen at -80°C following digestion until C18 Clean Up using 50 mg SepPak (Waters) cartridges.

C-18 Clean Up:

8. Desalting is performed following protein digestion using commercially available 50 mg SepPak (Waters) cartridges on a vacuum manifold. To prepare, samples are thawed on ice and centrifuged for 5 min at 5,000 x g to pellet. Undigested protein is removed from peptide mixture to avoid clogging C-18 cleanup columns.
9. Prior to loading samples onto the column, columns are wet using 1 mL of acetonitrile working with up to five columns at a time. Experiments requiring 20 samples such as in Chapter 4, are done in four sets of five.
10. A small amount of vacuum is used to maintain a constant flow of approximately 1 drop per second throughout the entire workflow until elution which is done without vacuum.
11. Columns are equilibrated using 2 mL of 1% TFA in water.
12. Peptide samples are passed through the column recovering flow through
13. Flow through is reapplied across the columns
14. Salts are removed by flowing 2 mL of 1% TFA in water following the flow through.

15. To elute desalted peptide mixture from column, 1.5 mL of 60% acetonitrile, 0.1% TFA in water is used. Elution is performed at ambient pressure with no additional vacuum applied.
    a. The desalted peptides are recovered using a 2 mL Eppendorf centrifuge tube.
    b. Once the 1.5 mL of 60% acetonitrile, 0.1% TFA in water have passed through the columns, the remaining amount is recovered by applying vacuum for approximately 5 sec.
16. Following peptide elution, samples are frozen at -80°C and vacuum centrifuged to dryness prior to phosphopeptide enrichment
    a. For samples that will not undergo peptide-level enrichment, they are ready for LC-MS/MS analysis following vacuum centrifugation to dryness (Section 2.7)

2.6 Phosphoproteomic Techniques

Reproducibility in sample preparation and processing is crucial for LFQ proteomics. When introducing an enrichment strategy and additional sample handling steps to the pipeline, variability is inherently increased. To reduce the variability introduced with the phosphopeptide enrichment step, the ideal protein:resin ratio was determined specifically for the Chlamydomonas cellular matrix (Figure 2.1). The following protocol uses commercially available 3 mg. TiO_2 phosphopeptide enrichment columns (GL Sciences) and was adapted from the protocol provided by the Duke Proteomics Core Facility (http://www.genome.duke.edu/cores/proteomics/) for Chlamydomonas. 2 mg. of peptide lysate starting material was used for each replicate in the LFQ phosphopeptide work described in Chapters 3-5.

Phosphopeptide Enrichment:

1. Columns are pre-eluted using 100 µL of elution buffer for each sample replicate.

    a. Elution buffer contains: 20% acetonitrile, 5% aqueous ammonia.

2. Columns are centrifuged at room temperature at 1000 x g for 2 min.
3. Conditioning is done by adding 100 µL of 80% acetonitrile, 1% TFA in water to each column.
4. Columns are centrifuged at room temperature at 1000 x g for 2 min.
5. Steps 3 and 4 are repeated one time.
6. Columns are conditioned using 100 µL of 80% acetonitrile, 1% TFA, 30 mg/mL phthalic acid.
7. Columns are centrifuged at room temperature at 1000 x g for 2 min.
8. Steps 6 and 7 are repeated twice.
9. Samples that were previously dried down following C18 clean-up (Section 2.4, step 16) are resuspended in 150 µL of 80% acetonitrile, 1% TFA, 30 mg/mL phthalic acid.
10. Following resuspension, samples are centrifuged at 10,000 x g for 5 min prior to loading onto the column to make sure there is no solid material that could clog the column.
11. 150 µL of peptide sample is added to each enrichment column.
12. The columns are centrifuged at room temperature at 1000 x g for 5 min recovering the flow through.
13. Flow through is reapplied following steps 11 and 12 twice.
14. Following peptide lysate binding, the columns are washed using 100 µL of 80% acetonitrile, 1% TFA in water, 30 mg/mL phthalic acid.
15. The columns are centrifuged at room temperature at 1000 x g for 2 min.
16. Steps 14 and 15 are repeated one time.
17. The columns are washed again using 100 µL of 80% acetonitrile, 1% TFA in water.

18. The columns are centrifuged at room temperature at 1000 x g for 2 min.
19. Steps 17 and 18 are repeated twice.
20. Phosphopeptide-enriched samples are eluted by adding 100 µL of elution buffer.
21. The columns are centrifuged at room temperature at 1000 x g for 5 min.
22. Steps 20 and 21 are repeated for a total of 200 µL of elution.
23. The elution is then frozen and vacuum centrifuged to dryness prior to ZipTip sample clean-up and subsequent LC-MS/MS acquisition.

2.7 LC-MS/MS Analysis

Following sample preparation techniques used throughout the LFQ proteomic and phosphoproteomic pipelines described above, reproducible LC-MS/MS sample preparation and acquisition is additionally required. To prepare samples for LC-MS/MS, samples are dried to completeness via vacuum centrifugation prior to resuspension in 3% MeCN, 0.1% TFA in water for phosphopeptide samples and resuspended in 3% MeCN, 0.1% formic acid (FA) in water for kinome and non-enriched samples. The LC-MS/MS system used throughout this dissertation is a NanoACQUITY coupled to a TripleTOF 5600 (AB Sciex) that is optimized for one microgram of lysate on column per sample. For general workflows, dried samples are prepared in 1µg/ 5µL concentrations with 5 µL injection volumes. For phosphopeptide-enriched samples, dried elutions following phosphopeptide enrichment are resuspended in 20 µL with 5 µL injection volumes for each replicate.

For peptide separation, a 90-min linear gradient from 95% H_2O/5% MeCN /0.1% FA to 65% H_2O/35% MeCN /0.1% FA was used. Each sample was loaded onto a trap column (NanoAcquity UPLC 2G-W/M Trap 5 µm Symmetry C18, 180 µm × 20 mm) at a flow rate of 5 µL min^{-1} for 5 min. Peptides were separated using a C18 column (NanoAcquity UPLC 1.8 µm HSS T3, 75 µm

× 250 mm) at a flow rate of 300 nL min^{-1}. For both MS acquisition strategies described below, the TripleTOF 5600 Q-TOF was operated in positive ionization nanoelectrospray and high-sensitivity mode for data acquisition as previously described[7]. Data-dependent acquisition was employed for all phosphoproteomic work described in the following research chapters and the data-independent acquisition workflow described below was employed for the kinome analysis in Chapter 3.

2.7.1 DDA and SWATH (DIA) Acquisition Parameters

Based on previous performance studies for the TripleTOF 5600 system[11] and our laboratory's assessment of our NanoACQUITY coupled to TripleTOF 5600 platform[7], DDA runs selected the first 20 features above 150 counts having a +2 to +5 charge state for fragmentation for each two second cycle. For DIA runs via SWATH (Sequential Windowed Acquisition of All Theoretical Fragment Ion Mass Spectra), fragmentation was instead performed across the entire mass range for each two second cycle. This was done using 20 sequential windows across the mass range with varying widths optimized to effectively cover the entire mass range while concurrently focusing on dense m/z regions with smaller Q1 windows and less dense m/z regions with larger Q1 windows (Figure 2.2). Sequential window widths optimized for the DIA kinome analysis can be found in Table 2.1.

2.8 Label-Free Quantitative Data Processing and Analysis Techniques

Following data acquisition, steps to align experimental runs, infer protein identifications, and provide quantitative information are necessary to infer biological significance. For DDA workflows, this was done using Progenesis QI for Proteomics (Nonlinear Dynamics) as discovery analysis software, Mascot Daemon (Matrix Science) for protein identification, and Python and Perseus for data filtering. For the SWATH workflow, this was done using PeakView

(AB Sciex) for quantitative review of MS/MS spectra and alignment to the ion library, which used Mascot Daemon database searching to generate the ion library identifications. The data processing steps for each acquisition type are outlined in the following sections.

2.8.1 DDA Data Processing and Analysis

DDA Data analysis workflow:

1. Acquired spectra files (*.wiff) are imported into Progenesis QI for Proteomics (v2.0, Nonlinear Dynamics).
2. Automatic processing is done, allowing a reference spectra to be assigned.
3. To minimize run-to-run differences, each file is aligned to reference spectra and the alignment is manually validated requiring ≥ 80% score for each *.wiff against the reference spectra.
    a. For alignments with <80% score, manual alignment vectors are included before redoing the automatic alignment.
4. Following alignment validation and review, the automatic processing is continued, setting up the experimental design specifying control and treatment runs.
5. A combined peak list (*.mgf) is then generated under the “identify peptides” tab for all runs.
6. The file is exported for peptide sequence determination and protein inference by Mascot (v2.5.1, Matrix Science) using parameters described in Figure 2.3.
7. Following database searching, Mascot Percolator algorithm is employed, requiring ≤ 1% peptide FDR.
8. Resulting matches are exported as *.xml file. Matches are also exported as *.csv file with query level raw peptide match data included.

9. *.xml file is uploaded into Progenesis QI for Proteomics to match peaks from the raw spectra.
10. Following this, peptide measurements as *.csv are exported for analysis of phosphoproteomic experiments and protein measurements are exported as *.csv for analysis of phosphoproteomics and kinome experiments. Prior to exporting protein measurements for phosphoproteomic experiments, the identifications are refined so protein scores of less than 13 are removed. Filtering steps to parse results were written as custom scripts in the Python programming language. Figure 2.4 displays an example output following Python filtering to be used for filtering and data visualization.
    a. For phosphoproteomic work, data filtering steps employed are shown in Figure 2.5 with the first three steps performed in Python and removal of rows with >50% zeros in each condition performed in Perseus.
    b. For kinome LFQ work, analysis was performed on protein measurements after filtering for proteins with ≥2 unique peptides used for identification in Excel.
11. Data normalization and visualization is performed as described in Section 2.10.

2.8.2 SWATH Data Processing and Analysis

Prior to LFQ analysis of SWATH files, an ion library composed of DDA runs to compare SWATH spectra against is required. For the SWATH ion library, 15 strong cation exchange (SCX) fractions in addition to kinome DDA runs were analyzed to compose a library of 4,198 protein identifications, which were used as the source for protein identifications for SWATH prior to LFQ analysis. The process of ion library generation in addition to SWATH file processing after ion library generation are described in this section.

Ion Library Generation for SWATH:

1. Raw *.wiff files from fractionated DDA runs and additional DDA runs that will compose the ion library are imported into ProteinPilot (AB Sciex, v.5.0) under the LC “Identify Proteins” tab.
2. Using Paragon processing, digestion and Cys alkylation type are specified as trypsin and iodoacetamide, respectively.
3. Thorough ID search with a biological modification ID focus and the database of interest are specified before searching.
4. Following searching, *.group file generated for ion library for SWATH data analysis is exported.

SWATH Data Analysis Workflow:

5. Following ion library generation, *.group file is imported into PeakView (AB Sciex, v.2.1) by selecting ion library from quantitation tab.
6. When prompted, a maximum number of proteins to import is specified that is above the amount of identifications specified in ProteinPilot for the ion library of interest.
7. Shared peptides are not imported and “unlabeled” sample type is selected.
8. Once ion library is loaded, raw *.wiff sample files are added to PeakView.
9. Retention time calibration is performed using 1-2 peptides every 10 minutes throughout gradient from 30-90 min.
10. SWATH data is processed using settings specified in Table 2.2.
11. The processed experiment is exported to an Excel workbook file.
12. In Excel, a confidence cutoff score is filtered to be >1.3 (95% confidence).
13. Data normalization and visualization is performed as described in Section 2.9.

2.9 Data Visualization and Biological Inference Techniques

To find significance in the quantitative data provided in the above workflow, strategies for statistical analysis, data visualization and biological inference such as pathway annotation are required. To perform this, multiple software and online tools are available. For this work, statistical analysis is performed using Perseus[12-13] and annotation data for Chlamydomonas is provided by Phytozome[14], the Plant Comparative Genomics portal of the Department of Energy's Joint Genome Institute (https://phytozome.jgi.doe.gov). Online tools such as KEGG pathway analysis[15-16] and DAVID functional annotation[17-18] allow for further understanding of pathways of interest from statistically significant proteins with annotation in the Chlamydomonas genome. Together, these resources provide downstream biological analysis from the quantitative data to better understand effects on cellular signaling from complex proteomic and phosphoproteomic datasets.

Statistical Analysis Workflow:

1. The quantitative dataset *.csv file is converted to a *.txt file in Excel to import to Perseus v1.6.0.0.
2. The *.txt file is imported specifying normalized abundance data for each replicate in the experiment as "Main" type columns.
3. Additional columns are specified as numerical, text, or categorical based on column characteristics. For phosphopeptide work, the Identifier column is imported and for kinome and unenriched work, the protein accession column is imported as a "text" column.
4. Following importing of the data matrix, the experimental design is specified for statistical testing by adding a categorical annotation row.

    a. Each replicate of a condition should have the same name in the categorical row.
5. The data are Log2 transformed to normalize prior to testing.
6. The appropriate test is performed based on the experimental design. Comparisons are specified using categorical rows.
    a. For example, if comparing two conditions, two-sample Student's T-test are performed. For comparison across multiple conditions, ANOVA testing is used.
7. Following testing, the final matrix is exported as *.txt file.
8. In Excel, *.txt file is filtered for the appropriate fold change. This is performed by comparing averages of each condition with a threshold for significance. For chapters 4 and 5, a fold change FC>2 and p-value<0.05 were used.
9. Sites or proteins significantly changing based on statistical testing are highlighted.
10. With matrix parsed for significantly changing rows, *.txt file is reimported into Perseus v.1.6.0.0 for data visualization and cluster analysis.
11. Abundance values are standardized by performing a Z-score.
12. Hierarchical clustering is performed following default parameters to compare site or protein trends across conditions.
13. Following Perseus analysis, the final matrix is exported with cluster assignment. Figure 2.6 shows an example block diagram to perform this analysis.
14. KEGG or DAVID pathway analysis is performed from Phytozome annotations for sites or proteins of interest following testing.

2.10 Tables

Table 2.1 Sequential window m/z values across Q1 mass range from 350.0-1250.0 m/z for SWATH acquisition employed during kinome analysis in Chapter 3.

Window	m/z range	Window	m/z range
1	350.0-358.0	11	665.0-698.2
2	357.0-411.9	12	697.2-731.8
3	410.9-445.5	13	730.8-767.5
4	444.5-474.9	14	766.5-805.3
5	473.9-507.1	15	804.3-848.7
6	506.1-541.4	16	847.7-893.5
7	540.4-574.4	17	892.5-943.9
8	573.4-605.1	18	942.9-1007.6
9	604.1-635.2	19	1006.6-1102.1
10	634.2-666.0	20	1101.1-1249.9

Table 2.2 Overview of processing settings for SWATH data processing.

Number of Peptides per Protein:	6
Number of Transitions per Protein	6
Peptide Confidence Threshold %	95
False Discovery Rate Threshold %	1.0
XIC Extraction Window (min)	10
XIC width (ppm)	20

2.11 Figures

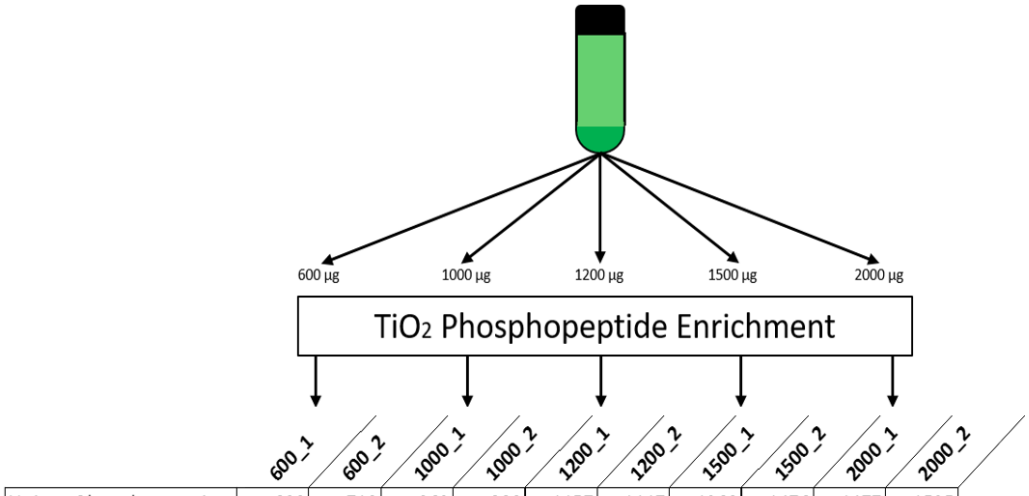

	600_1	600_2	1000_1	1000_2	1200_1	1200_2	1500_1	1500_2	2000_1	2000_2
Unique Phosphoproteins	603	719	962	883	1157	1117	1263	1476	1477	1525
Unique Phosphopeptides	1026	1241	1838	1632	2491	2287	2615	3105	3223	3377

Figure 2.1 Figure reproduced from [5]. Overview of coverage of phosphopeptides identified and phosphopeptide efficiency using 600, 1000, 1200, 1500, 2000 µg of digested protein lysate starting material

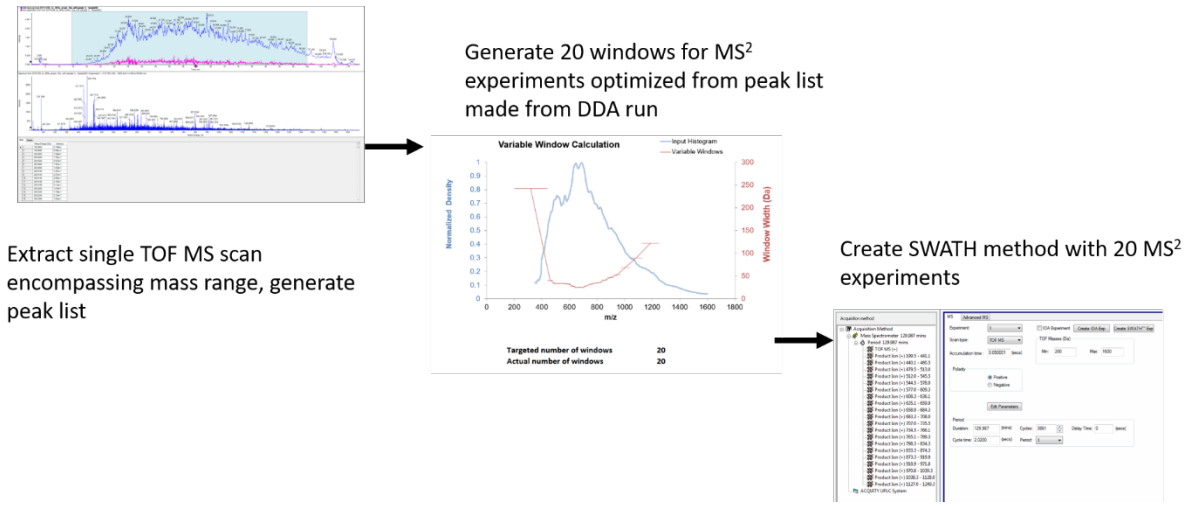

Figure 2.2 Variable windows used for SWATH acquisition. Window sizes are based on generating a peak list from DDA LC-MS/MS run representative of SWATH samples. Smaller Q1 windows are used for regions of the mass range where many peptide precursors are measured. Wider windows used where there are less precursors while still interrogating the entire mass range.

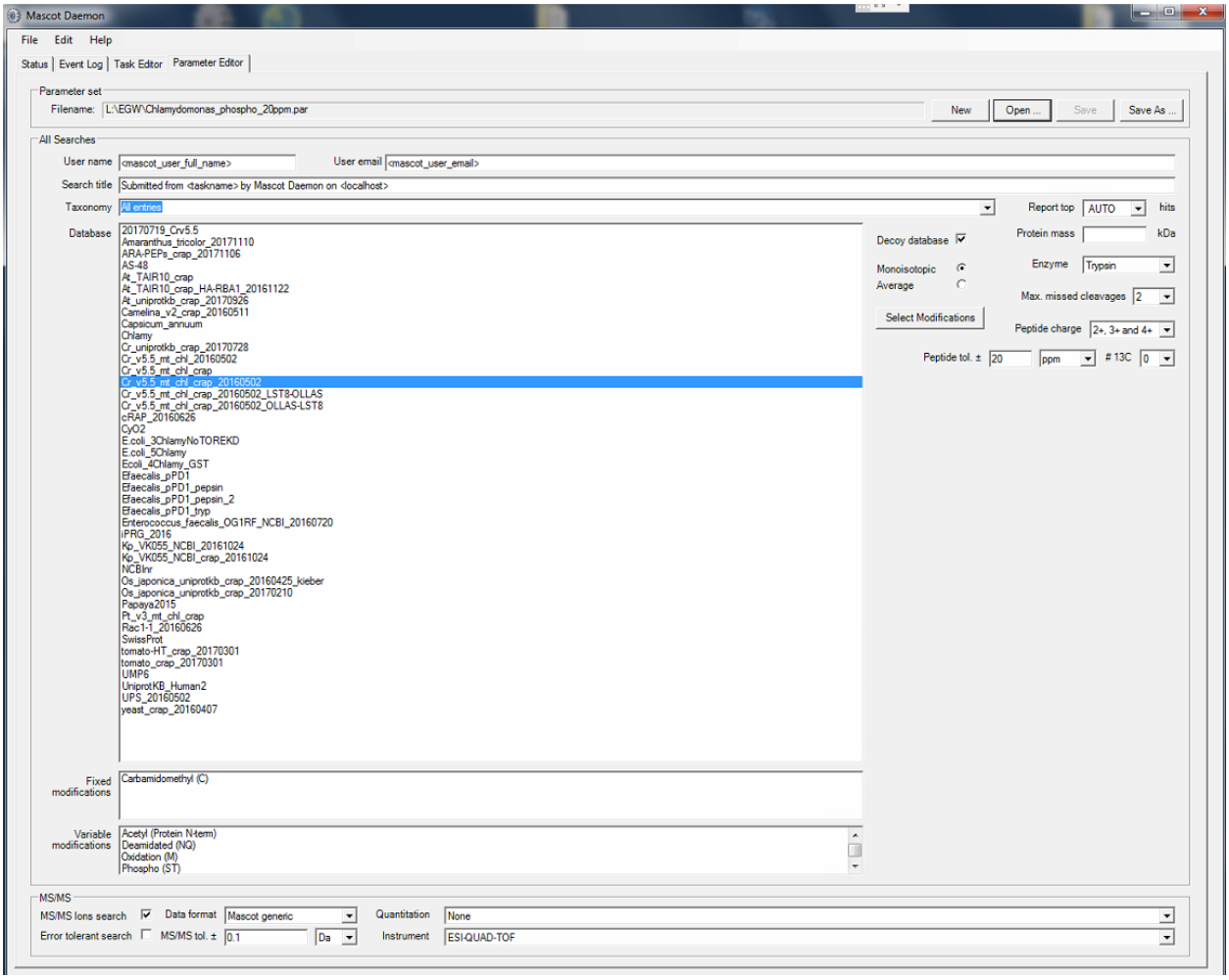

Figure 2.3 Overview of database searching requirements employed in LFQ proteomic experiments. Searches of MS/MS data used a trypsin protease specificity with the possibility of two missed cleavages, peptide/fragment mass tolerances of 20ppm/0.1 Da, and variable modifications of acetylation at the protein N-terminus, carbamidomethylation at cysteine, oxidation at methionine, and deamidation at asparagine or glutamine. Variable modifications of phosphorylation at serine or threonine and phosphorylation at tyrosine were appended to this list when working with phosphorylation enriched datasets.

```
***12020 pepm accessions / 12020 protm accesions matched

                                vip1_pepmeas.csv
Peptides                          114198.000000
Remove charge states               89720.000000
Remove score < 13                  12045.000000
Remove cRAP                        12020.000000
Filter raw                         12020.000000
Resolved raw                        9400.000000
Resolved phospho                    3669.000000
Resolved phospho unique             2551.000000
Resolved phospho peps percent         39.031915
                                             vip1_pepmeas.csv
Phosphopeptides                                   3669.000000
Unique phosphopeptides                            2551.000000
Mean CV                                             56.223329
Median CV                                           38.506574
80 percent of phosphopeptides at a CV of <          73.701627

                                                    vip1_pepmeas.csv
Proteins                                                        1514
Phosphopeptides with unique combinations of sites               2737
Total pS-pT-pY localized                                        1283
Total pS localized                                              1129
Total pT localized                                               136
Total pY localized                                                18
```

Figure 2.4 Example Python output following custom scripts written implemented to parse results.

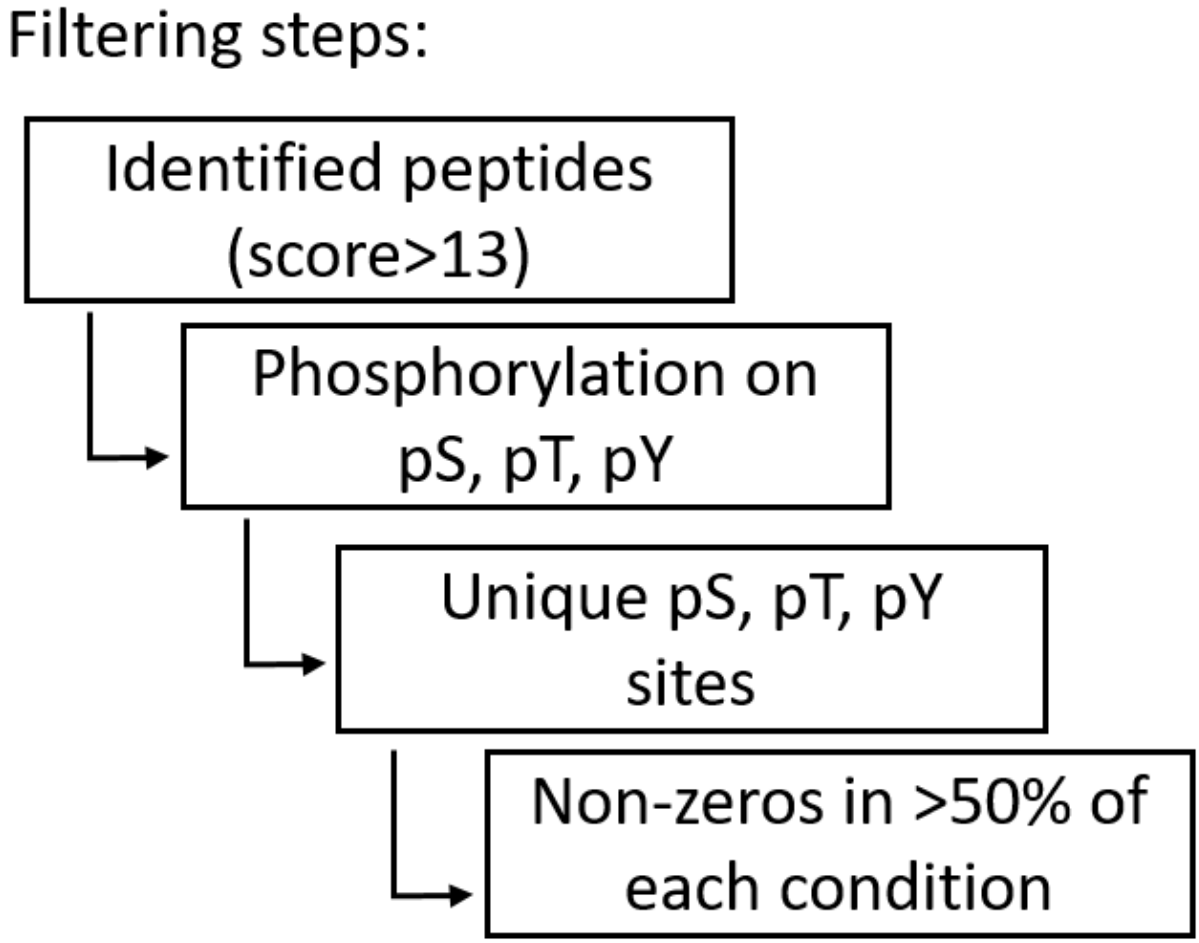

Figure 2.5 Overview of filtering steps in phosphoproteomic experiments required following Progenesis QI for Proteomics and Mascot database searching workflows described in Section 2.8.1.

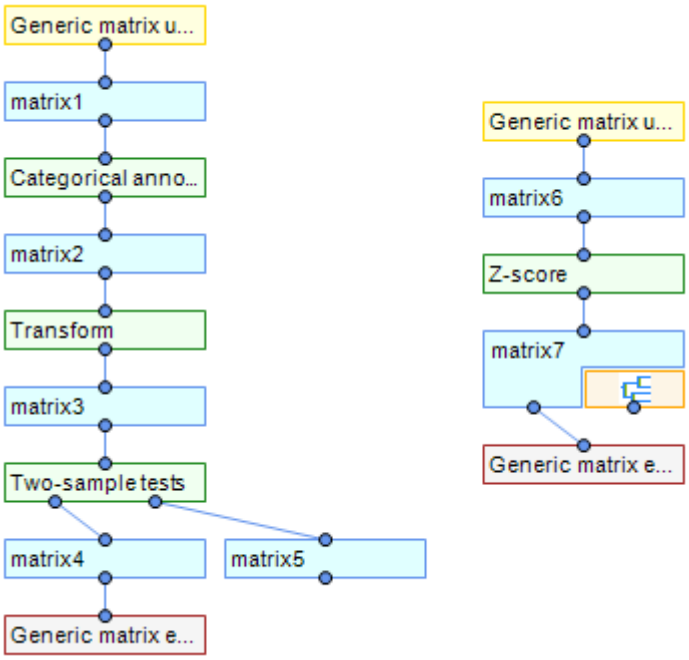

Figure 2.6 Block diagram of Perseus v.1.6.0.0 workflow highlighted in Section 2.9.

REFERENCES

1. Cross, F. R.; Umen, J. G., The Chlamydomonas cell cycle. *Plant J* **2015,** *82* (3), 370-392.

2. Gorman, D. S.; Levine, R., Cytochrome f and plastocyanin: their sequence in the photosynthetic electron transport chain of Chlamydomonas reinhardi. *Proceedings of the National Academy of Sciences* **1965,** *54* (6), 1665-1669.

3. Daub, H.; Olsen, J. V.; Bairlein, M.; Gnad, F.; Oppermann, F. S.; Korner, R.; Greff, Z.; Keri, G.; Stemmann, O.; Mann, M., Kinase-selective enrichment enables quantitative phosphoproteomics of the kinome across the cell cycle. *Mol Cell* **2008,** *31* (3), 438-448.

4. Dhabaria, A.; Cifani, P.; Reed, C.; Steen, H.; Kentsis, A., A High-Efficiency Cellular Extraction System for Biological Proteomics. *J Proteome Res* **2015,** *14* (8), 3403-3408.

5. Werth, E. G.; McConnell, E. W.; Gilbert, T. S. K.; Couso Lianez, I.; Perez, C. A.; Manley, C. K.; Graves, L. M.; Umen, J. G.; Hicks, L. M., Probing the global kinome and phosphoproteome in Chlamydomonas reinhardtii via sequential enrichment and quantitative proteomics. *The Plant Journal* **2017,** *89* (2), 416-426.

6. Maldonado, A. M.; Echevarría-Zomeño, S.; Jean-Baptiste, S.; Hernández, M.; Jorrín-Novo, J. V., Evaluation of three different protocols of protein extraction for Arabidopsis thaliana leaf proteome analysis by two-dimensional electrophoresis. *Journal of Proteomics* **2008,** *71* (4), 461-472.

7. Slade, W. O.; Werth, E. G.; McConnell, E. W.; Alvarez, S.; Hicks, L. M., Quantifying reversible oxidation of protein thiols in photosynthetic organisms. *J Am Soc Mass Spectrom* **2015,** *26* (4), 631-640.

8. Duncan, J. S.; Whittle, M. C.; Nakamura, K.; Abell, A. N.; Midland, A. A.; Zawistowski, J. S.; Johnson, N. L.; Granger, D. A.; Jordan, N. V.; Darr, D. B.; Usary, J.; Kuan, P. F.; Smalley, D. M.; Major, B.; He, X.; Hoadley, K. A.; Zhou, B.; Sharpless, N. E.; Perou, C. M.; Kim, W. Y.; Gomez, S. M.; Chen, X.; Jin, J.; Frye, S. V.; Earp, H. S.; Graves, L. M.; Johnson, G. L., Dynamic reprogramming of the kinome in response to targeted MEK inhibition in triple-negative breast cancer. *Cell* **2012,** *149* (2), 307-321.

9. Bräutigam, A.; Schaumlöffel, D.; Krauss, G.-J.; Wesenberg, D., Analytical approach for characterization of cadmium-induced thiol peptides—a case study using Chlamydomonas reinhardtii. *Analytical and bioanalytical chemistry* **2009,** *395* (6), 1737-1747.

10. Lee, D. Y.; Park, J.-J.; Barupal, D. K.; Fiehn, O., System response of metabolic networks in Chlamydomonas reinhardtii to total available ammonium. *Molecular & Cellular Proteomics* **2012,** *11* (10), 973-988.

11. Andrews, G. L.; Simons, B. L.; Young, J. B.; Hawkridge, A. M.; Muddiman, D. C., Performance characteristics of a new hybrid quadrupole time-of-flight tandem mass spectrometer (TripleTOF 5600). *Analytical chemistry* **2011,** *83* (13), 5442-5446.

12. Tyanova, S.; Temu, T.; Sinitcyn, P.; Carlson, A.; Hein, M. Y.; Geiger, T.; Mann, M.; Cox, J., The Perseus computational platform for comprehensive analysis of (prote) omics data. *Nature methods* **2016,** *13* (9), 731-740.

13. Cox, J.; Mann, M., 1D and 2D annotation enrichment: a statistical method integrating quantitative proteomics with complementary high-throughput data. *BMC bioinformatics* **2012,** *13* (16), S12.

14. Goodstein, D. M.; Shu, S.; Howson, R.; Neupane, R.; Hayes, R. D.; Fazo, J.; Mitros, T.; Dirks, W.; Hellsten, U.; Putnam, N., Phytozome: a comparative platform for green plant genomics. *Nucleic acids research* **2011,** *40* (D1), D1178-D1186.

15. Kanehisa, M.; Goto, S., KEGG: kyoto encyclopedia of genes and genomes. *Nucleic acids research* **2000,** *28* (1), 27-30.

16. Kanehisa, M.; Sato, Y.; Kawashima, M.; Furumichi, M.; Tanabe, M., KEGG as a reference resource for gene and protein annotation. *Nucleic acids research* **2015**, *44* (D1), D457-D462.

17. Huang, D. W.; Sherman, B. T.; Lempicki, R. A., Bioinformatics enrichment tools: paths toward the comprehensive functional analysis of large gene lists. *Nucleic acids research* **2008,** *37* (1), 1-13.

18. Huang, D. W.; Sherman, B. T.; Lempicki, R. A., Systematic and integrative analysis of large gene lists using DAVID bioinformatics resources. *Nature protocols* **2008,** *4* (1), 44-57.

CHAPTER 3: Probing the Global Kinome and Phosphoproteome in *Chlamydomonas reinhardtii* via Sequential Enrichment and Quantitative Proteomics

*****Reprinted with permission, from Werth, E.G., McConnell, E.M., Gilbert, T. S. K, Lianez, I. C., Perez, C. A., Manley, C. K., Graves, L. M., Umen, J. G., Hicks, L. M. Probing the global kinome and phosphoproteome in *Chlamydomonas reinhardtii* via sequential enrichment and quantitative proteomics. *Plant Journal* **2017,** 89, 416-426. doi: 10.1111/tpj.13384

3.1 Introduction

Expression and activity modulation of kinases is essential for organismal fitness and survival. Kinases regulate cellular signaling by site-specific phosphorylation of target proteins, thereby altering activity, subcellular localization, or complex formation[1]. Approaches for measuring kinase abundances have historically relied on highly specific antibody-based immunoassays[2], thus restricting coverage and throughput to a small subset of target kinases. Research aimed at dissecting the roles of kinases on a global "-omics" scale has grown within the past decade with the potential to become more comprehensive for discovery-based, untargeted kinome analyses. Utilization of immobilized kinase inhibitors [e.g., multiplexed inhibitor beads (MIBs)[3] or kinobeads[4]] preferentially capture low abundance protein kinases by targeting the ATP-binding domain of intact native kinases. This approach has enabled protein-level kinome analysis[2], the utility of which has been demonstrated in numerous studies in mammalian systems[5-8]. Herein, we employ a MIBs-based kinome enrichment in tandem with a phosphoproteome analysis from the same starting material. Development of this sequential enrichment strategy in a model eukaryotic photosynthetic organism, *Chlamydomonas reinhardtii* (Chlamydomonas), enabled simultaneous

coverage and quantification of its kinome and phosphoproteome using mass spectrometry-based quantitative label-free proteomics.

Chlamydomonas is an intensively-studied and well-developed model for investigating diverse biological processes including photosynthesis, chloroplast biogenesis, cell growth and motility[9-11]. The Chlamydomonas kinome contains an estimated 355 protein kinases[12] and forms a highly dynamic network of signaling pathways as illustrated by studies of the flagellar phosphoproteome[13] and proteomic analysis into the effects changes in kinase expression have on photosynthesis[14]. While global kinome enrichment has not yet been reported in Chlamydomonas, recent efforts by our laboratory to profile the global phosphoproteome identified 4,588 phosphoproteins and 15,862 unique phosphosites in this model organism[15].

Herein, a strategy is described for in-tandem kinome and phosphoproteome analysis from a single sample that provides quantitative information and increased coverage of expressed kinases and localized phosphosites on phosphoproteins potentially involved in kinase signaling pathways. We first optimized a native protein extraction for cell wall-containing Chlamydomonas strain CC-2895 (6145c *mt*-). Then, a MIBs global kinome enrichment strategy was used to enrich for intact kinases and ATP-binding proteins from the background via preferential binding to a mixture of moderate- to broadly-selective immobilized pan-kinase inhibitors. Quantitative reproducibility and overall coverage was compared between both data-dependent mass spectrometric acquisition (DDA) and data-independent mass spectrometric acquisition (DIA) via Sequential Windowed Acquisition of All Theoretical Fragment Ion Mass Spectra (SWATH) for the kinome-enriched samples. Proteolysis of unbound protein lysate from MIBs followed by TiO_2-based phosphopeptide enrichment and DDA enabled quantification of site-specific phosphorylation from the same samples. This workflow generates extensive

complementary datasets that may help increase understanding of kinase signaling pathways and regulated phosphorylation events in a quantitative manner.

3.2 Materials and Methods

3.2.1 Cell Growth and Native Extraction

Three biological replicates of *C. reinhardtii* strain CC-2895 6145c mt- (Chlamydomonas Resource Center) were grown at 22 ˚C in 350 mL Tris-acetate-phosphate (TAP) media[16] under continuous light (50 µE m^{-2} s^{-1}) on an Innova 2300 (New Brunswick Scientific, Enfield, CT, USA) shaker at 130 rpm. Cultures were harvested at early-log phase (OD_{750} 0.4 – 0.5) by centrifuging at 4,000*g* for 5 min and discarding the supernatant. Each replicate was resuspended in 50 mM HEPES, pH 7.5 buffer containing 0.5% Triton X-100 in the presence of EDTA-free cOmplete protease inhibitor cocktail (Roche) and phosphatase inhibitor cocktails 2 and 3 (Sigma) as previously described [3]. Samples were lysed by sonicating for 3 min at 200 cycles/burst, 100 W power, and 12% duty cycle using an E220 focused ultra-sonicator (Covaris, Woburn, MA, USA). Extracts were clarified via centrifugation (16,000*g*, 10 min) and adjusted to a final concentration of 1 M NaCl. Samples were normalized to 5.5 mg of protein per 3 mL of lysis buffer following determination of protein concentration using the CB-X protein assay (G-Biosciences, St. Louis, MO, USA).

3.2.2 Kinome Enrichment

Following native extraction, 5.5 mg of protein from each Chlamydomonas biological replicate was introduced on a MIBs column to isolate protein kinases and ATP-binding proteins from the lysate as previously described[3]. MIBs columns were composed of a 6 bead mix containing the following inhibitors: CTX0294885, VI16832, Purvalanol B, Shokat, PP58 and UNC21474 in the ratio of 1.5:1 (CTX0294885, VI16832): (Purvalanol B, Shokat, PP58 and

UNC21474). The flow through was reloaded once to the column before being collected and stored at -80°C for downstream applications employed in conjunction with enrichment due to the large amount of total protein remaining (~5.3 mg). Non-specifically bound proteins were removed using 5 mL each of wash buffer (50 mM HEPES, pH 7.5, 0.5% Triton X-100, 1 mM EDTA, 1 mM EGTA and 0.1% SDS) containing high-salt (1 M NaCl) or low-salt (150 mM NaCl). MIBs bound proteins were eluted from the column using 500 µL of 100 mM Tris-HCl, pH 6.8, 0.5% SDS, and 1% β-mercaptoethanol heated to 95°C for 15 min, twice.

3.2.3 Protein Digestion and Reduction

Enriched proteins were purified using a chloroform/methanol precipitation and resuspended in 50 mM HEPES, pH 8. Samples were reduced using 10 mM dithiothreitol and subsequently alkylated with 40 mM iodoacetamide prior to overnight digestion. For kinome-enriched and whole-cell (unenriched) samples, digestion was performed at 37 °C with Trypsin Gold (Promega) at a ratio of 1:100 protease:protein. For phosphoproteome analysis, digestion of MIBs flow through was performed at 25 °C at a ratio of 1:50 protease:protein.

3.2.4 Solid-Phase Extraction

After digestion, samples were acidified to 0.2% trifluoroacetic acid (TFA) following solid-phase extraction. For enriched and unenriched samples, desalting was performed using Pierce spin columns and C18 50 mg Sep-Pak cartridges (Waters) were used for phosphorylation-enriched samples. SPE columns were prepared by washing with acetonitrile (MeCN) followed by 80% MeCN/20% H_2O/0.1% TFA and 0.1% TFA. Digested protein lysates were applied to the columns and reloaded 2 times before being washed with 0.1% TFA and eluted using 80% MeCN/20% H_2O/0.1% TFA.

3.2.5 Phosphopeptide Enrichment

Following protein digestion and solid-phase extraction, 2 mg aliquots of flow through from MIBs enrichment were subjected to phosphorylation enrichment using 3 mg Titansphere Phos-TiO_2 Kit spin columns (GL Sciences). Replicates were dried by vacuum centrifugation and resuspended in 200 µL of 80% MeCN, 1% TFA and containing 25 mg/mL phthalic acid. Following each step in the enrichment, centrifugation at 1,000*g* for 2 min was performed. After pre-eluting the TiO_2 tips in 20% MeCN, 5% ammonium hydroxide, columns were conditioned with 80% MeCN, 1% TFA and peptide samples were loaded 3 times. Washes were performed 4 times using 80% MeCN, 1% TFA to remove non-specifically bound peptides. Phosphopeptides were eluted with 20% MeCN, 5% ammonium hydroxide and concentrated using vacuum centrifugation prior to LC-MS/MS analysis.

3.2.6 DDA and SWATH MS Acquisition

For all samples, peptides were resuspended in 95% H_20/5% MeCN/0.1% TFA before separation via a 100 min linear gradient from 95% H_20/5% MeCN/0.1% formic acid (FA) to 65% H_20/35% MeCN/0.1% FA via a NanoAcquity UPLC (Waters, Milford, MA, USA). Each sample was loaded onto a trap column (NanoAcquity UPLC 2G-W/M Trap 5 µm Symmetry C18, 180 µm × 20 mm) at a flow rate of 5 µL min^{-1} for 5 min. Peptides were separated using a C18 column (NanoAcquity UPLC 1.8 µm HSS T3, 75 µm × 250 mm) at a flow rate of 300 nL min^{-1}. A TripleTOF 5600 (AB Sciex, Concord, Canada) mass spectrometer was operated in positive ionization and high sensitivity mode for data acquisition as previously described[17], with the first 20 features above 150 counts threshold having a charge state of +2 to +5 selected for fragmentation during every 2 s cycle for DDA runs. SWATH samples were acquired using a variable acquisition window SWATH approach generated from previous MIBs-enriched or

whole cell lysate DDA runs with the 20 *m/z* windows used for both kinome enriched and no enrichment datasets. In addition to supplementary tables for MS datasets, the mass spectrometry proteomics data have been deposited to the ProteomeXchange Consortium (http://www.proteomexchange.org) via the PRIDE partner repository[18] with the dataset identifier PXD004681 and 10.6019/PXD004681.

3.2.7 DDA Data Processing

Acquired spectra (*.wiff) files were imported into Progenesis QI for proteomics (v2.0, Nonlinear Dynamics). A reference spectra was automatically assigned and total ion chromatograms were then aligned to minimize run-to-run differences in peak retention time. Alignment was validated (≥ 80% score) and a combined peak list (*.mgf) for all runs was exported for peptide sequence determination and protein inference by Mascot (v2.5.1, Matrix Science). Database searching was performed using the *C. reinhardtii* Phytozome v11 database (http://www.phytozome.net/; accessed May, 2015) appended with the NCBI chloroplast and mitochondria databases (19,603 entries). Sequences for common laboratory contaminants (http://www.thegpm.org/cRAP/; 116 entries) were appended to the database. Searches of MS/MS data used a trypsin protease specificity with the possibility of two missed cleavages, peptide/fragment mass tolerances of 10ppm/0.08 Da, and variable modifications of acetylation at the protein N-terminus, carbamidomethylation at cysteine, oxidation at methionine, and deamidation at asparagine or glutamine. Variable modifications of phosphorylation at serine or threonine and phosphorylation at tyrosine were appended to this list when working with phosphorylation enriched datasets. Significant peptide identifications above the identity or homology threshold were adjusted to ≤ 1% peptide FDR using the Mascot Percolator algorithm [19] and resulting matches were exported (*.xml) for further analysis. Peptide identifications in the

result file were uploaded to Progenesis QI for proteomics and matched to peaks from the raw spectra. Peptide measurements were then exported (*.csv) and custom scripts written in the Python programming language were implemented to parse results. Briefly, only peptides with Mascot ion score ≥ 13 and abundance > 0 across all samples, requiring detection in every biological replicate, were considered. Homologous proteins with shared peptides were then grouped together to satisfy the principle of parsimony. After grouping, the script performed site localization of variable modifications using an implementation of the Mascot Delta Score[20]. Confident site localization was considered if the difference between the best and second best Mascot ion score was ≥ 10 for alternative modification sites on an otherwise identical peptide-spectrum match.

3.2.8 Ion Library Generation

Raw (*.wiff) files from 8 MIBs-enriched DDA runs in addition to 15 SCX fraction DDA runs were combined and processed using ProteinPilot (Sciex, v5.0). Trypsin and iodoacetamide were specified for digestion and cysteine alkylation, respectively. A thorough ID search effort with a biological modification ID focus were specified and searched against the *C. reinhardtii* Phytozome v11 database concatenated with NCBI chloroplast and mitochondria entries as mentioned above. Following search, the resulting file (*.group) was imported into PeakView (v.2.1, AB Sciex) for SWATH data analysis.

3.2.9 SWATH Data Processing

Raw (*.swath) files were imported into PeakView for quantitative review of MS/MS spectra and alignment to ion library allowing for 6 peptides per protein and 6 transitions per peptide. Peptide confidence threshold was set to 95% with an FDR threshold of < 1%. XIC extraction window was opened to 10 minutes with 20 ppm mass tolerance. Following retention time

calibration in the PeakView software and processing, an Excel workbook file was exported and filtered for a confidence cutoff score > 1.3 (95% confidence). Logarithm base 2 transformation and data normalization by the central tendency approach were performed using the R package Inferno[21] with subsequent data analysis in the Python and R programming languages.

3.3 Results and Discussion

3.3.1 Native Protein Extraction of Chlamydomonas

The MIBs kinome enrichment strategy utilizes the affinity of kinases for ATP analogs and therefore requires non-denaturing protein extraction techniques. Cell lysis via adaptive focused acoustics is an alternative to traditional sonication methods that reduces protein degradation and aggregation during cell disruption by avoiding sample overheating[22], and this method has previously been found effective for disrupting Chlamydomonas cells[23]. We optimized and implemented an acoustic-wave sonication method for native protein extraction from Chlamydomonas with the goal of maximizing yield to accommodate the requirement for high protein amounts in kinome and phosphoproteome enrichment steps used downstream.

Our method (detailed in the Materials and Methods section) yielded an average of 7.8 mg of protein per g of wet cell pellet from each replicate that was only slightly reduced compared to a denaturing Tris-buffered phenol extraction routinely used for protein extractions from photosynthetic organisms that yields 8.0-9.5 mg/g[17, 24]. Coverage was also similar when comparing global profiles of whole cell lysates: 2,093 proteins were inferred from 9,607 unique peptides for native extraction and 2,063 proteins were inferred from 10,533 unique peptides for Tris-buffered phenol extraction based on standard DDA LC-MS/MS acquisition performed as previously described[17]. Importantly, the optimized native extraction provided sufficient material (5.5 mg protein extracted from 0.7 g wet pellet) for subsequent kinome and phosphopeptide

enrichments. As outlined in Figure 3.1, lysates from three biological replicates containing 5.5 mg each of native protein were subjected to a MIBs-based method to enrich for ATP-binding proteins (Figure 3.1B)[25]. Eluates were proteolyzed and processed via quantitative label-free proteomics as described below.

3.3.2 Kinome DDA and SWATH Data Acquisition

Both data-dependent acquisition (DDA) and data-independent acquisition (DIA) via SWATH were performed to compare depth of coverage of the kinome as well as quantitative accuracy of each acquisition approach. Untargeted methods relying on DDA are ubiquitous in bottom-up proteomics, but pose a challenge for identifying low abundance proteins because they require a minimum signal for specific ions to trigger a tandem MS (MS^2) analysis within a finite duty cycle[25]. SWATH acquisition can improve detection of low abundance proteins because it is not limited by such parameters. Instead, SWATH acquisition allows for fragmentation of all transmitted ions simultaneously by iteratively stepping the quadrupole (Q1) through 20 separate windows across the mass range (350-1250 *m/z*) and passing all ions through to the collision cell. This DIA strategy is further enhanced by using narrower Q1 windows in dense regions of the mass range and wider Q1 windows in sparse regions.

Implementation of a SWATH platform requires initial DDA runs with fractionation for exhaustive coverage to generate a spectral library for peptide matching and protein identification (Figure 3.2). The resulting ion library comprised of 15 strong-cation exchange (SCX) fractions and 8 MIBs runs contains 4,198 proteins (64,124 distinct peptides) with a confidence cutoff score > 1.3 (95% confidence in ProteinPilot), serving as the basis for SWATH spectral matching/identification. These 4,198 proteins represent 21% (4,198/19,603) of the predicted *C.*

reinhardtii proteome and includes 235/355 protein kinases[12] and 404/553 additional ATP-binding proteins classified by gene ontology.

Data from total lysates and MIBs-enriched samples showed improved coverage using SWATH acquisition over DDA alone, with lower between-replicate median variability in the kinome-enriched and total lysate samples from SWATH acquisition (Figure 3.3). Proteins identified through SWATH acquisition (Table S1) increased MIBs enriched data coverage by 597 proteins (37%) relative to DDA (Figure 3.3A, Table S2) including 36 more kinases. Three biological replicates were used to compare quantitative reproducibility for both SWATH and DDA methods. For the kinome-enriched samples, 90% of the 1,391 quantified proteins from SWATH acquisition had a coefficient of variation (CV) below 10%, and 90% of the 974 proteins via the DDA workflow had a CV below 11% (Figure 3.3C). The overall trend of increased coverage while maintaining low variability with SWATH is also evident with whole cell lysate samples (Figure 3.3B, C) where 253 (16%) additional proteins were identified using SWATH (Figure 3.3D) versus DDA alone. Compared to DDA acquisition, SWATH-MS maintains high reproducibility while providing additional coverage and is therefore preferential for label-free differential studies of MIBs enriched proteins. A breakdown of the chemical characteristics of the peptides identified in the MIB-enrichment dataset can be found in Figure 3.4.

3.3.3 Phosphopeptide Enrichment

Tandem investigation of the phosphoproteome and kinome from the same starting biological material simplifies analysis and may help generate or constrain hypotheses concerning kinase-substrate relationships. Following lysate loading onto MIBs columns, the flow through that contained >95% of the starting protein was processed for phosphopeptides using a titanium dioxide-based enrichment (Figure 3.1C)[26].

Variability between replicates for phosphopeptide enrichment was minimized by optimizing the protein-to-resin ratio and by use of a chemical additive that was selected from several tested candidates to minimize non-specific binding to the resin. A range of peptide loading levels from 0.5-2.5 mg was tested for enrichment on pre-packed 3 mg TiO_2 tip-columns and 2 mg was chosen for further experiments based on maximum reproducible phosphopeptide coverage. Numerous chemical additives have proven successful for decreasing non-specific binding during phosphopeptide enrichment, and were assessed here by their effect on recovery of non-phosphorylated peptides identified in post-enrichment samples. Among the additives tested [*e.g.*, glycerol, glycolic acid, and lactic acid[27-28]], phthalic acid yielded the greatest reduction in non-specific binding with a phosphopeptide enrichment efficiency of approximately 67% (~33% of the dataset was not phosphorylated) and a 10% increase in phosphopeptide coverage over the second best additive, glycolic acid.

Following enrichment for three biological replicates and DDA acquisition, retention time alignment, normalization of intensity across otherwise identical replicates and log transformation were performed. Ninety percent of the 2,304 phosphopeptides had < 11% CV (Figure 3.5C) with 1,314 unique phosphosites localized among the 1,052 proteins (Table S5, highlighted in yellow). Among these 1,077 proteins were 243 identified from the kinome enrichment experiment (Figure 3.5A) containing 484 phosphosites. Approximately 86.6% of the phosphosites detected were pSer, 12.8% pThr and 0.6% pTyr (Figure 3.5B) with >80% of the phosphopeptides singly phosphorylated (Figure 3.5D), similar to the distribution reported previously for Chlamydomonas[15]. A breakdown of chemical characteristics of the peptides identified in the phosphopeptide-enrichment dataset can be found in Figure 3.6.

3.3.4 Kinome and Phosphoproteome Coverage Using MIBs and TiO_2 Enrichment

Our enrichment method identified 115 protein kinases, >50% (62/115) of which were not detected without kinome enrichment (Figure 3.7A; Table S3). Gene ontology (GO) classification of proteins only identified following kinome enrichment (Table S4) revealed significant enrichment for the terms protein phosphorylation, ATP-binding, and MAP kinase (Figure 3.7B) validating the effectiveness of a MIBs approach for kinome analysis in Chlamydomonas. Among the kinases identified with MIBs enrichment and not from the total proteome, 57 serine/threonine protein kinases were identified whose homologs in other species are associated with signaling cascades which influence cell growth, survival, and differentiation. Of the 115 kinases identified using MIBs, 36 were themselves phosphoproteins (Table S5, bolded) with a total of 71 phosphosites quantified from the TiO_2 enrichment experiment (Table 1). Nine of these phosphosites (Table 1, asterisk) could not be confidently identified in our prior global phosphoproteomics study[15]. Maintaining high reproducibility between replicates despite the MIBs enrichment not being exhaustive allows for capture during TiO_2 enrichment of MIBs flow through - with 30 of the 36 kinases detected in the phosphopeptide dataset also appearing as high confidence proteins in the MIBs dataset (<11% CV). The phosphoproteomics dataset is also helpful in providing additional coverage on phosphoproteins/substrates not revealed in the kinome-enriched dataset. Figure 3.5A highlights the overlap between proteins identified in the kinome and phosphoproteome datasets, of which 834 phosphoproteins inferred from 1,584 phosphopeptides were identified and quantified only from the phosphoproteome dataset. Protein kinases found from MIBs or phosphopeptide enrichment include Chlamydomonas homologs of mitogen-activated protein (MAP) kinases 4 and 5 (Cre01.g010000.t1.2, Cre12.g509000.t1.1, Cre12.g530000.t1.2, Cre13.g607300.t1.2) and MEKK protein kinase (Cre01.g016570.t1.1) in the

MIBs data set, along with MAP kinase related proteins Cre13.g563733.t2.1 (MAPK kinase 6) and Cre10.g461150.t1.2 (MAPK/ERK kinase kinase 1) from the phosphoproteome dataset.

This combination of localizing phosphosites on kinases as well as coverage on downstream targets has the potential to provide quantitative information into dynamic protein phosphorylation events occurring in Chlamydomonas. For example, Table 3.2 shows the quantitative coverage provided by the kinome and phosphoproteome enrichments on 13 proteins with KEGG ontology (KO) terms[29-30] mapping to the cell cycle. These proteins, three of which are Chlamydomonas cell-cycle regulatory genes with available Chlamydomonas mutants[31], include cyclin-dependent kinases (Cre10.g465900.t1.2, Cre08.g372550.t1.1), a Chlamydomonas homolog of GSK3B (Cre12.g511850.t1.2) and phosphosite coverage on minichromosome maintenance (MCM2/3/5) family proteins (Cre07.g316850.t1.2 [pSer S119], Cre06.g295700.t1.1[pSer 545]) in addition to phosphosite localization on pSer25 of E2F transcription factor (Cre01.g052300.t1.1). Without this tandem enrichment approach, only 5 of the 13 proteins mapping to the cell cycle were identified without the benefit of site specificity.

Kinases uniquely found in the kinome enrichment involved with cellular energy status include SNF1 kinase homolog 10 (Cre04.g211600.t1.1), 3'-phosphoinositide-dependent protein kinase 1 (Cre11.g467568.t1.1), and 5'-AMP-activated protein kinase beta-2 subunit protein (Cre10.g457500.t1.1). Previous work has shown energy dependent protein kinases, specifically SNF1 and phosphatidylinositol 3-kinase (PI3K), as important regulatory factors upon triggering of autophagy with SNF1 kinase, a key factor in glucose sensing in yeast, completely blocking autophagy induced by nitrogen starvation following gene deletion in Chlamydomonas[32-33]. Along with these, AMP-activated protein kinases (AMPKs) have been shown as important upstream positive regulators of autophagy in mammalian cells[34]. A relationship of positive regulation

between protein kinase expression levels and autophagy was evident in the *Arabidopsis thaliana* ATG1/13 kinase complex following nutrient limitation indicating ATG1/13 as both a regulator and a target of autophagy[35], with possible relevance to stress adaptation in Chlamydomonas upon similar stresses. Because autophagy is such a crucial cellular response to stress, obtaining quantitative coverage of energy dependent protein kinases that might control autophagy and their possible downstream targets may facilitate experiments to elucidate autophagy related signaling mechanisms. For example, through the induction of stress in Chlamydomonas and the use of differential proteomic studies of the kinome and phosphoproteome, future studies using this tandem enrichment have the potential to target specific pathways and investigate global kinome and phosphoproteome changes in a quantitative fashion. While this method is capable of extensive coverage into the kinome, this approach is only an initial screen for proteins of interest and would require subsequent studies to further validate kinase activity and conformational changes occurring upon various physiological conditions.

3.4 Conclusion/Summary

Herein, a dual enrichment strategy first targeting intact protein kinases via capture on MIBs with subsequent proteolytic digestion of unbound proteins and peptide-based phosphorylation enrichment from the same sample is presented. MIBs enrichment permits a >50% increase in coverage of the kinome compared with unenriched samples, and increases the potential to investigate protein kinases and their predicted substrates in the same experiment. With high quantitative reproducibility among replicates and increased coverage of the kinome, studies aimed at investigating changes in kinase expression levels under different conditions could reveal kinases and ATP-binding proteins involved in specific signaling pathways. Further, tandem probing of the phosphoproteome allows for simultaneous discovery of differential

phosphorylation of substrate proteins in the same experiment. Ultimately, this approach can link changes in the kinome with the phosphoproteome to help elucidate intracellular kinase signaling networks.

3.5 Tables

Table 3.1 Phosphosite coverage on MIBs-identified kinases. * previously undetected. Based on phosphopeptide enrichment on the MIBs flow through, 71 phosphosites were localized from 36 protein kinases identified in the kinome enrichment dataset and 9 sites were not previously detected.

Kinase Accession	Description	Phosphosites
Cre01.g031300.t1.1	calcium dependent protein kinase 1	T1245
Cre02.g076900.t1.1	serine/threonine protein kinase 2	S71
Cre02.g113600.t1.2	ataurora3	T137, S432*, S434*
Cre02.g120250.t1.1	STT7 homolog STN7	S533, S740
Cre02.g147900.t1.1	Pyruvate kinase family protein	S463, S584, T587*, S597
Cre03.g168150.t1.2	VH1-interacting kinase	S15
Cre03.g199000.t1.2	phototropin 2	S577
Cre05.g232750.t1.2	NIMA-related kinase 5	T300
Cre06.g262900.t1.2	phosphofructokinase 5	S77, S81
Cre06.g280950.t1.2	Pyruvate kinase family protein	S463, S466, S490, S494, S497, S676
Cre06.g292700.t1.2	Protein kinase superfamily protein	S167
Cre06.g302800.t1.2	with no lysine (K) kinase 3	S283
Cre07.g317300.t1.1	Protein kinase superfamily protein	S524
Cre07.g328900.t1.2	calcium-dependent protein kinase 17	S472*, S481
Cre07.g337300.t1.1	Protein kinase superfamily protein	S70, S76, S82, S274, S507*, T508, S509, S532, S712
Cre08.g382800.t1.2	calcium-dependent protein kinase 17	S645, S647
Cre08.g385850.t1.2	cyclin dependent kinase group C2	T206
Cre10.g428650.t1.2	geminivirus rep interacting kinase 2	T631
Cre10.g457500.t1.1	5\'-AMP-activated protein kinase beta-2 subunit protein	S25
Cre10.g457700.t1.2	calmodulin-domain protein kinase cdpk isoform 2	S324
Cre12.g485600.t1.2	Protein kinase superfamily protein	S222*, S526*
Cre12.g499500.t1.1	Protein kinase superfamily protein	S173, S177
Cre12.g508900.t1.2	MAP kinase 4	T202, Y204
Cre12.g511850.t1.2	shaggy-like kinase 13	Y323
Cre12.g527000.t1.2	calcium-dependent protein kinase 34	S612, S615
Cre12.g551250.t1.2	Protein kinase superfamily protein	S835
Cre13.g566450.t1.2	Protein kinase superfamily protein with octicosapeptide/Phox/Bem1p domain	S104*, S266, S274, T405
Cre13.g571700.t1.1	calmodulin-domain protein kinase cdpk isoform 2	T365*, S448, S474
Cre13.g575300.t1.1	Protein kinase family protein with ARM repeat domain	S800
Cre13.g584100.t1.1	PB1 domain-containing protein tyrosine kinase	S661
Cre13.g591400.t1.1	pantothenate kinase 2	S577, S1070
Cre13.g607300.t1.2	MAP kinase 5	S403
Cre16.g661100.t1.2	Protein kinase superfamily protein	T156, Y158
Cre16.g664850.t1.1	Protein kinase superfamily protein with octicosapeptide/Phox/Bem1p domain	S772
Cre16.g665364.t1.1	phosphoenolpyruvate carboxylase-related kinase 1	S92, T121
Cre17.g734250.t1.1	PB1 domain-containing protein tyrosine kinase	S848, S1003

Table 3.2 Identified proteins in the cell cycle signaling pathway in Chlamydomonas. * indicates Chlamydomonas cell-cycle regulatory genes with available Chlamydomonas mutants based on (Cross and Umen 2015). Bolded accessions indicate proteins unique to the kinome enrichment and italicized rows indicate proteins unique to phosphopeptide enrichment.

Protein	Protein Description	KEGG/ec	KO
Cre07.g341700.t1.1	**putative protein kinase 1**	2.7.12.2	K08866
Cre08.g372550.t1.1*	**cyclin-dependent kinase B1;2**	2.7.11.22	K07760
Cre10.g465900.t1.2*	**cell division control 2**	2.7.11.22, 2.7.11.23	K02206
Cre07.g316850.t1.2--S119	**Minichromosome maintenance (MCM2/3/5) family protein**	3.6.4.12	K02212
Cre12.g543450.t1.2--S2	**RING-box 1**		K03868
*Cre01.g052300.t1.1--S25**	*E2F transcription factor 1*		K06620
Cre06.g295700.t1.1--S545	*Minichromosome maintenance (MCM2/3/5) family protein*	3.6.4.12	K02541
Cre09.g387393.t1.1--S426	histone deacetylase 1	3.5.1.98	K06067
Cre12.g511850.t1.2--Y323	shaggy-like kinase 13	2.7.11.1	K03083
Cre06.g257500.t1.2	general regulatory factor 7		K06630
Cre12.g515850.t1.2	proliferating cellular nuclear antigen 1		K04802
Cre12.g559250.t1.2	general regulatory factor 7		K06630

3.6 Figures

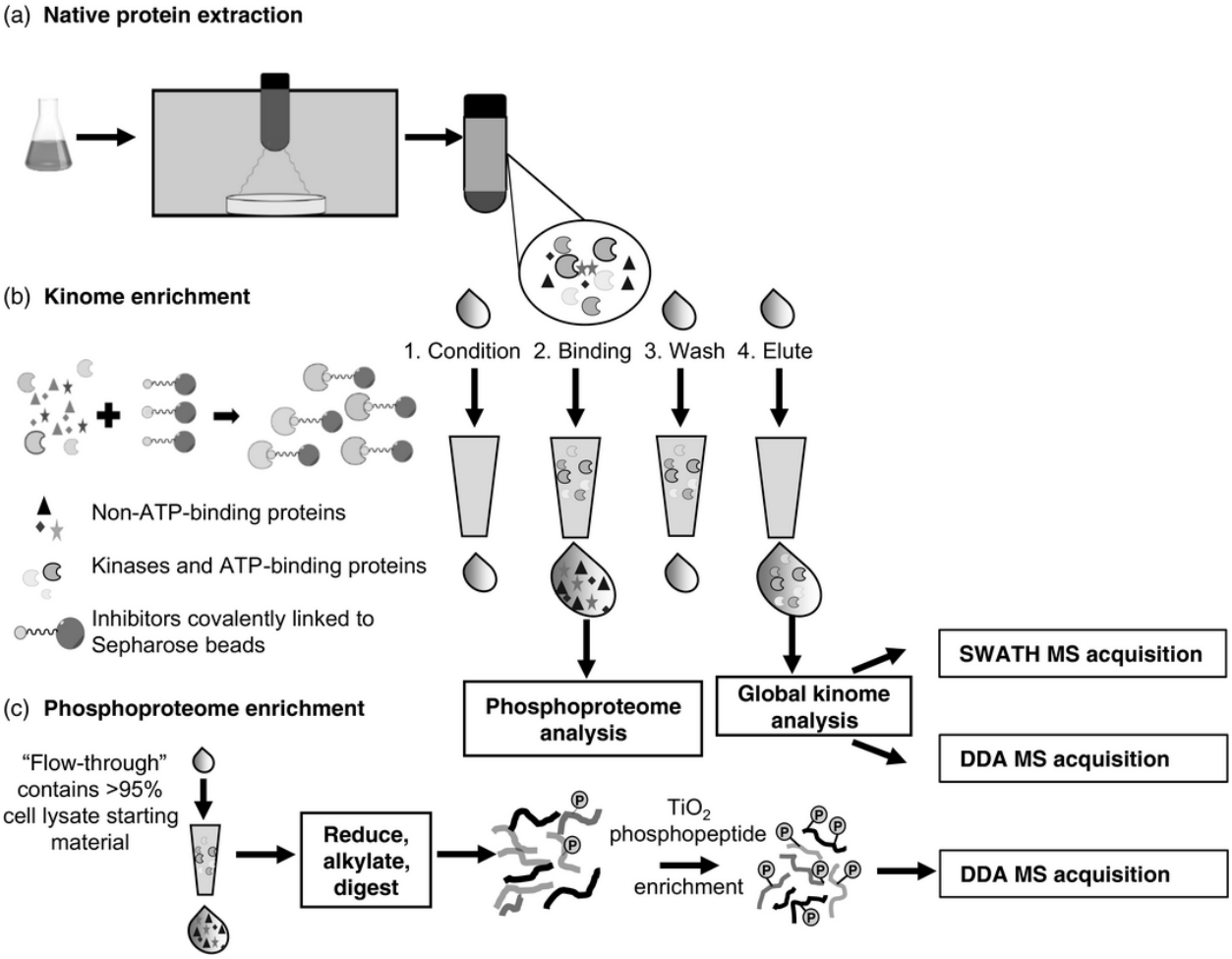

Figure 3.1 Figure reproduced from ref [36]. Overview of kinome and phosphoproteome workflow. (A) Schematic highlighting the focused ultrasonication performed during native protein extraction before MIBs kinome enrichment. (B) Following protein extraction, 5.5 mg of cell lysate is incubated with Sepharose beads covalently bound to a mixture of moderate and pan-kinase inhibitors. Proteins that are not bound to the MIBs beads (flow through) are saved for subsequent phosphopeptide enrichment. After washes, intact kinases and additional ATP-binding proteins are eluted from the columns and subjected to DDA and SWATH-MS analysis. (C) For the proteins collected in the flow through of the MIBs enrichment, phosphopeptide enrichment using TiO_2 is performed on 2 mg of each of the cell lysates.

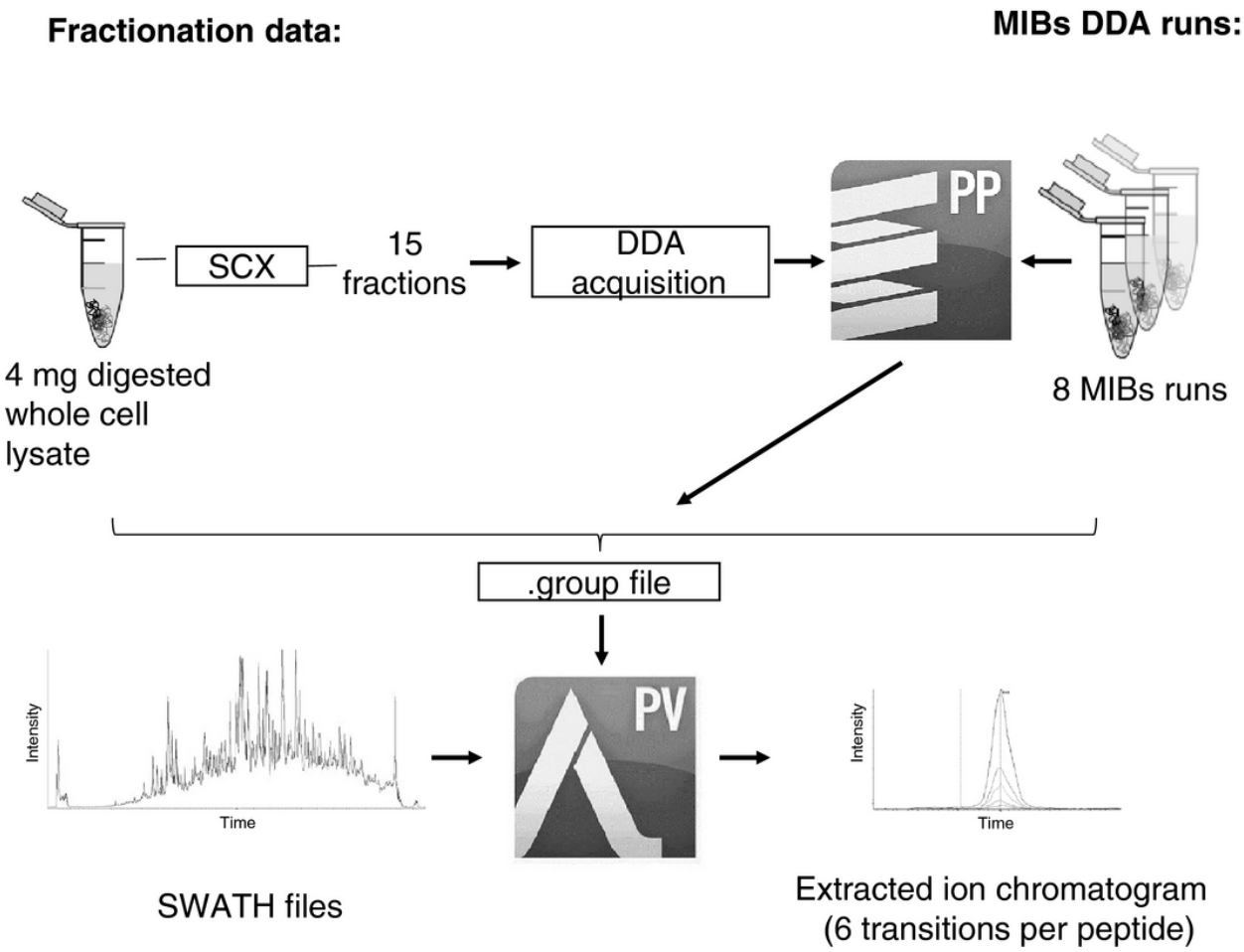

Figure 3.2 Figure reproduced from [36]. SWATH ion library generation. Schematic depicting ion library generation for SWATH data spectral matching and protein identification. An ion library was generated from a combination of 15 fractions derived from digested whole cell lysate separated by SCX and acquired via DDA. Additionally, 8 DDA runs of MIBs-enriched samples were included to assure exhaustive coverage of proteins in the ion library. After acquisition of all DDA runs, database searching was performed using ProteinPilot v5.0 and the result file (*.group file) was imported into PeakView v2.1 for SWATH data analysis.

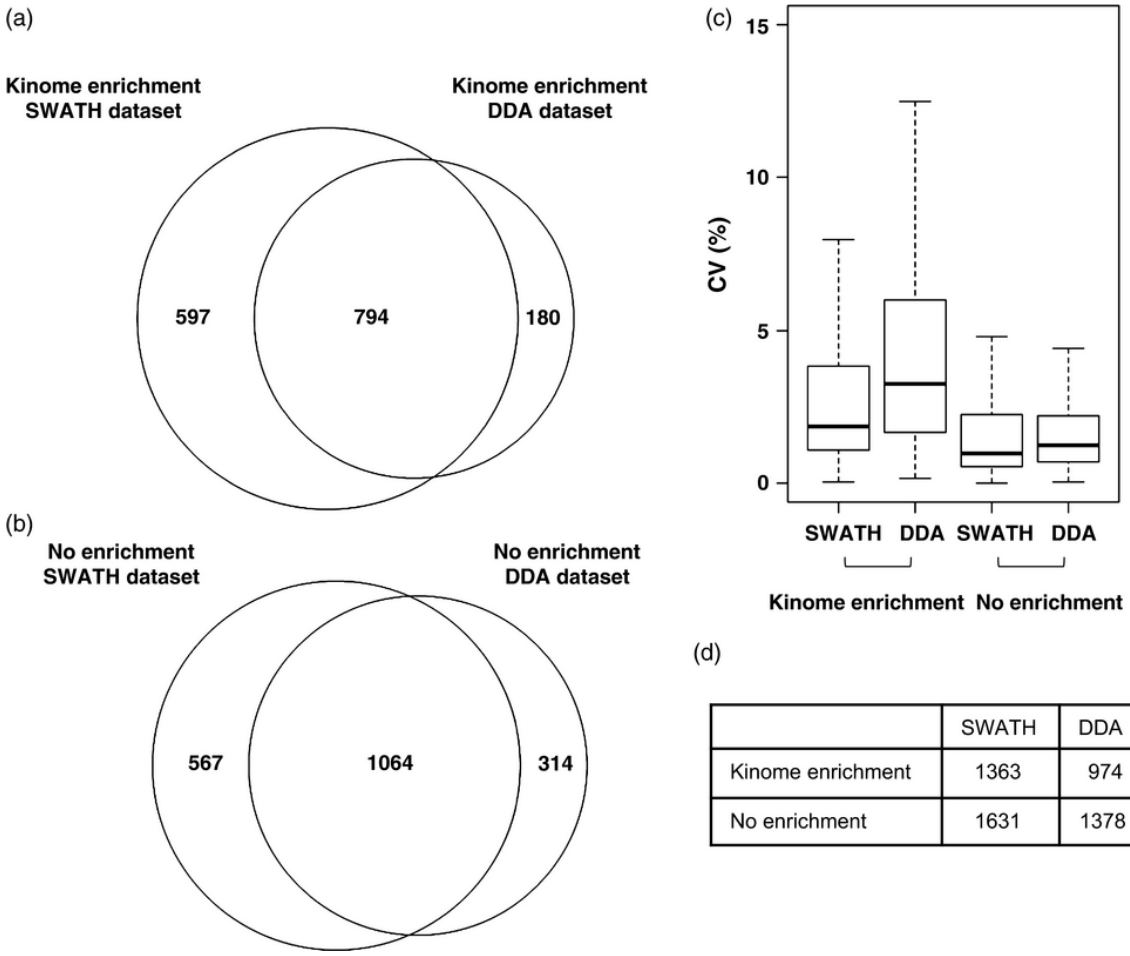

(d)

	SWATH	DDA	Total
Kinome enrichment	1363	974	1550
No enrichment	1631	1378	1945

Figure 3.3 Figure reproduced from [36]. Comparison of data independent (SWATH) and data dependent acquisition (DDA) methods for kinome identification. Venn diagram showing overlap of proteins identified between SWATH and DDA acquisition strategies for kinome enrichment (A) and no kinome enrichment (B) datasets. (C) Box-whisker plot showing distribution of CV values for 90% of proteins identified using DDA and SWATH acquisition strategies with and without enrichment. (D) Breakdown of coverage for both SWATH and DDA MS acquisition for kinome and no enrichment along with total unique proteins identified for each.

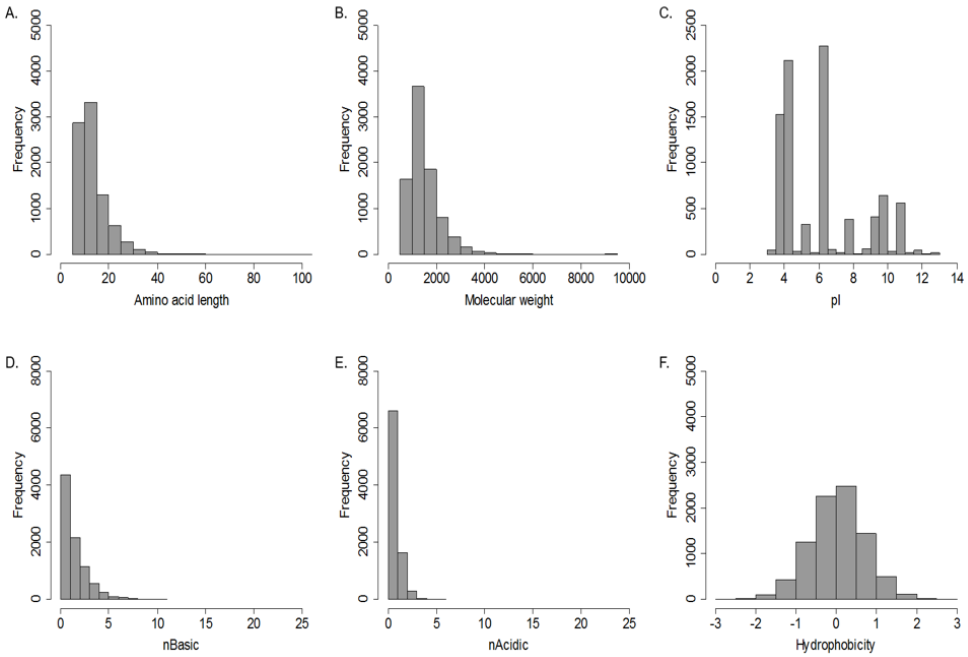

Figure 3.4 Figure reproduced from [36]. Chemical characteristics of the peptides identified in the MIBs dataset including (A) Amino acid length, (B) Molecular Weight, (C) pI, (D) amount of basic residues, (E) amount of acidic residues and (F) Hydrophobicity.

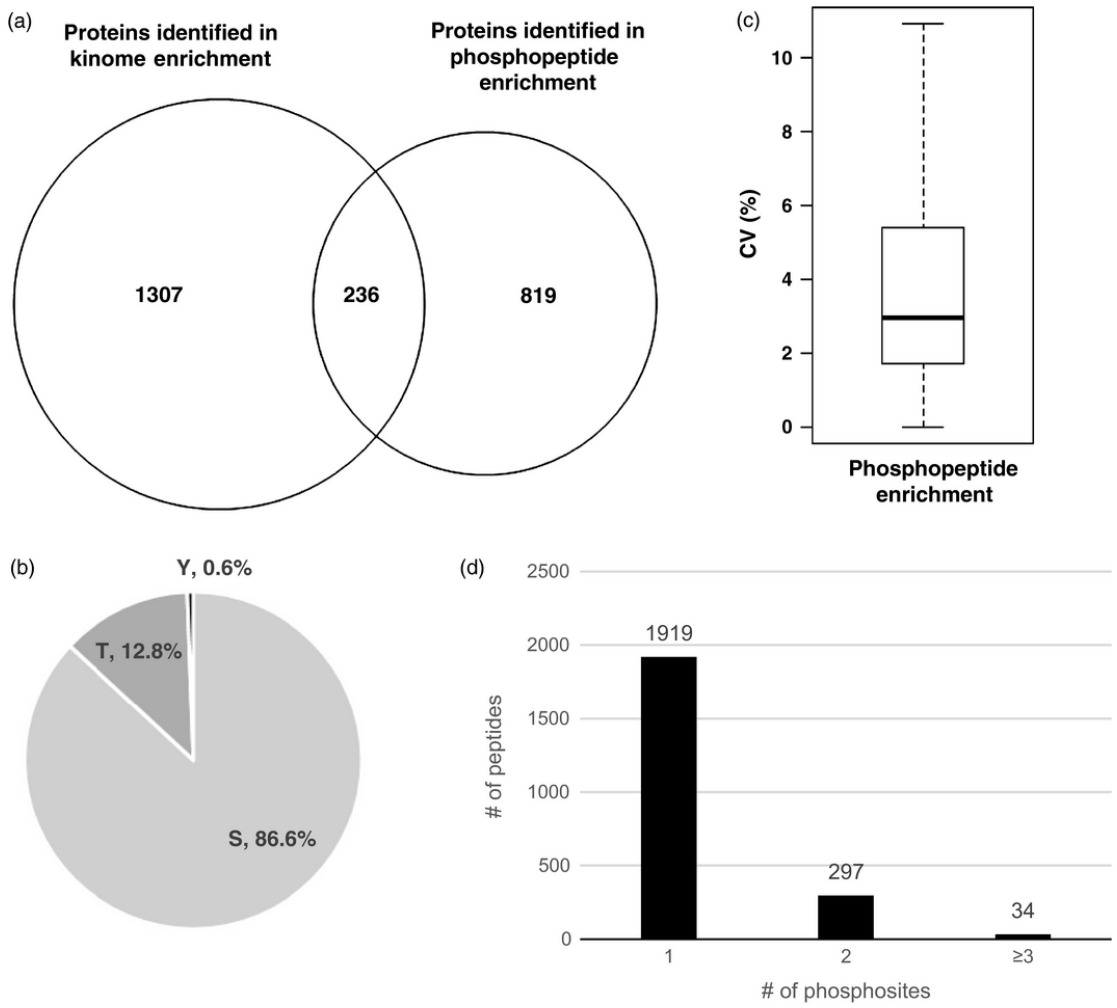

Figure 3.5 Figure reproduced from [36]. Comparison of proteins identified in MIBs and phosphopeptide enrichments. (A) Venn diagram comparing the overlap and unique proteins identified from kinome enrichment versus phosphopeptide enrichment. 243 proteins were found in both data sets, with 1307 identified solely in MIBs and 834 via phosphopeptide enrichment. (B) Of the phosphorylation sites confidently localized, 86.6% were pSer, 12.8% were pThr, and 0.6% were pTyr. (C) Box-whisker plot showing distribution of %CV of each protein for DDA from TiO_2 enrichment. (D) Distribution of phophosites among peptides showing that 80% (1394/1765) were singly phosphorylated.

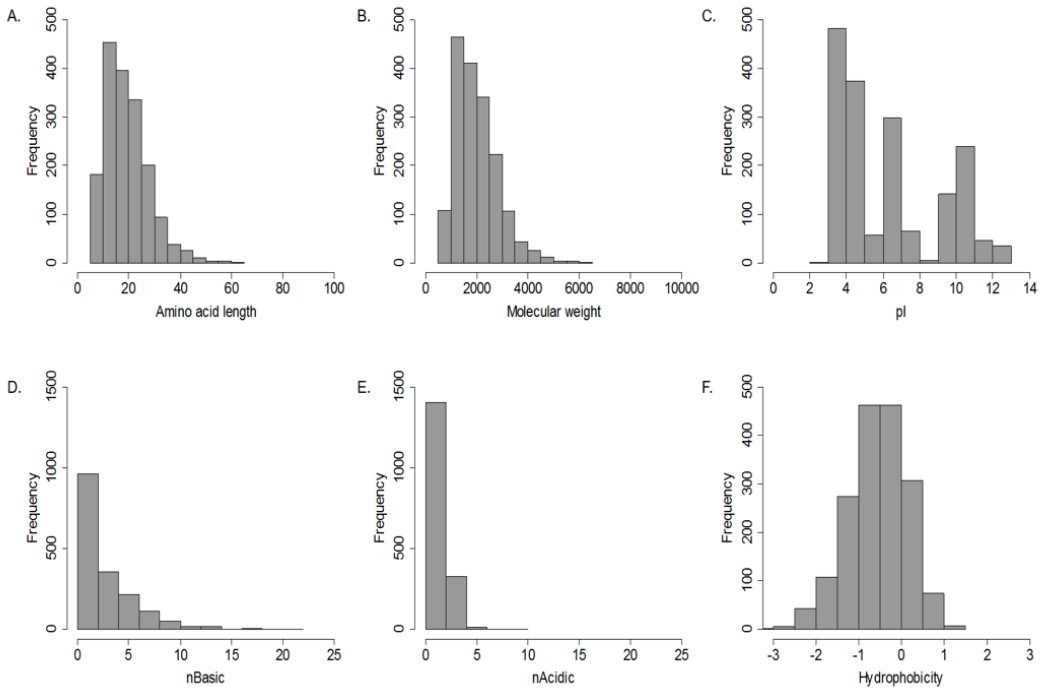

Figure 3.6 Figure reproduced from ref [36]. Chemical characteristics of the peptides identified in the phosphopeptide dataset including (A) Amino acid length, (B) Molecular Weight, (C) pI, (D) amount of basic residues, (E) amount of acidic residues and (F) Hydrophobicity.

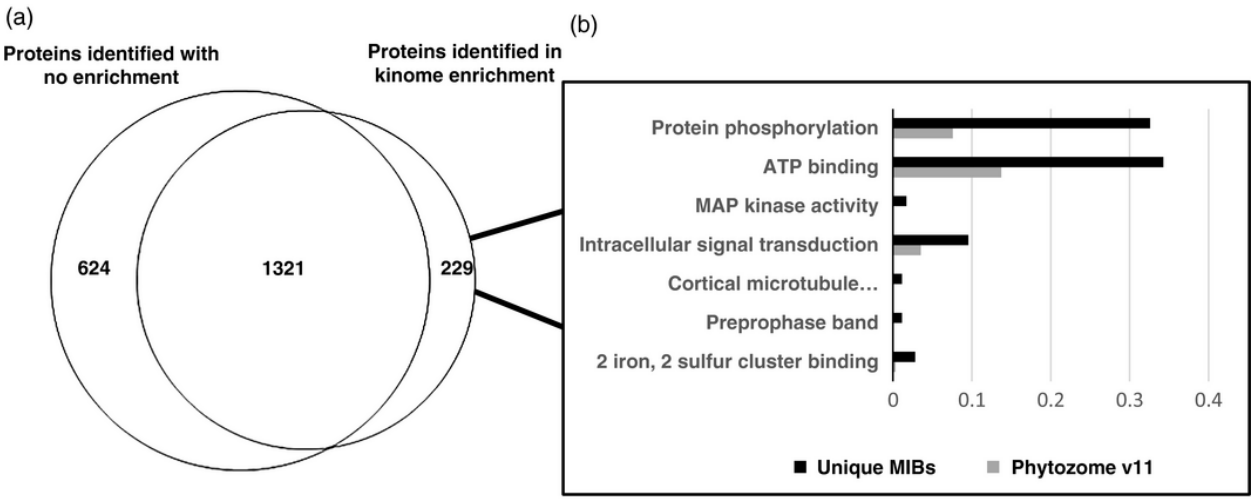

Protein group	# of proteins
Kinases	62
MAP kinases	5
Additional ATP-binding proteins	6

Figure 3.7 Figure reproduced from [36]. Comparison of proteins identified and enriched GO terms from MIBs. (A) Venn diagram comparing the overlap and unique proteins identified with and without enrichment in addition to a table highlighting protein groups of interest in the 229 proteins unique to MIBs enrichment. (B) Bar graph highlighting the GO terms enriched following enrichment of Gene Ontology terms for biological processes, molecular functions, and cellular processes using default parameters in Blast2GO (http://www.Blast2GO.com/b2ghome, BioBam, Valencia, Spain) using the Fisher method with multiple testing correction based on Benjamani Hochberg FDR cutoff of 0.05 with the Phytozome v11 *C. reinhardtii* predicted proteome as background.

REFERENCES

1. Daub, H.; Olsen, J. V.; Bairlein, M.; Gnad, F.; Oppermann, F. S.; Korner, R.; Greff, Z.; Keri, G.; Stemmann, O.; Mann, M., Kinase-selective enrichment enables quantitative phosphoproteomics of the kinome across the cell cycle. *Mol Cell* **2008,** *31* (3), 438-448.

2. Xiao, Y.; Wang, Y., Global discovery of protein kinases and other nucleotide-binding proteins by mass spectrometry. *Mass Spectrom Rev* **2014,** *35* (5), 601-619.

3. Duncan, J. S.; Whittle, M. C.; Nakamura, K.; Abell, A. N.; Midland, A. A.; Zawistowski, J. S.; Johnson, N. L.; Granger, D. A.; Jordan, N. V.; Darr, D. B.; Usary, J.; Kuan, P. F.; Smalley, D. M.; Major, B.; He, X.; Hoadley, K. A.; Zhou, B.; Sharpless, N. E.; Perou, C. M.; Kim, W. Y.; Gomez, S. M.; Chen, X.; Jin, J.; Frye, S. V.; Earp, H. S.; Graves, L. M.; Johnson, G. L., Dynamic reprogramming of the kinome in response to targeted MEK inhibition in triple-negative breast cancer. *Cell* **2012,** *149* (2), 307-321.

4. Bantscheff, M.; Eberhard, D.; Abraham, Y.; Bastuck, S.; Boesche, M.; Hobson, S.; Mathieson, T.; Perrin, J.; Raida, M.; Rau, C.; Reader, V.; Sweetman, G.; Bauer, A.; Bouwmeester, T.; Hopf, C.; Kruse, U.; Neubauer, G.; Ramsden, N.; Rick, J.; Kuster, B.; Drewes, G., Quantitative chemical proteomics reveals mechanisms of action of clinical ABL kinase inhibitors. *Nat Biotechnol* **2007,** *25* (9), 1035-1044.

5. Cooper, M. J.; Cox, N. J.; Zimmerman, E. I.; Dewar, B. J.; Duncan, J. S.; Whittle, M. C.; Nguyen, T. A.; Jones, L. S.; Ghose Roy, S.; Smalley, D. M.; Kuan, P. F.; Richards, K. L.; Christopherson, R. I.; Jin, J.; Frye, S. V.; Johnson, G. L.; Baldwin, A. S.; Graves, L. M., Application of multiplexed kinase inhibitor beads to study kinome adaptations in drug-resistant leukemia. *PLoS One* **2013,** *8* (6), e66755.

6. Graves, L. M.; Duncan, J. S.; Whittle, M. C.; Johnson, G. L., The dynamic nature of the kinome. *Biochem J* **2013,** *450* (1), 1-8.

7. Stuhlmiller, T. J.; Miller, S. M.; Zawistowski, J. S.; Nakamura, K.; Beltran, A. S.; Duncan, J. S.; Angus, S. P.; Collins, K. A.; Granger, D. A.; Reuther, R. A.; Graves, L. M.; Gomez, S. M.; Kuan, P. F.; Parker, J. S.; Chen, X.; Sciaky, N.; Carey, L. A.; Earp, H. S.; Jin, J.; Johnson, G. L., Inhibition of Lapatinib-Induced Kinome Reprogramming in ERBB2-Positive Breast Cancer by Targeting BET Family Bromodomains. *Cell Rep* **2015,** *11* (3), 390-404.

8. Johnson, G. L.; Stuhlmiller, T. J.; Angus, S. P.; Zawistowski, J. S.; Graves, L. M., Molecular pathways: adaptive kinome reprogramming in response to targeted inhibition of the BRAF-MEK-ERK pathway in cancer. *Clin Cancer Res* **2014,** *20* (10), 2516-2522.

9. Zones, J. M.; Blaby, I. K.; Merchant, S. S.; Umen, J. G., High-Resolution Profiling of a Synchronized Diurnal Transcriptome from Chlamydomonas reinhardtii Reveals Continuous Cell and Metabolic Differentiation. *Plant Cell* **2015,** *27* (10), 2743-2769.

10. Crespo, J. L.; Diaz-Troya, S.; Florencio, F. J., Inhibition of target of rapamycin signaling by rapamycin in the unicellular green alga Chlamydomonas reinhardtii. *Plant Physiol* **2005,** *139* (4), 1736-1749.

11. Merchant, S. S.; Prochnik, S. E.; Vallon, O.; Harris, E. H.; Karpowicz, S. J.; Witman, G. B.; Terry, A.; Salamov, A.; Fritz-Laylin, L. K.; Maréchal-Drouard, L., The Chlamydomonas genome reveals the evolution of key animal and plant functions. *Science* **2007,** *318* (5848), 245-250.

12. Wheeler, G. L.; Miranda-Saavedra, D.; Barton, G. J., Genome analysis of the unicellular green alga Chlamydomonas reinhardtii Indicates an ancient evolutionary origin for key pattern recognition and cell-signaling protein families. *Genetics* **2008,** *179* (1), 193-197.

13. Boesger, J.; Wagner, V.; Weisheit, W.; Mittag, M., Analysis of flagellar phosphoproteins from Chlamydomonas reinhardtii. *Eukaryot Cell* **2009,** *8* (7), 922-932.

14. Lee, C.; Rhee, J.-K.; Kim, D.; Choi, Y.-E., Proteomic study reveals photosynthesis as downstream of both MAP kinase and cAMP signaling pathways in Chlamydomonas reinhardtii. *Photosynthetica* **2015,** *53* (4), 625-629.

15. Wang, H.; Gau, B.; Slade, W. O.; Juergens, M.; Li, P.; Hicks, L. M., The global phosphoproteome of Chlamydomonas reinhardtii reveals complex organellar phosphorylation in the flagella and thylakoid membrane. *Molecular & Cellular Proteomics* **2014,** *13* (9), 2337-2353.

16. Harris, E. H.; Stern, D. B.; Witman, G. B., *The chlamydomonas sourcebook*. Cambridge Univ Press: **2009**; Vol. 1.

17. Slade, W. O.; Werth, E. G.; McConnell, E. W.; Alvarez, S.; Hicks, L. M., Quantifying reversible oxidation of protein thiols in photosynthetic organisms. *J Am Soc Mass Spectrom* **2015,** *26* (4), 631-640.

18. Vizcaíno, J. A.; Côté, R. G.; Csordas, A.; Dianes, J. A.; Fabregat, A.; Foster, J. M.; Griss, J.; Alpi, E.; Birim, M.; Contell, J., The PRoteomics IDEntifications (PRIDE) database and associated tools: status in 2013. *Nucleic acids research* **2013,** *41* (D1), D1063-D1069.

19. Käll, L.; Canterbury, J. D.; Weston, J.; Noble, W. S.; MacCoss, M. J., Semi-supervised learning for peptide identification from shotgun proteomics datasets. *Nature methods* **2007,** *4* (11), 923-925.

20. Savitski, M. M.; Lemeer, S.; Boesche, M.; Lang, M.; Mathieson, T.; Bantscheff, M.; Kuster, B., Confident phosphorylation site localization using the Mascot Delta Score. *Molecular & Cellular Proteomics* **2011,** *10* (2), M110. 003830.

21. Polpitiya, A. D.; Qian, W. J.; Jaitly, N.; Petyuk, V. A.; Adkins, J. N.; Camp, D. G., 2nd; Anderson, G. A.; Smith, R. D., DAnTE: a statistical tool for quantitative analysis of -omics data. *Bioinformatics* **2008,** *24* (13), 1556-1558.

22. Dhabaria, A.; Cifani, P.; Reed, C.; Steen, H.; Kentsis, A., A High-Efficiency Cellular Extraction System for Biological Proteomics. *J Proteome Res* **2015,** *14* (8), 3403-3408.

23. Bigelow, T. A.; Xu, J.; Stessman, D. J.; Yao, L.; Spalding, M. H.; Wang, T., Lysis of Chlamydomonas reinhardtii by high-intensity focused ultrasound as a function of exposure time. *Ultrason Sonochem* **2014,** *21* (3), 1258-1264.

24. Maldonado, A. M.; Echevarría-Zomeño, S.; Jean-Baptiste, S.; Hernández, M.; Jorrín-Novo, J. V., Evaluation of three different protocols of protein extraction for Arabidopsis thaliana leaf proteome analysis by two-dimensional electrophoresis. *Journal of Proteomics* **2008,** *71* (4), 461-472.

25. Oppermann, F. S.; Gnad, F.; Olsen, J. V.; Hornberger, R.; Greff, Z.; Kéri, G.; Mann, M.; Daub, H., Large-scale proteomics analysis of the human kinome. *Molecular & Cellular Proteomics* **2009,** *8* (7), 1751-1764.

26. Thingholm, T. E.; Jorgensen, T. J.; Jensen, O. N.; Larsen, M. R., Highly selective enrichment of phosphorylated peptides using titanium dioxide. *Nat Protoc* **2006,** *1* (4), 1929-1935.

27. Sugiyama, N.; Masuda, T.; Shinoda, K.; Nakamura, A.; Tomita, M.; Ishihama, Y., Phosphopeptide enrichment by aliphatic hydroxy acid-modified metal oxide chromatography for nano-LC-MS/MS in proteomics applications. *Molecular & Cellular Proteomics* **2007,** *6* (6), 1103-1109.

28. Jensen, S. S.; Larsen, M. R., Evaluation of the impact of some experimental procedures on different phosphopeptide enrichment techniques. *Rapid Communications in Mass Spectrometry* **2007,** *21* (22), 3635-3645.

29. Kanehisa, M.; Goto, S., KEGG: kyoto encyclopedia of genes and genomes. *Nucleic acids research* **2000,** *28* (1), 27-30.

30. Kanehisa, M.; Sato, Y.; Kawashima, M.; Furumichi, M.; Tanabe, M., KEGG as a reference resource for gene and protein annotation. *Nucleic acids research* **2015**, gkv1070.

31. Cross, F. R.; Umen, J. G., The Chlamydomonas cell cycle. *Plant J* **2015,** *82* (3), 370-392.

32. Perez-Perez, M. E.; Florencio, F. J.; Crespo, J. L., Inhibition of target of rapamycin signaling and stress activate autophagy in Chlamydomonas reinhardtii. *Plant Physiol* **2010,** *152* (4), 1874-1888.

33. Wang, Z.; Wilson, W. A.; Fujino, M. A.; Roach, P. J., Antagonistic controls of autophagy and glycogen accumulation by Snf1p, the yeast homolog of AMP-activated protein kinase, and the cyclin-dependent kinase Pho85p. *Molecular and cellular biology* **2001,** *21* (17), 5742-5752.

34. Pérez-Pérez, M. E.; Lemaire, S. D.; Crespo, J. L., Reactive oxygen species and autophagy in plants and algae. *Plant physiology* **2012,** *160* (1), 156-164.

35. Suttangkakul, A.; Li, F.; Chung, T.; Vierstra, R. D., The ATG1/ATG13 protein kinase complex is both a regulator and a target of autophagic recycling in Arabidopsis. *The Plant Cell* **2011,** *23* (10), 3761-3779.

36. Werth, E. G.; McConnell, E. W.; Gilbert, T. S. K.; Couso Lianez, I.; Perez, C. A.; Manley, C. K.; Graves, L. M.; Umen, J. G.; Hicks, L. M., Probing the global kinome and phosphoproteome in Chlamydomonas reinhardtii via sequential enrichment and quantitative proteomics. *The Plant Journal* **2017,** *89* (2), 416-426.

CHAPTER 4: Investigating the Effect of Target of Rapamycin Kinase Inhibition on the *Chlamydomonas reinhardtii* Phosphoproteome: From Known Homologs to New Targets.

*****Manuscript submitted for publication. Authors: Werth, E.G., McConnell, E.M., Couso, I., Perrine, Z., Crespo, J. L., Umen, J. G., Hicks, L. M. Investigating the effect of Target of Rapamycin kinase inhibition on the *Chlamydomonas reinhardtii* phosphoproteome: from known homologs to new targets. **2018**

4.1 Introduction

The Target of Rapamycin (TOR) protein kinase is a conserved eukaryotic growth regulator whose activity is modulated in response to stress, nutrients and energy supply[1-5]. In metazoans and fungi, TOR is found in two compositionally and functionally distinct multiprotein complexes (TORC1) and (TORC2) that control rates of biosynthetic growth and cytoskeletal dynamics respectively[2, 6]. In the green lineage (algae and land plants), only homologs of TORC1 proteins have been identified[3, 7-8]. TORC1 kinase activity is modulated by nutrients and stress, and serves to control protein biosynthesis and other metabolic processes in response to environmental conditions[6]. Selective chemical inhibitors of TOR kinase including rapamycin, AZD8055, and Torin1 have been instrumental in dissecting the TOR signaling pathway[9-12]. Rapamycin (Rap) inhibits TORC1 activity through an allosteric mechanism requiring formation of a FKBP12-Rap complex[13-15]. Recent studies support the notion that several functions of TOR kinase are not inhibited by rapamycin[11]. Instead, novel drugs like Torin1 and AZD8055 have been reported to more completely inhibit TOR kinase by acting as ATP-competitors[10-11]. Torin1 has slower off-binding kinetics than other mTOR inhibitors in mammalian cell lines, possibly due to

conformational change induction in the kinase that is energetically more difficult to recover from leading to a more pronounced and longer inhibition of the TORC1 pathway[16]. AZD8055 is an ATP-competitive inhibitor of mTOR and all PI3K class I isoforms noted to inhibit the mTORC1 and mTORC2 substrate phosphorylation[17]. These drugs were used to inhibit TOR activity in plants where rapamycin treatment is not highly effective[18-19].

The role of TOR in mammalian and fungal cell metabolism has been extensively investigated[20-21], while its role in photosynthetic eukaryotes is less well established[3, 22-23]. TOR has been shown to control growth, metabolism and life span in the model plant *Arabidopsis thaliana* (Arabidopsis)[24-27] where the TOR gene is essential[28]. The model green alga *Chlamydomonas reinhardtii* (Chlamydomonas) has key TORC1 complex proteins encoded by single-copy genes including TOR (Cre09.g400553.t1.1), regulatory associate protein target of rapamycin (RAPTOR) (Cre08.g371957.t1.1), and lethal with sec-13 protein 8 (LST8) (Cre17.g713900.t1.2) [7-8]. Treatment of Chlamydomonas cultures with rapamycin has been shown to slow but not completely arrest cell growth[29], activate autophagy [30], and induce lipid droplet formation[31-32]. Recent work reported a connection between TOR kinase and inositol polyphosphate signaling that governs carbon metabolism and lipid accumulation[33]. Chlamydomonas cells are sensitive to Torin1 and AZD8055 that are potent inhibitors of cell growth at saturating doses[33] and induce triacylglycerol accumulation[34]. However, the TOR pathway in Chlamydomonas has yet to be extensively characterized and, to date, only a limited number of candidate TOR kinase substrates have been identified.

We characterized the phosphoproteome of Chlamydomonas that produced a conservative estimate of 4,588 phosphoproteins / 15,862 unique phosphosites[35] through a qualitative strategy involving extensive fractionation and complementary enrichment strategies, and have now

developed label-free quantification (LFQ) to allow simultaneous quantification of 2,547 Chlamydomonas phosphosites[36]. Herein we characterized the effects of TOR inhibition on the Chlamydomonas phosphoproteome. Cultures treated with saturating doses of different TOR inhibitors (rapamycin, AZD8055 and Torin1) revealed hundreds of affected phosphosites with a significant overlap observed between those seen with different inhibitors. Phosphosites from an AZD-resistant mutant were compared with wild type after AZD treatment revealing very few potential off target effects. Hierarchical clustering was used to classify sites and motif analysis was used to assess consensus motifs in clusters.

4.2 Materials and Methods

4.2.1 Cell Culturing and Drug Treatment

Strain CC-1690 wild-type mt+ (Sager 21 gr) (Sager, 1955) was used for the wild-type Chlamydomonas analysis across all chemical inhibitors. For the control AZD-insensitive strain experiments, strain was obtained from the Umen laboratory (Donald Danforth Plant Science Center). All cultures were maintained on TAP (Tris acetate phosphate) agar plates and grown in 350-mL TAP liquid cultures at 25ºC as previously described[33]. Experiments were done using five replicate cultures grown to exponential phase (1-2x10^6 cells/mL) for each drug condition and control and quenched with 40% methanol prior to harvesting by centrifuging at 4000 *g* for 5 min and discarding supernatant. To limit batch effects, replicate "n" of each drug and control were harvested together (Figure 4.1) prior to downstream processing. Cell pellets were then flash frozen using liquid nitrogen and stored at -80ºC until use. For AZD8055-, Torin 1-, and rapamycin- treated (LC Laboratories) cultures, drug was added to a final concentration of 500 nM for rapamycin and Torin 1, and 700 nM for AZD8055 from 1mM stocks in DMSO for 15

min prior to harvesting. For control replicates, just drug vehicle (DMSO) without a chemical inhibitor was added to each replicate culture for 15 min prior to harvesting.

4.2.2 Protein Extraction

Cell pellets were resuspended in lysis buffer containing 100 mM Tris, pH 8.0 with 1x concentrations of cOmplete protease inhibitor and phosSTOP phosphatase inhibitor cocktails (Roche, Indianapolis, IN, USA). Cells were lysed via sonication using an E220 focused ultrasonicator (Covaris, Woburn, MA, USA) for 120 s at 200 cycles/burst, 100 W power and 13% duty cycle. Following ultrasonication, the supernatant was collected from cellular debris by centrifugation for 10 min at 15,000 *g* at 4ºC and proteins were precipitated using 5 volumes of cold 100 mM ammonium acetate in methanol. Following 3 hr incubation at -80ºC, protein was pelleted by centrifugation for 5 min at 2,000 *g* followed by two washes with fresh 100 mM ammonium acetate in methanol and a final wash with 70% ethanol. Cell pellets were resuspended in 8M urea and protein concentration was determined using the CB-X assay (G-Biosciences, St. Louis, MO, USA).

4.2.3 Protein Digestion and Reduction.

Samples were reduced using 10 mM dithiothreitol for 30 min at RT and subsequently alkylated with 40 mM iodoacetamide for 45 min in darkness at RT prior to overnight digestion. Samples were diluted 5-fold in 100 mM Tris following alkylation and digestion was performed at 25°C for 16 h with Trypsin Gold (Promega) at a protease:protein ratio of 1:50.

4.2.4 Solid-Phase Extraction.

After digestion, samples were acidified to pH<3.0 with trifluoroacetic acid (TFA). Pelleted, undigested protein was cleared from the supernatant by centrifugation for 5 min at 5,000 *g* prior to solid-phase extraction. Desalting was performed using C18 50 mg Sep-Pak cartridges

(Waters). Columns were prepared by washing with acetonitrile (MeCN) followed by 80% MeCN/20%H_2O/0.1% TFA and 0.1% TFA. Digested protein lysates were applied to the columns and reloaded twice before being washed with 0.1% TFA and eluted using 80% MeCN/20% H_2O/0.1% TFA.

4.2.5 Phosphopeptide Enrichment and Clean-Up.

Following protein digestion and solid-phase extraction, replicates were dried down using vacuum centrifugation and phosphopeptide enrichment was performed on 2-mg aliquots of each sample using 3 mg Titansphere Phos-TiO_2 kit spin columns (GL Sciences) as previously described[36]. After enrichment, samples were dried down and desalted again using ZipTips (Millipore) as per manufacturers protocol prior to LC-MS/MS acquisition.

4.2.6 LC-MS/MS Acquisition and Data Processing.

Following ZipTip clean-up, peptides were dried down and resuspended in 20 µL of 0.1% TFA, 5% MeCN before separation via a 90-min linear gradient from 95% H_2O/5% MeCN/0.1% formic acid (FA) to 65% H_2O/35% MeCN/0.1% FA via a NanoAcquity UPLC (Waters). Each sample was loaded onto a trap column (NanoAcquity UPLC 2G-W/M Trap 5 µm Symmetry C18, 180 µm × 20 mm) at a flow rate of 5 µL min^{-1} for 5 min. Peptides were separated using a C18 column (NanoAcquity UPLC 1.8 µm HSS T3, 75 µm × 250 mm) at a flow rate of 300 nL min^{-1}. A TripleTOF 5600 (AB Sciex) Q-TOF was operated in positive-ionization nanoelectrospray and high-sensitivity mode for data acquisition as previously described[37]. In addition to the Supporting Information tables for MS datasets, the mass spectrometry proteomics data have been deposited to the ProteomeXChange Consortium via PRIDE partner repository[38] identifier PXD007221. Acquired spectra (*.wiff) files were imported into Progenesis QI for proteomics (v2.0, Nonlinear Dynamics) as previously described[36] with peptide sequence

determination and protein inference done by Mascot (v.2.5.1; Matrix Science) using the *C. reinhardtii* Phytozome v.11 database (www.phytozome.net/; accessed May 2015) appended with the NCBI chloroplast and mitochondrial databases (19,603 entries) and sequences for common laboratory contaminants (http://thegpm.org/cRAP/; 116 entries). For database searching, trypsin protease specificity with up to two missed cleavages, peptide/fragment mass tolerances of 20 ppm/0.1 Da, a fixed modification of carbamidomethylation at cysteine, and variable modifications of acetylation at the protein N-terminus, oxidation at methionine, deamidation at asparagine or glutamine, phosphorylation at serine or threonine and phosphorylation at tyrosine were used. Peptide false discovery rates (FDR) were adjusted to ≤1% using the Mascot Percolator algorithm[39] and only peptides with a Mascot ion score over 13 were considered.

Custom scripts written in Python were implemented to parse results following data normalization and quantification in Progenesis QI for proteomics. Shared peptides between proteins were grouped together to satisfy the principle of parsimony and represented in Table S1 by the protein accession with the highest amount of unique peptides, otherwise the largest confidence score assigned by Progenesis QI for proteomics. Additionally, the script appended site localization of variable modifications using an implementation of the Mascot Delta Score[40] to the peptide measurements (*.csv) export from Progenesis QI for proteomics with confident site localization considered a Mascot Delta score >90%. Following scoring, only peptides with phosphorylation at serine, threonine, or tyrosine were considered for further processing and analysis.

4.2.7 Downstream Bioinformatics Analysis.

Missing value imputation was performed on logarithmized normalized abundances in Perseus v1.6.0.0[41-42] requiring at least three of the five replicates in all drug conditions and control to be

nonzero to continue through the workflow. For t-test analyses, replicates were grouped and the statistical tests were performed with fold change threshold of ±2 and $p \leq 0.05$ significance threshold. KEGG pathway annotation[43], Gene Ontology (GO)[44] term annotation, hierarchical clustering, and motif analysis were performed following statistical testing to glean biological insight on modulated sites found in the study. For hierarchical clustering, visualization was performed in Perseus v1.6.0.0. Following data normalization and missing value imputation, intensity values were z-score normalized and grouped using k-means clustering with default parameters. For motif analysis, sequence logo visualizations were performed using pLOGO with serine or threonine residues fixed at position 0. Positions with significant residue presence are depicted as amino acid letters sized above the red line[45].

4.2.8 Carotenoid Analysis.

Chlamydomonas cells were collected by centrifugation (4000 g for 5 min) and resuspended in 80% acetone. Samples were heat up for 5 min in a water bath at 90ºC and then centrifuge at 10000g 10min. The supernatant evaporated under N2, and then resuspended in 80%acetone. The separation and chromatographic analysis of pigments was performed in a HPLC using a Waters Spherisorb ODS2 column (4.6 · 250 mm, 5 lm particle size). The chromatographic method described by Baroli et al., 2003[46]. Pigments were eluted at a flow rate of 1.0 mL min^{-1} with a linear gradient from 100% solvent A (acetonitrile:methanol:0.1mM Tris-HCl pH 8.0 [84:2:14]) to 100% solvent B (methanol:ethyl acetate [68:32]) for 20 min, followed by 7 min of solvent B, then 1 min with a linear gradient from 100% solvent B to 100% solvent A, and finally 6 min with solvent A. The carotenoids were detected at 440 nm using a Waters 2996 photodiode-array detector. The different carotenoids were identified using standards from Sigma (USA) and DHI (Germany). This analysis was normalized by dry cell weight.

4.2.9 Dry Weight Determination

Dry weight was determined by filtering an exact volume of microalgae culture (30 ml) on pre-targeted glass-fiber filters (1μm pore size). The filter was washed with a solution of ammonium formate (0.5 M) to remove salts and dried at 100 ◦C for 24 h. The dried filters were weighed in an analytical balance and the dry weight calculated by difference.

4.2.10 SDS-PAGE and Western Blotting

Chlamydomonas cells from liquid cultures were collected by centrifugation (4000 g for 5 min), washed in 50 mM Tris-HCl (pH 7.5), 10 mM NaF, 10 mM NaN3, 10 mM p-nitrophenylphosphate, 10 mM sodium pyrophosphate, and 10 mM b-glycerophosphate), and resuspended in a minimal volume of the same solution supplemented with Protease Inhibitor Cocktail (Sigma). Cells were lysed by two cycles of slow freezing to –80 °C followed by thawing at room temperature. The soluble cell extract was separated from the insoluble fraction by centrifugation (15 000 g for 20 min) in a microcentrifuge at 4 °C. For immunoblot analyses, total protein extracts (20 μg) were subjected to 12% SDS–PAGE and then transferred to PVDF membranes (Millipore). Anti-P-RPS6(Ser242) and Anti-RPS6 primary antibodies were generated as described in Dobrenel et al., 2016[47] and produced by Proteogenix, (France). Phospho-p70 S6 kinase (Thr(P)-389) polyclonal antibody (Cell Signaling, 9205) was used as described in Xiong et al., 2012[48]. Primary antibodies were diluted 1:2000 and 1:1000 respectively. Secondary anti-rabbit (Sigma) antibodies were diluted 1:5000 and 1:10 000, respectively, in phosphate-buffered saline (PBS) containing 0.1% (v/v) Tween-20 (Applichem) and 5% (w/v) milk powder. The Luminata Crescendo Millipore immunoblotting detection system (Millipore) was used to detect the proteins. Proteins were quantified with the Coomassie dye binding method (BioRad).

4.3 Results and Discussion

4.3.1 Parameter Selection for TORC1-Specific Inhibition

Previous studies in Chlamydomonas have shown rapamycin drug saturation ranging from 500 nM-1μM[29]. For this study, 500 nM rapamycin was selected and saturating doses for Torin1 and AZD8055 in wild-type Chlamydomonas strain CC-1690 were determined using serial dilutions with previously published target concentrations[33]. Growth inhibition saturated at 500 nM for Torin1 and 700 nM for AZD8055 (Figure 4.2).

While reports have shown phosphorylation changes as early as 2 minutes after rapamycin treatment [49], a 15-minute time point was chosen based on the high number of changes seen in mammalian cell lines at this time point[49-51] and to ensure reproducibility in treatment and harvesting across 20 samples (control, AZD8055-, Torin1-, and rapamycin-treated with n=5) from the early logarithmic phase of growth. Growth for each replicate was staggered, and to limit batch-effects replicates were harvested in sets, each containing a control sample and the three different drug-tested samples (Figure 1) prior to downstream processing.

Prior rapamycin phosphoproteomic experiments in mammalian studies have shown that phosphopeptide ratios in general were not affected by normalization to protein levels at a 15 min time point[51]. To confirm this in *Chlamydomonas reinhardtii*, a whole-cell proteomics experiment (n=4) was performed to test the overlap between quantitative coverage on whole-cell and phospho-enriched results after 15 min of rapamycin inhibition. These results showed that protein abundance levels in general are not affected with only 18 of the 1,539 proteins quantified significantly changing (Supplemental Table S4) with no significant differences in protein abundances between control and treatment (Figure 4.3). While 4 of the 18 proteins changing at the protein level were identified in the phosphoproteomics study detailed below, they were not

detected as phospho-modulated following chemical inhibition and thus not proteins of interest in this study. Thus, we have confidence that the statistically significant phosphorylation sites detected are from changes in the phosphorylation status and not an artefact of protein expression or turnover.

4.3.2 Quantitative Coverage of the TOR-Inhibited Phosphoproteome

Label- free quantitative phosphoproteomics was used to compare normalized abundance values of control samples (n=5) versus samples treated with each of the chemical inhibitors (n=5) using an area under the curve (AUC) MS1 intensity-based quantitation method. For this approach, the change in chromatographic peak area between control and chemically-inhibited replicates for each phosphopeptide was the basis for determining relative phosphopeptide abundance. Tip-based TiO_2 phosphopeptide enrichment that previously showed high reproducibility between samples[36] was used for sample preparation. As part of the LFQ pipeline, quantitative data was filtered for only peptides containing a phosphorylation site on Ser, Thr, or Tyr after peak picking and peptide sequence determination. At least 3 of the 5 replicates for each condition were required to have nonzero abundances to remain in the final dataset presented in Table S1 and missing value imputation was performed on log-transformed normalized abundances[41-42]. Highly variable sites remaining in the dataset were then removed by filtering out those with a coefficient of variation of >25% in >2 experimental conditions. The resulting dataset contained 2,547 unique phosphosites from 1,432 different proteins (Table S1) in untreated control samples. To determine sites of interest following chemical inhibition with Torin1, AZD8055, or rapamycin, two sample Student's T-tests were performed between samples from each chemical inhibitor compared and control samples. From this, 258 phosphosites from 219 phosphopeptides showed at least a two-fold change and a p-value ≤ 0.05 (Figure 4.4A, Table

S2). High confidence phosphorylation site assignments (90% site-localization based on Mascot Delta scoring[40]) were achieved for 48% of the dataset (1,123 of the 2,363 phosphopeptides) listed in Table S1. AZD8055 treatment resulted in 97 phosphopeptides modulated in the wild-type strain (Figure 4.4A). A matched control experiment using an AZD-insensitive strain which grow similar to wild-type (Figure 4.5) showed only 13 low abundance phosphosites differentially changing (Table S3, Figure 4.4B). Of the 13, no overlap was found with the 258 modulated phosphosites in the main dataset.

Torin1 treatment caused the largest number of significant changes with 103 up- and 57 down-modulated phosphosites. AZD8055 treatment caused 75 up- and 19 down-modulated phosphosites, while rapamycin treatment caused 40 up- and 35 down-modulated phosphosites. Overlap analysis of the differential sites for each drug revealed 88% (57/66) of all the down-modulated sites were in the Torin1 subset, while 42% (24/57) of the Torin1 down-modulated sites were not detected with AZD or rapamycin. Up-regulated sites were also compared for each condition and to determine if the conditions had significant overlap between down- and up-modulated sites, a hypergeometric test was performed with p-values of 3.76×10^{-25} and 2.87×10^{-34}, respectively, showing significant overlap.

4.3.3 Cluster Analysis and Phosphosite Motif Identification

Kinase specificity can be dictated by amino acid residues immediately surrounding phosphorylation sites on substrates[52]. Mammalian TOR has been shown to mainly (but not exclusively) phosphorylate (S/T)P motifs and motifs with hydrophobic residues surrounding the phosphorylation site making it a relatively promiscuous kinase whose substrate choices may also be influenced by additional interactions outside the phosphosite region[53]. Hierarchical clustering of Chlamydomonas modulated phosphosites generated 2 distinct clusters (Figure 4.6A,B), and

motif analysis[45] was performed on decreasing (cluster 1) and increasing (cluster 2) clusters . Cluster 1 phosphosites, which contained 94% of sites that significantly decrease in phosphorylation upon TOR inhibition, had significant enrichment for a proline in the +1 position and arginine in the -3 position with respect to the phosphorylation site (position 0) that showed strong enrichment for serine over threonine (Figure 4.6C). Cluster 2 phosphosites also had significant enrichment for a proline in the +1 position and arginine in the -3 position in addition to enrichment for an aspartic acid at the +3 position. Thus, CrTOR may have a preference for phosphorylation of (S/T)P motifs on substrates, similar to mTOR[53] and other diverse proline-directed kinases including cyclin-dependent protein kinases (CDKs) and mitogen-activated protein kinases (MAPKs)[54]. Additionally, a phosphoproteomic study using mammalian cell line MCF7 identified the RXXS/TP motif identified in clusters 1 and 2 as a rapamycin-sensitive motif[49]. Other studies have also found RXRXXS/T and RXXS/T motifs[50-51] enriched among rapamycin-sensitive phosphosites that are recognized by mTOR-regulated kinases Akt, S6K1 and SGK1[55]. Cluster 2 additionally has an acidic motif also found in casein kinase- II substrates[56].

4.3.4 Phosphosites in TORC1 Complex Proteins

Numerous phosphosites in mammalian homologs of TORC1 complex proteins are regulated by the TOR pathway and/or are phosphorylated autocatalytically[57]. This includes sites on Raptor and mTOR homologs. Therefore, phosphosites found on CrTORC1 complex proteins could be affected by TOR inhibition. TORC1 complex proteins conserved in Chlamydomonas include TOR (Cre09.g400553.t1.1), Raptor (Cre08.g371957.t1.1), and LST8 (Cre17.g713900.t1.2)[8, 30, 33, 58]. While there is a known LST8 homolog in Chlamydomonas, it is not known to be phosphorylated[35]. Phosphosites on Raptor (Ser782/783:NL) (Not Localized:NL) and TOR

(Ser2598) were detected in this study, however no statistically significant modulation in their abundance was detected. BLASTP alignment of human Raptor (Uniprot Q8N122) with CrRaptor revealed high sequence overlap on the N-terminal region of the protein (residues 9-627 with 57% identity), however known TORC1-sensitive phosphosites in the human Raptor homolog (i.e. Ser719, Ser721, Ser722, Ser859, and Ser863[57, 59]) were not conserved in CrRaptor. Similarly, human mTOR (Uniprot P42345) phosphosites Ser2159/Thr2164 that are within the kinase domain promoting mTORC1-associated mTOR Ser2481 autophosphorylation[60] are not conserved in CrTOR. The limited sequence conservation among CrTORC1 phosphosites with mammalian TOR phosphosites precludes any predictions about functions of CrTORC1 protein phosphorylation. Other phosphosites on CrTORC1 complex proteins that were detected in previous work on the global phosphoproteome in Chlamydomonas[35] might be significant for regulation but they were not observed in our data. Future experiments with additional fractionation to increase the dynamic range of quantitative coverage could allow for deeper coverage and more comprehensive detection of phosphosites.

4.3.5 Sites Modulated by TORC1 Inhibition – Known and Putative Substrates.

In animal cells TORC1-inhibition blocks phosphorylation of multiple substrates including S6 kinases and eukaryotic translation initiation factors, leading to a reduction in translation initiation rates for a subset of mRNAs[61-63]. Phosphorylation of Ser371 and Thr389 in human p70S6K1 (Uniprot P23443-2) are reduced by treatment of cells with TOR inhibitors[64-65]. While we identified one potential site (site was not localized) (Thr771/Ser773/Thr777:NL) on a Chlamydomonas homolog of ribosomal protein S6 kinase (S6K; Cre13.g579200.t1.2), its phosphorylation state was not significantly altered by TOR inhibitors (Table 1). No coverage was obtained on predicted conserved sites Ser915 and Thr932, which align to human p70S6K1

Ser371 and Thr389, respectively, although these sites have been detected previously in Chlamydomonas[35]. Moreover, while commercial anti-phospho S6K antibodies have been shown to detect phospho-S6K in plants[48, 66] they have not detected a signal in Chlamydomonas in our hands (Figure 4.7A) and in another study [33], thus limiting our ability to independently validate Chlamydomonas TOR substrate phosphopeptides. On the other hand, Chlamydomonas ribosomal protein S6 (RPS6, Cre09.g400650.t1.2), a predicted target of S6K, showed a 2.1-fold decrease in phosphorylation on Thr127 following Torin1 treatment (Figure 4.8, Table 1). While this site is potentially TORC1-regulated, antibodies specific for this phosphosite needed for validation are not available. In Arabidopsis, a phosphosite on the C-terminal extremity peptide of RPS6, Ser240, had decreased phosphorylation following TOR inactivation[47]. While this exact site is not conserved in Chlamydomonas, the phosphoserine next to it, Ser241 in Arabidopsis (aligning to Ser242 in Chlamydomonas) has been detected in prior work[35]; however it was not detected in this study (Figure 4.7B). To determine if Ser242 in Chlamydomonas is TORC1-regulated, a western blot of proteins fractionated from wild-type cells under different drug treatments for 0, 5, 15, 30, and 60 min was performed with antibodies raised for phosphorylated and non-phosphorylated Ser242 (Figure 4.7C), the latter used as a control for monitoring protein level. Interestingly, this site does not seem to change drastically with Torin1, AZD8055, or rapamycin treatment contrary to results on the C-terminal phosphosite in Arabidopsis.

4.3.6 Sites Modulated by TORC1 Inhibition – Known TOR Pathway Association.

Of the 258 phosphosites detected as significantly modulated in this study, 10 are in homologs of proteins associated with the TOR signaling pathway (Figure 4.8, Table 1). In addition to four sites of decreasing phosphorylation, six proteins related to the TOR pathway had an increase in protein phosphorylation following chemical inhibition. While initially an unexpected

observation, similar increases were previously reported for some phosphosites in a phosphoproteomic study of TOR inhibition in mouse liver[50]. In our study, sites with increasing phosphorylation after TOR inhibition include elongation factor 2 (EEF2, Cre12.g516200.t1.2) whose animal homologs showed reduced activity upon phosphorylation. In human cells, phosphorylation of EEF2 Thr57 by elongation factor 2 kinase (EEF2K, Cre17.g721850.t1.2) inactivates EEF2 activity, an essential factor for protein synthesis [67]. This site is conserved in Chlamydomonas EEF2 (Thr57/Thr59:NL) where we detect a 4.75-fold increase in phosphorylation with AZD8055 treatment with a predicted effect of reduced translation initiation rates. From these data we predict that CrTOR signaling may inhibit EEF2 kinase activity, and that this inhibition is relieved in the presence of TOR inhibitors.

LA RNA-binding protein (LARP1, Cre10.g441200.t1.2) had two phosphosites that both underwent large decreases in phosphorylation upon treatment with the three chemical inhibitors. Ser817 was decreased $0.06_{AZD8055}$, 0.05_{Torin1}, and 0.13_{RAP} and Ser 737/738:NL was decreased $0.08_{AZD8055}$ and $0.01_{Torin\ 1}$ but no change in rapamycin (0.99_{RAP}) (Figure 4.8). In mammals, LARP1 phosphorylation also requires mTORC1[55, 68-69] with studies in human cell lines establishing LARP1 as a target of mTORC1 and S6K with non-phosphorylated LARP1 interacting with both 5' and 3' UTRs of RP mRNAs and inhibiting their translation[70]. Additional reports have shown LARP1 as a direct substrate of mTORC1 in mammalian cells with mTORC1 controlling Terminal Oligopyrimidine (TOP) mRNA translation via LARP1[70-71]. The dramatic modulation of LARP1 phosphorylation detected in our study indicates that LARP1 may have a parallel role in Chlamydomonas. The human LARP1 phosphosites are not conserved with those we found in Chlamydomonas. However, based on the NCBI conserved domain searching[72], the DM15 domain required for the interaction of LARP1 with mTORC1 in human cell lines is

conserved in Chlamydomonas LARP1, and the phospho-Ser817 detected in our study is adjacent to the DM15 domain (877-915) in Chlamydomonas, a region in mammalian LARP1shown to be required for interaction with mTORC1[70].

4.3.7 Additional Proteins with Phosphosites Altered by TORC1 Inhibition

The majority of differential phosphosites we identified were not previously linked to TOR signaling, including in Chlamydomonas. These include sites on a translation-related protein (Cre17.g696250.t1.1) and RNA-binding proteins (Cre10.g441200.t1.2, Cre10.g466450.t1.1, Cre16.g659150.t1.1, Cre16.g662702.t1.1 Cre17.g729150.t1.2). One of the most down-modulated proteins annotated as CTC-interacting domain 4 (CID4, Cre01.g063997.t1.1), has been shown to have an important function in regulation of translation and mRNA stability in eukaryotes[73-74]. CID4 had 2 sites, Ser441 ($FC=0.2_{AZD8055}$, $FC=0.14_{TORIN1}$) and Ser439/Ser441/Ser446:NL ($FC=0.03_{AZD8055}$, $FC=0.05_{TORIN1}$) with a large decrease in phosphorylation upon inhibitor treatment. While little is known about the relationship between this protein and TORC1 signaling, the CTC domain, more recently referred to as the MLLE domain[75], is also found in evolutionarily conserved Poly (A)-binding proteins (PABPs). The large decrease in CID4 phosphorylation seen upon inhibition of the CrTORC1 pathway in our study implies a potential role for TORC1 mediated control of translation through CID4.

Another differential phosphosite of interest following TORC1 inhibition that was not previously linked to TOR regulation is a site on lycopene beta/epsilon cyclase protein (Cre04.g221550.t1.2--Thr800/Ser802:NL). This phosphosite is significantly increased upon Torin1 treatment (FC=4.02) and the total protein level remained constant upon rapamycin treatment (Supplementary Table S4, FC=0.88). Lycopene beta/epsilon cyclases are required for carotenoid biosynthesis, carrying out cyclation of lycopene to yield α- and β- carotenes[76-78]

which have been shown to be high-value compounds participating in light harvesting and in the protection of the photosynthetic apparatus against photo-oxidation damage[79]. To further investigate the effect of TORC1 inhibition on carotenoid biosynthesis based on this phosphoproteomic finding, carotenoid levels in AZD-, Torin1- and rapamycin-treated cells were assessed after eight hours of treatment with three biological and two technical replicates (Figure 4.9, Table 2). After eight hours of treatment, there was a significant increase in various carotenoids measured in TOR-inhibited samples including β-carotene, which is directly downstream of cyclase activity (Figure 4.9, Table 2). While the effects on carotenoid biosynthesis and secondary metabolism following TORC1 inhibition required eight hours to become detectable, this is the first evidence that carotenoid production is modulated by TOR signaling. Additionally, altered cyclase protein levels are not likely responsible for this finding since previous studies showed no change in lycopene beta/epsilon cyclase protein level after up to 24 hours of nitrogen stress[80-81], a condition that is metabolically similar to TOR inhibition[30, 82].

Numerous phosphosites from proteins without Phytozome database descriptions were also found to be down-regulated upon CrTORC1 inhibition, including some sites with large decreases (>five-fold). For all unannotated proteins, we searched for pfam, Panther, KOG, KEGG, KO, and GO pathway terms and domain conservation using Phytozome and NCBI annotations (Table S4). Numerous proteins had conserved domains including structural maintenance of chromosomes (Accession: cl25732), autophagy protein (Accession: cl27196), transmembrane proteins (Accession: cl24526), and small acidic protein (Accession: pfam15477). While the large changes upon chemical inhibition are potentially interesting, especially the five proteins containing sites with at least a five-fold decrease in phosphorylation (Cre03.g152150.t1.2, Cre06.g263250.t1.1, Cre11.g469150.t1.2, Cre05.g236650.t1.1, Cre13.g582800.t1.2), future targeted work would be

required to infer biological significance to this observation. To aid in this, the fifty-eight modulated sites without Phytozome database annotation were also homology searched for best BLAST hit IDs in Volvox, Gonium, and Arabidopsis to find homologs among green lineage (Table S5) and Table S2 displays all of the experimentally derived sites modulated by AZD8055, Torin1, and/or rapamycin and will serve as a guide in follow-up studies.

4.4 Conclusion/Summary

In summary, we obtained a candidate list of phosphosites modulated following TORC1 inhibition. We achieved extensive coverage of the TOR-modulated phosphoproteome in Chlamydomonas using a quantitative label-free approach. Our approach was validated by the overlap of phosphosites altered using different TOR inhibitors and by our identification of Chlamydomonas homologs of TOR signaling-related proteins such as RPS6 and LARP1 that had decreased phosphorylation upon TORC1 inhibition. Follow-up experiments guided by our phosphoproteomic findings in lycopene beta/epsilon cyclase showed that carotenoid levels are affected by TORC1 inhibition, the first evidence that carotenoid production is under TOR control. Conserved TOR substrate motifs were also identified such as RXXS/TP and RXXS/TP. Our study provides a new resource for investigating the phosphorylation networks governed by the TOR kinase pathway in Chlamydomonas.

4.5 Tables

Table 4.1 TOR targets identified with fold change values for drug condition versus control. Fold change values shaded red indicate a statistically significant increase in phosphopeptide abundance for specified drug treatment versus control. Fold change values shaded blue indicate a statistically significant decrease in phosphopeptide abudance for specified drug treatment versus control. Level of p-value statistical significance is denoted by p-value ≤ 0.05 (*) and ≤ 0.01 (**)

			Fold-change		
Accession	**Common Name**	**Sites**	**AZD8055**	**Torin1**	**Rapamycin**
CrTORC1 proteins					
Cre09.g400553.t1.1	TOR	S2598	0.99	0.90	1.12
Cre08.g371957.t1.1	RAPTOR	S782/S783:NL	1.56	1.94	1.54
homologs of known substrates					
Cre13.g579200.t1.2	RPS6KB	T771/S773/T777:NL	1.17	1.35	1.05
Cre09.g400650.t1.2	RPS6	T127	0.90	0.48**	0.61*
homologs of TOR pathway-associated proteins					
Cre10.g441200.t1.2	LARP1	T668/S670:NL	1.50	1.91*	1.96*
		S737/738:NL	0.08**	0.01**	0.99
		T809/S810:NL	0.41	0.46	0.81
		S817	0.06**	0.05**	0.13**
Cre17.g721850.t1.2	EEF2K	S306	0.75	0.42**	0.58
		S589/S591:NL	1.13	1.24	1.20
		S853/S857	2.00*	2.73**	1.69
Cre12.g516200.t1.2	EEF2	T57/T59:NL	4.75*	1.88	2.76
Cre12.g511850.t1.2	GSK3B	S322	1.27	1.15	1.25*
Cre09.g391245.t1.1	ATG1	T802/S803:NL	1.80	1.65	1.53
Cre06.g251050.t1.1	PRKAA	S699/S702:NL	0.64	0.29	0.97
Cre10.g457500.t1.1	PRKAB	S25/S29:NL	1.67*	1.75	2.27**
Cre02.g100300.t1.1	PI-3K/PI-4-like	T149/S150:NL	1.11	0.82	0.92
Cre05.g245550.t1.1	PI3KA	S794	1.04	0.91	1.51
Cre06.g304650.t1.1	PI3KB2	S403	1.25	1.39	0.88
		T478/S479/S482:NL	0.94	1.19	1.06
Cre03.g192000.t1.2	SEH1	S337	4.22	2.64	1.43
Cre02.g076900.t1.1	PRKG1	S71	2.20*	1.54	1.59**
		S71/S78:NL	1.44	1.76*	1.41
		S126, S128	1.84	1.23	0.82
		T857/T859:NL	1.12	0.97	0.98
		T857/T859:NL	0.89	0.97	0.92
		T857/T859/T863:NL	1.45	1.17	1.22*
Cre10.g461050.t1.2	ATP synthase A	S378	1.25	0.79	0.94
Cre02.g076350.t1.2	ATP6B, ATPase	S7/S8:NL	2.24	1.12	2.09**
Cre11.g468550.t1.2	ATP synthase G2	S7	2.52*	1.62*	2.33
		S77	1.60	1.24	1.33

*p-value ≤ 0.05 **p-value ≤ 0.01 Up- Down-

Table 4.2 Carotenoid content in WT Chlamydomonas after 8 hours of treatment with Rapamycin, Torin1, and AZD8055 compared to control.

Carotenoids Content (mg g^{-1} DW)

	Control	500nM Rap	500nM Torin	700nM Azd
Neoxanthin	0.64±0.01	1.12±0.01*	1.25±0.04*	1.65±0.00*
Violaxanthin	0.50±0.00	0.57±0.00	0.93±0.07*	1.02±0.00*
Anteraxanthin	0.04±0.00	0.12±0.00*	0.16±0.01*	0.11±0.00*
Lutein	1.60±0.03	2.56±0.02*	3.42±0.14*	3.29±0.00*
B-carotene	1.82±0.03	1.80±0.03	2.09±0.02*	3.02±0.02*

4.6 Figures

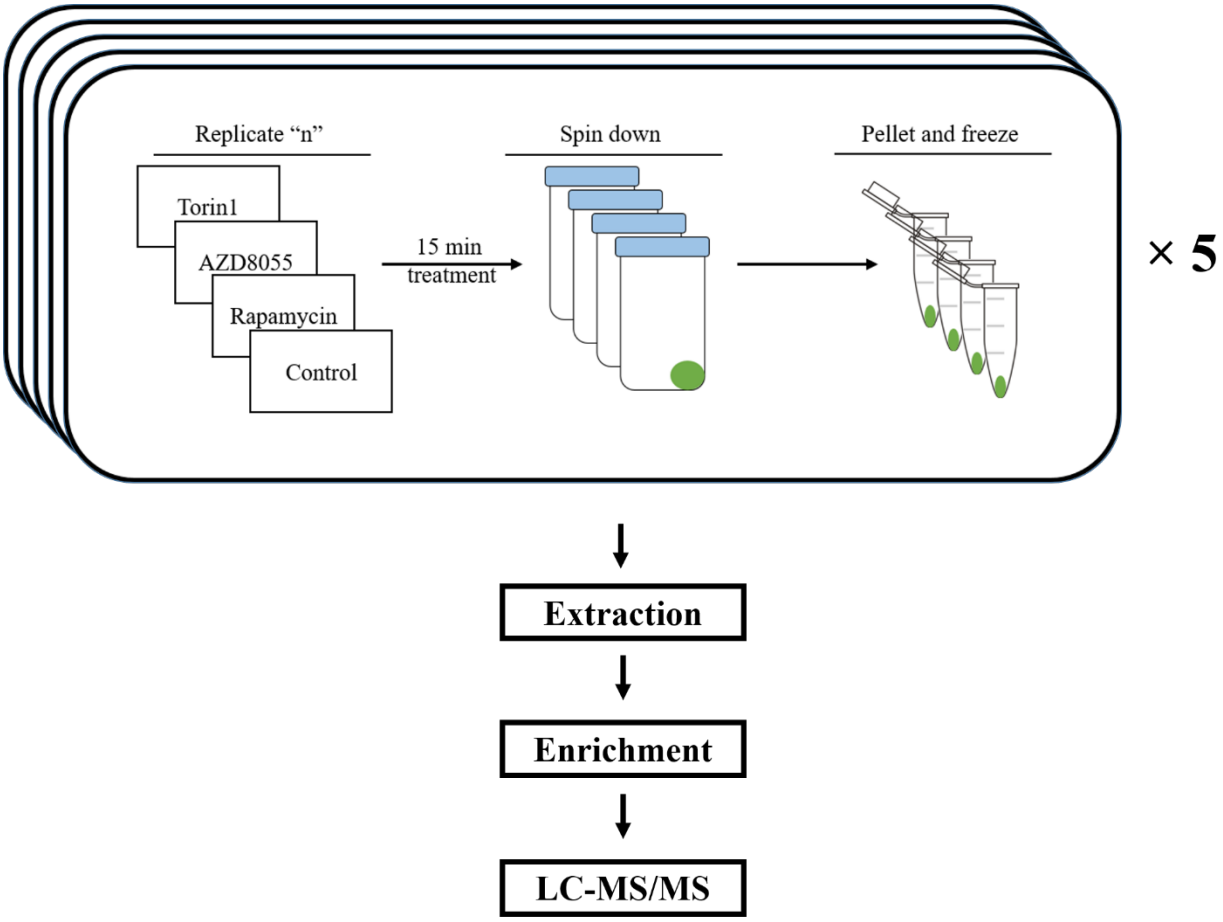

Figure 4.1 Figure reproduced from ref [83]. Drug treatment and cell harvesting workflow in Chlamydomonas cells. Replicate "n" (1-5) of each drug condition and control were harvested together prior to downstream processing. To minimize inter-condition batch effects, "n" replicate of each condition was harvested together and frozen until protein extraction.

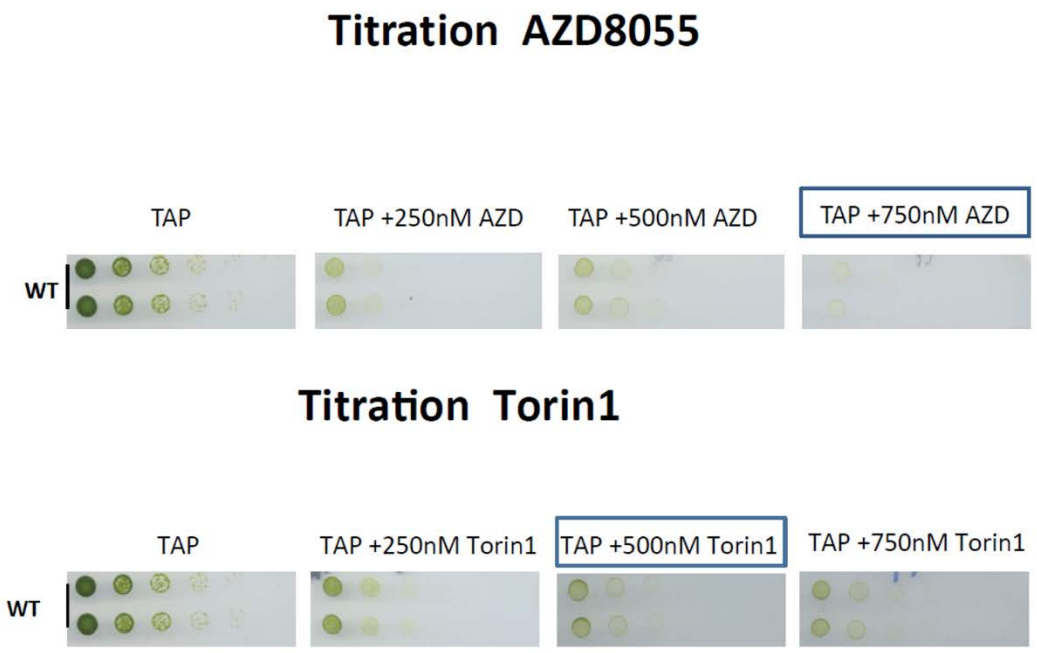

Figure 4.2 Figure reproduced from ref [83]. Titration experiment for AZD8055 and Torin1 to determine drug concentrations required for saturation

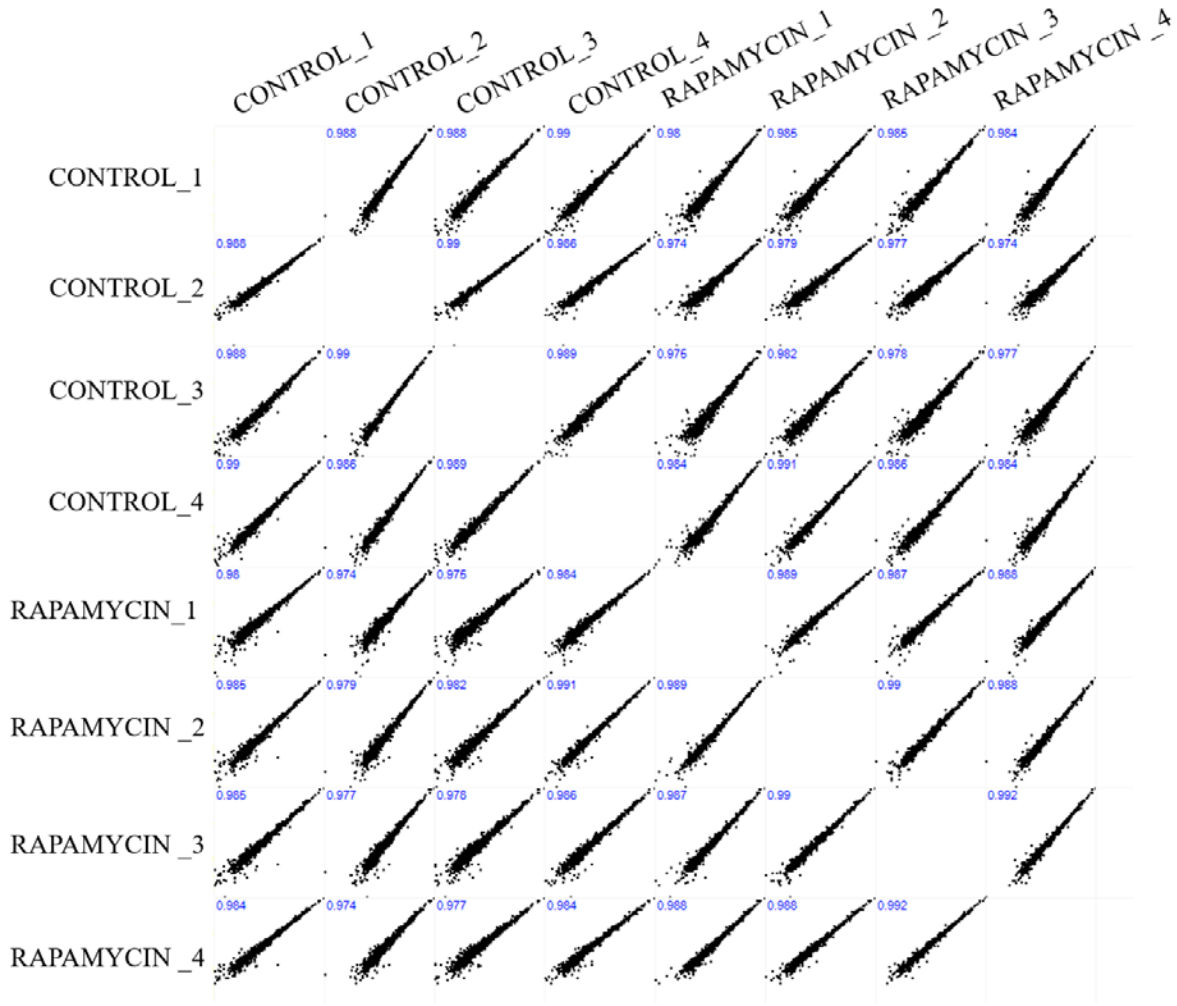

Figure 4.3 Figure reproduced from ref [83]. Pearson correlation coefficient between replicates of control and rapamycin-treated cells following protein-level analysis. Logarithmized protein abundances across 4 replicates for control and 15 min. rapamycin-treated cells showing high correlation regardless of treatment with no significant differences in protein abundances between control and treatment replicates.

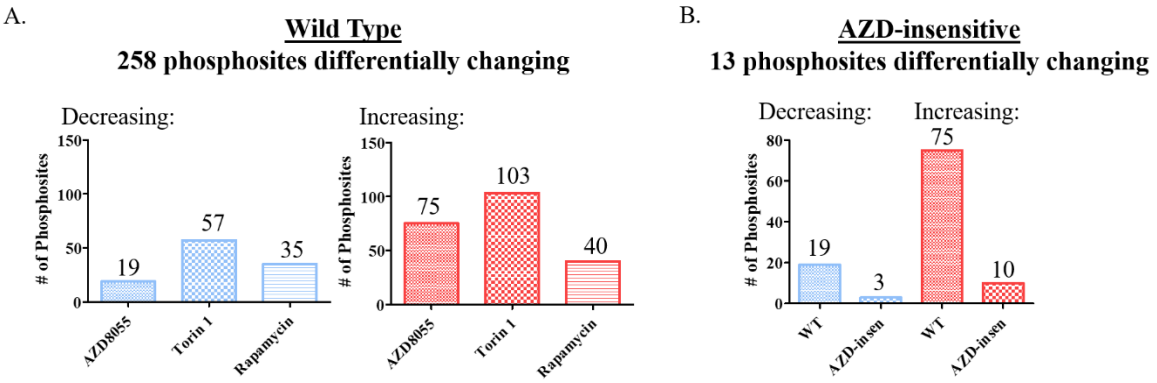

Figure 4.4 Figure reproduced from ref [83]. Sites modulated by chemical inhibition. Results of differential analysis between each chemical inhibitor drug treatment compared to control for both wild-type (A) and AZD-insensitive (B) Chlamydomonas strains. For comparison of overlap between the drug conditions in the WT dataset, a Pearson's correlation was performed comparing all condition types. From this, the highest correlation among conditions was between AZD8055 and Torin1 at 0.986 and the lowest 3 were all drug inhibitor vs. controls.

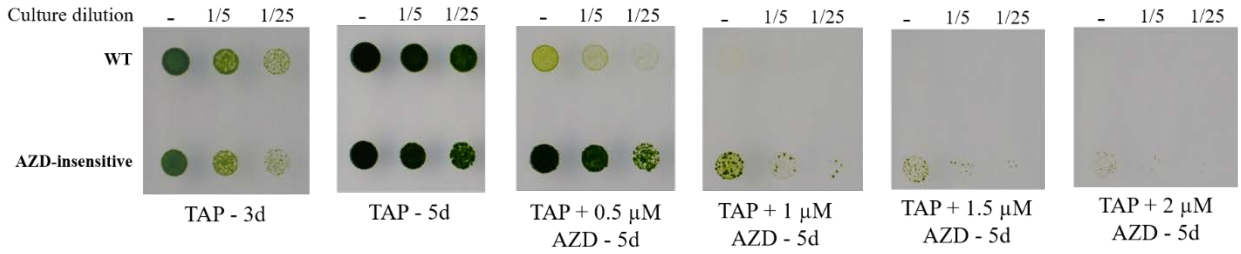

Figure 4.5 Figure reproduced from ref [83]. Spot test for comparison of growth between WT and AZD-insensitive Chlamydomonas cultures after 3 and 5 days of growth. WT and AZD-insensitive strains were grown on solid TAP media and cultures were diluted 1/5 and 1/25. Additionally, after 5 days of growth, spot tests for 0.5 uM- 2 uM AZD8055 treatment between WT and AZD-insensitive Chlamydomonas cultures were compared showing continued growth of the AZD-insensitive strain following AZD8055 treatment.

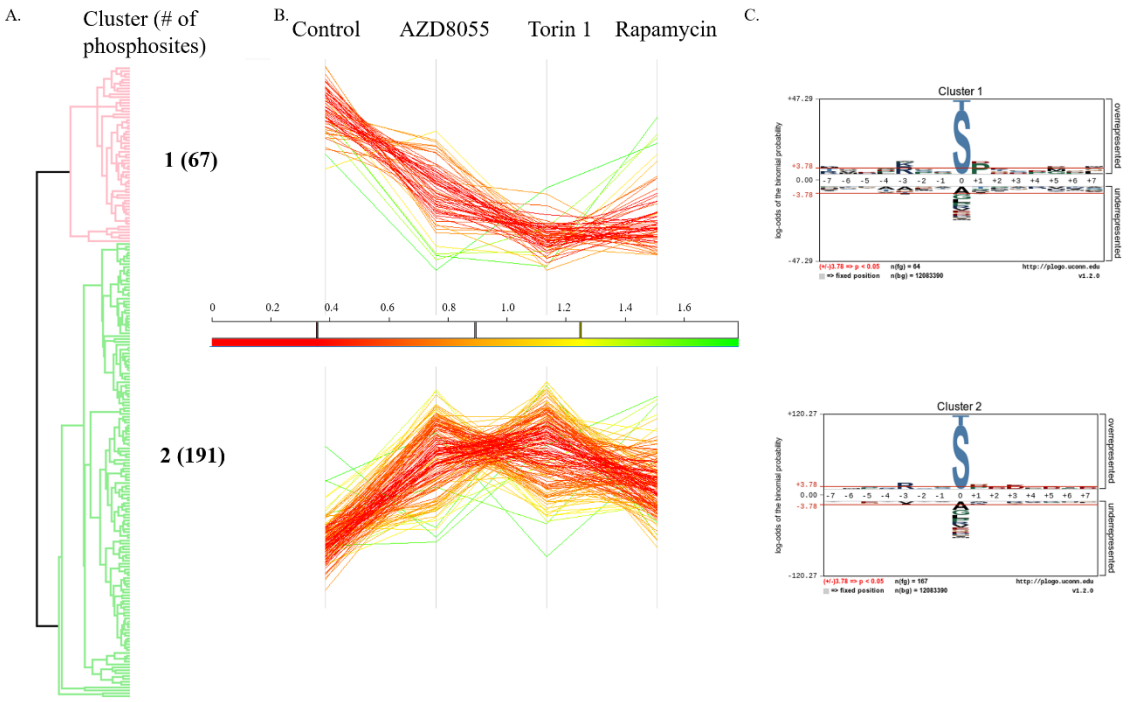

Figure 4.6 Figure reproduced from ref [83]. Hierarchical clustering of differentially changing sites into 2 clusters (A). Visualization was performed in Perseus v1.6.0.0. Following data normalization and missing value imputation, intensity values were z-score normalized and grouped using k-means clustering with default parameters. Overall trends in site intensity were graphed and colored based on intensity (B). For each of the two clusters, motif analysis was performed (C) : motif analysis on clusters 1 and 2 from hierarchical clustering. Sequence logo visualizations were performed using pLOGO with serine or threonine residues fixed at position 0. Positions with significant residue presence are depicted as amino acid letters sized above the red line. For cluster 1, there was significant enrichment for a proline in the +1 position and arginine in the -3 position, RXXS/TP. For cluster 2, there was again significant enrichment for a proline in the +1 position and arginine in the -3 position in addition to an aspartic acid in the +3 position, RXXS/TPXD.

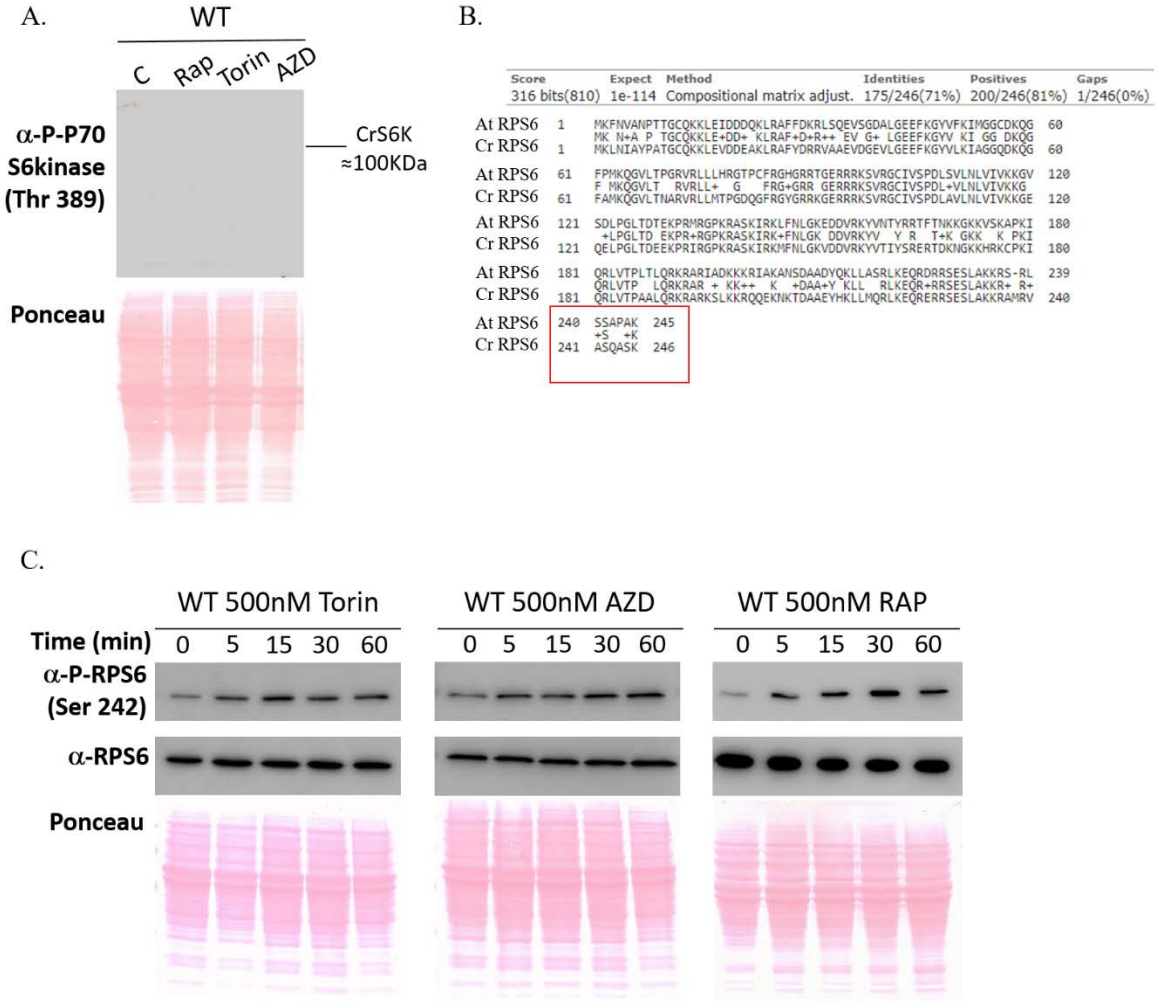

Figure 4.7 Figure reproduced from ref [83]. Commercial anti-phospho S6K antibody reactivity in Chlamydomonas with no signal (A). Comparison of RPS6 protein sequence between Arabidopsis and Chlamydomonas (B). a western blot in wild-type under different drug treatments for 0, 5, 15, 30, and 60 min with antibodies raised for Ser242 (C).

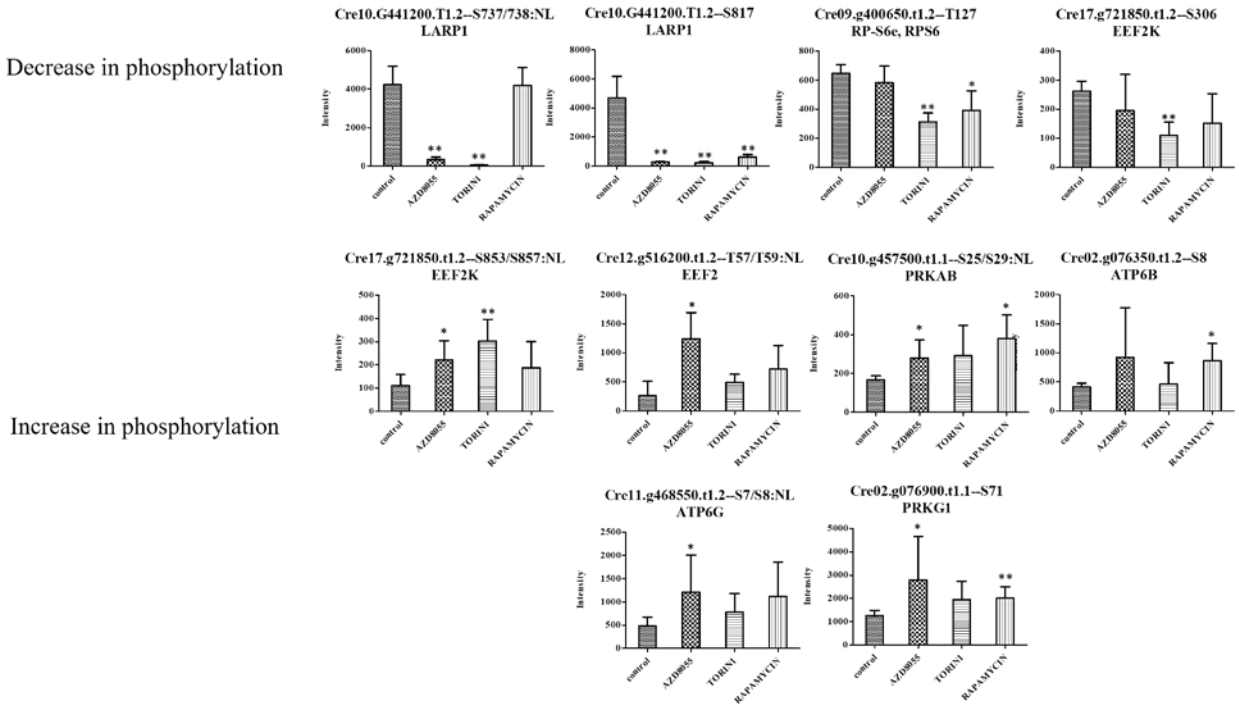

Figure 4.8 Figure reproduced from ref [83]. Bar charts of 10 modulated phosphosites on TOR pathway-associated proteins based on homology. Level of p-value statistical significance is denoted by p-value ≤ 0.05 (*) and ≤ 0.01 (**)

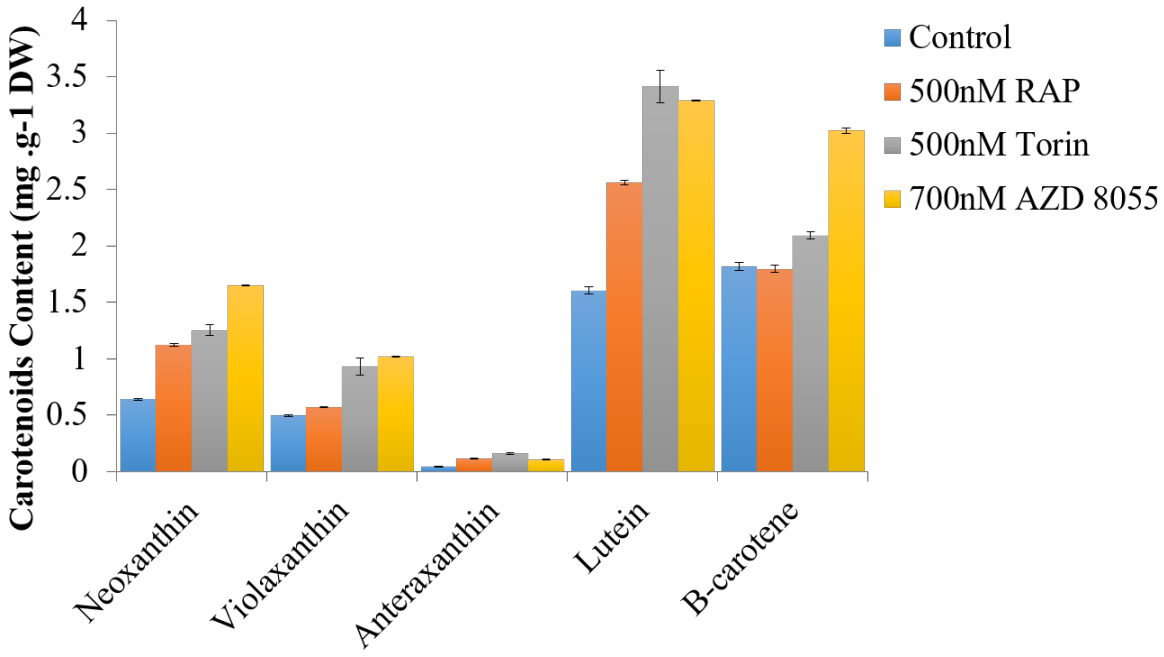

Figure 4.9 Figure reproduced from ref [83]. Bar chart of carotenoid content in WT Chlamydomonas after 8 hours of treatment with Rapamycin, Torin1, and AZD8055 compared to control

REFERENCES

1. Loewith, R.; Hall, M. N., Target of rapamycin (TOR) in nutrient signaling and growth control. *Genetics* **2011,** *189* (4), 1177-1201.

2. Wullschleger, S.; Loewith, R.; Hall, M. N., TOR signaling in growth and metabolism. *Cell* **2006,** *124* (3), 471-484.

3. Dobrenel, T.; Caldana, C.; Hanson, J.; Robaglia, C.; Vincentz, M.; Veit, B.; Meyer, C., TOR Signaling and Nutrient Sensing. *Annual review of plant biology* **2016,** *67*, 261-285.

4. Pérez-Pérez, M. E.; Couso, I.; Crespo, J. L., The TOR Signaling Network in the Model Unicellular Green Alga Chlamydomonas reinhardtii. *Biomolecules* **2017,** *7* (3), 54.

5. González, A.; Hall, M. N., Nutrient sensing and TOR signaling in yeast and mammals. *The EMBO journal* **2017**, e201696010.

6. Raught, B.; Gingras, A. C.; Sonenberg, N., The target of rapamycin (TOR) proteins. *Proc Natl Acad Sci U S A* **2001,** *98* (13), 7037-7044.

7. van Dam, T. J.; Zwartkruis, F. J.; Bos, J. L.; Snel, B., Evolution of the TOR pathway. *J Mol Evol* **2011,** *73* (3-4), 209-220.

8. Diaz-Troya, S.; Florencio, F. J.; Crespo, J. L., Target of rapamycin and LST8 proteins associate with membranes from the endoplasmic reticulum in the unicellular green alga Chlamydomonas reinhardtii. *Eukaryot Cell* **2008,** *7* (2), 212-222.

9. Fingar, D. C.; Blenis, J., Target of rapamycin (TOR): an integrator of nutrient and growth factor signals and coordinator of cell growth and cell cycle progression. *Oncogene* **2004,** *23* (18), 3151-3171.

10. Chresta, C. M.; Davies, B. R.; Hickson, I.; Harding, T.; Cosulich, S.; Critchlow, S. E.; Vincent, J. P.; Ellston, R.; Jones, D.; Sini, P.; James, D.; Howard, Z.; Dudley, P.; Hughes, G.; Smith, L.; Maguire, S.; Hummersone, M.; Malagu, K.; Menear, K.; Jenkins, R.; Jacobsen, M.; Smith, G. C.; Guichard, S.; Pass, M., AZD8055 is a potent, selective, and orally bioavailable ATP-competitive mammalian target of rapamycin kinase inhibitor with in vitro and in vivo antitumor activity. *Cancer Res* **2010,** *70* (1), 288-298.

11. Thoreen, C. C.; Kang, S. A.; Chang, J. W.; Liu, Q.; Zhang, J.; Gao, Y.; Reichling, L. J.; Sim, T.; Sabatini, D. M.; Gray, N. S., An ATP-competitive mammalian target of rapamycin inhibitor reveals rapamycin-resistant functions of mTORC1. *J Biol Chem* **2009,** *284* (12), 8023-8032.

12. Benjamin, D.; Colombi, M.; Moroni, C.; Hall, M. N., Rapamycin passes the torch: a new generation of mTOR inhibitors. *Nature reviews Drug discovery* **2011,** *10* (11), 868-880.

13. Brown, E. J.; Albers, M. W.; Shin, T. B.; Keith, C. T.; Lane, W. S.; Schreiber, S. L., A mammalian protein targeted by G1-arresting rapamycin–receptor complex. *Nature* **1994,** *369* (6483), 756-758.

14. Sabatini, D. M.; Erdjument-Bromage, H.; Lui, M.; Tempst, P.; Snyder, S. H., RAFT1: a mammalian protein that binds to FKBP12 in a rapamycin-dependent fashion and is homologous to yeast TORs. *Cell* **1994,** *78* (1), 35-43.

15. Heitman, J.; Movva, N. R.; Hall, M. N., Targets for cell cycle arrest by the immunosuppressant rapamycin in yeast. *Science* **1991,** *253* (5022), 905-909.

16. Liu, Q.; Xu, C.; Kirubakaran, S.; Zhang, X.; Hur, W.; Liu, Y.; Kwiatkowski, N. P.; Wang, J.; Westover, K. D.; Gao, P., Characterization of Torin2, an ATP-competitive inhibitor of mTOR, ATM, and ATR. *Cancer research* **2013,** *73* (8), 2574-2586.

17. Roohi, A.; Hojjat-Farsangi, M., Recent advances in targeting mTOR signaling pathway using small molecule inhibitors. *Journal of drug targeting* **2017,** *25* (3), 189-201.

18. Montane, M. H.; Menand, B., ATP-competitive mTOR kinase inhibitors delay plant growth by triggering early differentiation of meristematic cells but no developmental patterning change. *J Exp Bot* **2013,** *64* (14), 4361-4374.

19. Zhang, Y. J.; Duan, Y.; Zheng, X. F., Targeting the mTOR kinase domain: the second generation of mTOR inhibitors. *Drug Discov Today* **2011,** *16* (7-8), 325-331.

20. Dibble, C. C.; Manning, B. D., Signal integration by mTORC1 coordinates nutrient input with biosynthetic output. *Nature cell biology* **2013,** *15* (6), 555-564.

21. Saxton, R. A.; Sabatini, D. M., mTOR signaling in growth, metabolism, and disease. *Cell* **2017,** *168* (6), 960-976.

22. Zhang, Y.; Persson, S.; Giavalisco, P., Differential regulation of carbon partitioning by the central growth regulator target of rapamycin (TOR). *Molecular plant* **2013,** *6* (6), 1731-1733.

23. Xiong, Y.; Sheen, J., The role of target of rapamycin signaling networks in plant growth and metabolism. *Plant physiology* **2014,** *164* (2), 499-512.

24. Dobrenel, T.; Marchive, C.; Sormani, R.; Moreau, M.; Mozzo, M.; Montane, M. H.; Menand, B.; Robaglia, C.; Meyer, C., Regulation of plant growth and metabolism by the TOR kinase. *Biochem Soc Trans* **2011,** *39* (2), 477-481.

25. Xiong, Y.; Sheen, J., Rapamycin and glucose-target of rapamycin (TOR) protein signaling in plants. *J Biol Chem* **2012,** *287* (4), 2836-2842.

26. Xiong, Y.; McCormack, M.; Li, L.; Hall, Q.; Xiang, C.; Sheen, J., Glucose-TOR signalling reprograms the transcriptome and activates meristems. *Nature* **2013,** *496* (7444), 181-186.

27. Ren, M.; Venglat, P.; Qiu, S.; Feng, L.; Cao, Y.; Wang, E.; Xiang, D.; Wang, J.; Alexander, D.; Chalivendra, S.; Logan, D.; Mattoo, A.; Selvaraj, G.; Datla, R., Target of rapamycin signaling regulates metabolism, growth, and life span in Arabidopsis. *Plant Cell* **2012,** *24* (12), 4850-4874.

28. Menand, B.; Desnos, T.; Nussaume, L.; Berger, F.; Bouchez, D.; Meyer, C.; Robaglia, C., Expression and disruption of the Arabidopsis TOR (target of rapamycin) gene. *Proc Natl Acad Sci U S A* **2002,** *99* (9), 6422-6427.

29. Crespo, J. L.; Diaz-Troya, S.; Florencio, F. J., Inhibition of target of rapamycin signaling by rapamycin in the unicellular green alga Chlamydomonas reinhardtii. *Plant Physiol* **2005,** *139* (4), 1736-1749.

30. Perez-Perez, M. E.; Florencio, F. J.; Crespo, J. L., Inhibition of target of rapamycin signaling and stress activate autophagy in Chlamydomonas reinhardtii. *Plant Physiol* **2010,** *152* (4), 1874-1888.

31. Rodrigues, S. P.; Alvarez, S.; Werth, E. G.; Slade, W. O.; Gau, B.; Cahoon, E. B.; Hicks, L. M., Multiplexing strategy for simultaneous detection of redox-, phospho- and total proteome – understanding TOR regulating pathways in Chlamydomonas reinhardtii. *Anal. Methods* **2015,** *7* (17), 7336-7344.

32. Imamura, S.; Kawase, Y.; Kobayashi, I.; Sone, T.; Era, A.; Miyagishima, S.-y.; Shimojima, M.; Ohta, H.; Tanaka, K., Target of rapamycin (TOR) plays a critical role in triacylglycerol accumulation in microalgae. *Plant molecular biology* **2015,** *89* (3), 309-318.

33. Couso, I.; Evans, B. S.; Li, J.; Liu, Y.; Ma, F.; Diamond, S.; Allen, D. K.; Umen, J. G., Synergism between Inositol Polyphosphates and TOR Kinase Signaling in Nutrient Sensing, Growth Control, and Lipid Metabolism in Chlamydomonas. *The Plant Cell* **2016,** *28* (9), 2026-2042.

34. Imamura, S.; Kawase, Y.; Kobayashi, I.; Shimojima, M.; Ohta, H.; Tanaka, K., TOR (target of rapamycin) is a key regulator of triacylglycerol accumulation in microalgae. *Plant signaling & behavior* **2016,** *11* (3), e1149285.

35. Wang, H.; Gau, B.; Slade, W. O.; Juergens, M.; Li, P.; Hicks, L. M., The global phosphoproteome of Chlamydomonas reinhardtii reveals complex organellar phosphorylation in the flagella and thylakoid membrane. *Molecular & Cellular Proteomics* **2014,** *13* (9), 2337-2353.

36. Werth, E. G.; McConnell, E. W.; Gilbert, T. S. K.; Couso Lianez, I.; Perez, C. A.; Manley, C. K.; Graves, L. M.; Umen, J. G.; Hicks, L. M., Probing the global kinome and phosphoproteome in Chlamydomonas reinhardtii via sequential enrichment and quantitative proteomics. *The Plant Journal* **2017,** *89* (2), 416-426.

37. Slade, W. O.; Werth, E. G.; McConnell, E. W.; Alvarez, S.; Hicks, L. M., Quantifying reversible oxidation of protein thiols in photosynthetic organisms. *J Am Soc Mass Spectrom* **2015,** *26* (4), 631-640.

38. Vizcaíno, J. A.; Côté, R. G.; Csordas, A.; Dianes, J. A.; Fabregat, A.; Foster, J. M.; Griss, J.; Alpi, E.; Birim, M.; Contell, J., The PRoteomics IDEntifications (PRIDE) database and associated tools: status in 2013. *Nucleic acids research* **2013,** *41* (D1), D1063-D1069.

39. Käll, L.; Canterbury, J. D.; Weston, J.; Noble, W. S.; MacCoss, M. J., Semi-supervised learning for peptide identification from shotgun proteomics datasets. *Nature methods* **2007,** *4* (11), 923-925.

40. Savitski, M. M.; Lemeer, S.; Boesche, M.; Lang, M.; Mathieson, T.; Bantscheff, M.; Kuster, B., Confident phosphorylation site localization using the Mascot Delta Score. *Molecular & Cellular Proteomics* **2011,** *10* (2), M110. 003830.

41. Tyanova, S.; Temu, T.; Sinitcyn, P.; Carlson, A.; Hein, M. Y.; Geiger, T.; Mann, M.; Cox, J., The Perseus computational platform for comprehensive analysis of (prote) omics data. *Nature methods* **2016,** *13* (9), 731-740.

42. Cox, J.; Mann, M., 1D and 2D annotation enrichment: a statistical method integrating quantitative proteomics with complementary high-throughput data. *BMC bioinformatics* **2012,** *13* (16), S12.

43. Kanehisa, M.; Goto, S., KEGG: kyoto encyclopedia of genes and genomes. *Nucleic acids research* **2000,** *28* (1), 27-30.

44. Ashburner, M.; Ball, C. A.; Blake, J. A.; Botstein, D.; Butler, H.; Cherry, J. M.; Davis, A. P.; Dolinski, K.; Dwight, S. S.; Eppig, J. T., Gene Ontology: tool for the unification of biology. *Nature genetics* **2000,** *25* (1), 25-29.

45. O'shea, J. P.; Chou, M. F.; Quader, S. A.; Ryan, J. K.; Church, G. M.; Schwartz, D., pLogo: a probabilistic approach to visualizing sequence motifs. *Nature methods* **2013,** *10* (12), 1211-1212.

46. Baroli, I.; Do, A. D.; Yamane, T.; Niyogi, K. K., Zeaxanthin accumulation in the absence of a functional xanthophyll cycle protects Chlamydomonas reinhardtii from photooxidative stress. *The Plant Cell* **2003,** *15* (4), 992-1008.

47. Dobrenel, T.; Mancera-Martínez, E.; Forzani, C.; Azzopardi, M.; Davanture, M.; Moreau, M.; Schepetilnikov, M.; Chicher, J.; Langella, O.; Zivy, M., The Arabidopsis TOR kinase specifically regulates the expression of nuclear genes coding for plastidic ribosomal proteins and the phosphorylation of the cytosolic ribosomal protein S6. *Frontiers in plant science* **2016,** *7*, 1611.

48. Xiong, Y.; Sheen, J., Rapamycin and glucose-target of rapamycin (TOR) protein signaling in plants. *Journal of Biological Chemistry* **2012,** *287* (4), 2836-2842.

49. Rigbolt, K. T.; Zarei, M.; Sprenger, A.; Becker, A. C.; Diedrich, B.; Huang, X.; Eiselein, S.; Kristensen, A. R.; Gretzmeier, C.; Andersen, J. S.; Zi, Z.; Dengjel, J., Characterization of early autophagy signaling by quantitative phosphoproteomics. *Autophagy* **2014,** *10* (2), 356-371.

50. Demirkan, G.; Yu, K.; Boylan, J. M.; Salomon, A. R.; Gruppuso, P. A., Phosphoproteomic profiling of in vivo signaling in liver by the mammalian target of rapamycin complex 1 (mTORC1). *PLoS One* **2011,** *6* (6), e21729.

51. Harder, L. M.; Bunkenborg, J.; Andersen, J. S., Inducing autophagy: a comparative phosphoproteomic study of the cellular response to ammonia and rapamycin. *Autophagy* **2014,** *10* (2), 339-355.

52. Chou, M. F.; Schwartz, D., Biological sequence motif discovery using motif-x. *Current Protocols in Bioinformatics* **2011**, 13.15.1-13.15.24.

53. Robitaille, A. M.; Christen, S.; Shimobayashi, M.; Cornu, M.; Fava, L. L.; Moes, S.; Prescianotto-Baschong, C.; Sauer, U.; Jenoe, P.; Hall, M. N., Quantitative phosphoproteomics reveal mTORC1 activates de novo pyrimidine synthesis. *Science* **2013,** *339* (6125), 1320-1323.

54. Lu, K. P.; Liou, Y.-C.; Zhou, X. Z., Pinning down proline-directed phosphorylation signaling. *Trends in cell biology* **2002,** *12* (4), 164-172.

55. Hsu, P. P.; Kang, S. A.; Rameseder, J.; Zhang, Y.; Ottina, K. A.; Lim, D.; Peterson, T. R.; Choi, Y.; Gray, N. S.; Yaffe, M. B.; Marto, J. A.; Sabatini, D. M., The mTOR-regulated phosphoproteome reveals a mechanism of mTORC1-mediated inhibition of growth factor signaling. *Science* **2011,** *332* (6035), 1317-1322.

56. Lv, D.-W.; Ge, P.; Zhang, M.; Cheng, Z.-W.; Li, X.-H.; Yan, Y.-M., Integrative network analysis of the signaling cascades in seedling leaves of bread wheat by large-scale phosphoproteomic profiling. *Journal of proteome research* **2014,** *13* (5), 2381-2395.

57. Foster, K. G.; Acosta-Jaquez, H. A.; Romeo, Y.; Ekim, B.; Soliman, G. A.; Carriere, A.; Roux, P. P.; Ballif, B. A.; Fingar, D. C., Regulation of mTOR complex 1 (mTORC1) by raptor Ser863 and multisite phosphorylation. *J Biol Chem* **2010,** *285* (1), 80-94.

58. Merchant, S. S.; Prochnik, S. E.; Vallon, O.; Harris, E. H.; Karpowicz, S. J.; Witman, G. B.; Terry, A.; Salamov, A.; Fritz-Laylin, L. K.; Maréchal-Drouard, L., The Chlamydomonas genome reveals the evolution of key animal and plant functions. *Science* **2007,** *318* (5848), 245-250.

59. Carrière, A.; Cargnello, M.; Julien, L.-A.; Gao, H.; Bonneil, É.; Thibault, P.; Roux, P. P., Oncogenic MAPK signaling stimulates mTORC1 activity by promoting RSK-mediated raptor phosphorylation. *Current biology* **2008,** *18* (17), 1269-1277.

60. Ekim, B.; Magnuson, B.; Acosta-Jaquez, H. A.; Keller, J. A.; Feener, E. P.; Fingar, D. C., mTOR kinase domain phosphorylation promotes mTORC1 signaling, cell growth, and cell cycle progression. *Molecular and cellular biology* **2011,** *31* (14), 2787-2801.

61. Wang, X.; Proud, C. G., Nutrient control of TORC1, a cell-cycle regulator. *Trends in cell biology* **2009,** *19* (6), 260-267.

62. Terada, N.; Patel, H. R.; Takase, K.; Kohno, K.; Nairn, A. C.; Gelfand, E. W., Rapamycin selectively inhibits translation of mRNAs encoding elongation factors and ribosomal proteins. *Proceedings of the National Academy of Sciences* **1994,** *91* (24), 11477-11481.

63. Jefferies, H.; Reinhard, C.; Kozma, S.; Thomas, G., Rapamycin selectively represses translation of the" polypyrimidine tract" mRNA family. *Proceedings of the National Academy of Sciences* **1994,** *91* (10), 4441-4445.

64. Dennis, P. B.; Pullen, N.; Kozma, S. C.; Thomas, G., The principal rapamycin-sensitive p70 (s6k) phosphorylation sites, T-229 and T-389, are differentially regulated by rapamycin-insensitive kinase kinases. *Molecular and cellular biology* **1996,** *16* (11), 6242-6251.

65. Burnett, P. E.; Barrow, R. K.; Cohen, N. A.; Snyder, S. H.; Sabatini, D. M., RAFT1 phosphorylation of the translational regulators p70 S6 kinase and 4E-BP1. *Proceedings of the National Academy of Sciences* **1998,** *95* (4), 1432-1437.

66. Ahn, C. S.; Ahn, H.-K.; Pai, H.-S., Overexpression of the PP2A regulatory subunit Tap46 leads to enhanced plant growth through stimulation of the TOR signalling pathway. *Journal of experimental botany* **2014,** *66* (3), 827-840.

67. Hizli, A. A.; Chi, Y.; Swanger, J.; Carter, J. H.; Liao, Y.; Welcker, M.; Ryazanov, A. G.; Clurman, B. E., Phosphorylation of eukaryotic elongation factor 2 (eEF2) by cyclin A–cyclin-dependent kinase 2 regulates its inhibition by eEF2 kinase. *Molecular and cellular biology* **2013,** *33* (3), 596-604.

68. Yu, Y.; Yoon, S. O.; Poulogiannis, G.; Yang, Q.; Ma, X. M.; Villen, J.; Kubica, N.; Hoffman, G. R.; Cantley, L. C.; Gygi, S. P.; Blenis, J., Phosphoproteomic analysis identifies Grb10 as an mTORC1 substrate that negatively regulates insulin signaling. *Science* **2011,** *332* (6035), 1322-1326.

69. Kang, S. A.; Pacold, M. E.; Cervantes, C. L.; Lim, D.; Lou, H. J.; Ottina, K.; Gray, N. S.; Turk, B. E.; Yaffe, M. B.; Sabatini, D. M., mTORC1 phosphorylation sites encode their sensitivity to starvation and rapamycin. *Science* **2013,** *341* (6144), 1236566.

70. Hong, S.; Freeberg, M. A.; Han, T.; Kamath, A.; Yao, Y.; Fukuda, T.; Suzuki, T.; Kim, J. K.; Inoki, K., LARP1 functions as a molecular switch for mTORC1-mediated translation of an essential class of mRNAs. *eLife* **2017,** *6*.

71. Fonseca, B. D.; Zakaria, C.; Jia, J.-J.; Graber, T. E.; Svitkin, Y.; Tahmasebi, S.; Healy, D.; Hoang, H.-D.; Jensen, J. M.; Diao, I. T., La-related protein 1 (LARP1) represses terminal oligopyrimidine (TOP) mRNA translation downstream of mTOR complex 1 (mTORC1). *Journal of Biological Chemistry* **2015,** *290* (26), 15996-16020.

72. Marchler-Bauer, A.; Bryant, S. H., CD-Search: protein domain annotations on the fly. *Nucleic acids research* **2004,** *32* (suppl_2), W327-W331.

73. Bravo, J.; Aguilar-Henonin, L.; Olmedo, G.; Guzman, P., Four distinct classes of proteins as interaction partners of the PABC domain of Arabidopsis thaliana Poly (A)-binding proteins. *Molecular genetics and genomics* **2005,** *272* (6), 651-665.

74. Jiménez-López, D.; Bravo, J.; Guzmán, P., Evolutionary history exposes radical diversification among classes of interaction partners of the MLLE domain of plant poly (A)-binding proteins. *BMC evolutionary biology* **2015,** *15* (1), 195.

75. Jiménez-López, D.; Guzmán, P., Insights into the evolution and domain structure of Ataxin-2 proteins across eukaryotes. *BMC research notes* **2014,** *7* (1), 453.

76. Cunningham, F. X.; Pogson, B.; Sun, Z.; McDonald, K. A.; DellaPenna, D.; Gantt, E., Functional analysis of the beta and epsilon lycopene cyclase enzymes of Arabidopsis reveals a mechanism for control of cyclic carotenoid formation. *The Plant Cell* **1996,** *8* (9), 1613-1626.

77. Cunningham, F. X.; Gantt, E., One ring or two? Determination of ring number in carotenoids by lycopene ε-cyclases. *Proceedings of the National Academy of Sciences* **2001,** *98* (5), 2905-2910.

78. Cordero, B. F.; Obraztsova, I.; Martín, L.; Couso, I.; León, R.; Ángeles Vargas, M.; Rodríguez, H., ISOLATION AND CHARACTERIZATION OF A LYCOPENE β-CYCLASE GENE FROM THE ASTAXANTHIN-PRODUCING GREEN ALGA CHLORELLA ZOFINGIENSIS (CHLOROPHYTA). *Journal of phycology* **2010,** *46* (6), 1229-1238.

79. Frank, H. A.; Cogdell, R. J., Carotenoids in photosynthesis. *Photochemistry and photobiology* **1996,** *63* (3), 257-264.

80. Valledor, L.; Furuhashi, T.; Recuenco-Muñoz, L.; Wienkoop, S.; Weckwerth, W., System-level network analysis of nitrogen starvation and recovery in Chlamydomonas reinhardtii reveals potential new targets for increased lipid accumulation. *Biotechnology for biofuels* **2014,** *7* (1), 171.

81. Cunningham Jr, F.; Gantt, E., Genes and enzymes of carotenoid biosynthesis in plants. *Annual review of plant biology* **1998,** *49* (1), 557-583.

82. Roustan, V.; Bakhtiari, S.; Roustan, P.-J.; Weckwerth, W., Quantitative in vivo phosphoproteomics reveals reversible signaling processes during nitrogen starvation and

recovery in the biofuel model organism Chlamydomonas reinhardtii. *Biotechnology for biofuels* **2017,** *10* (1), 280.

83. Werth, E. G.; McConnell, E. W.; Couso, I.; Perrine, Z.; Crespo, J. L.; Umen, J. G.; Hicks, L. M., Investigating the effect of Target of Rapamycin kinase inhibition on the Chlamydomonas reinhardtii phosphoproteome: from known homologs to new targets. *Submitted.* **2018**.

CHAPTER 5: Pathway Inhibition of Rapamycin-Hypersensitive Vip-1 Mutant Chlamydomonas Strain Revealed via Phosphoproteomics

*****Manuscript to be submitted for publication. Authors: Werth, E.G., Couso, I., Umen, J. G., Hicks, L. M. Pathway Inhibition of Rapamycin-Hypersensitive Vip-1 Mutant Chlamydomonas Strain Revealed via Phosphoproteomics.

5.1 Introduction

Characterizing cellular regulation of carbon metabolism and triacylglycerol (TAG) accumulation in algae is required to harness its potential as a biofuel feedstock[1-6]. Elucidation of intracellular carbon regulatory networks and the interplay between them will provide better strategies for improving yields and storage of fixed carbon. Many interconnected signaling networks are tied to lipid and TAG accumulation in algae including target of rapamycin (TOR)[1, 7-8] and inositol polyphosphate (InsPs) signaling[9-10]. Recently, a connection between the TOR kinase pathway and inositol polyphosphate signaling has been reported in Chlamydomonas[11], an interaction previously only suggested in yeast and animals[12-13].

TOR kinase signaling is a master regulator of cellular processes from cell cycle to autophagy and modulates activity in response to nutrients and stress to control protein biosynthesis and other metabolic processes[14-19]. Highly studied in metazoans and fungi[15, 20], TOR is found in two compositionally and functionally distinct multiprotein complexes, TORC1 and TORC2[15, 19], but only homologs of TORC1 are found in the green lineage[14, 21-22]. In the model green alga *Chlamydomonas reinhardtii* (Chlamydomonas), key TORC1 complex proteins such as TOR (Cre09.g400553.t1.1), regulatory associate protein target of rapamycin (RAPTOR) (Cre08.g371957.t1.1), and lethal with sec-13 protein 8 (LST8) (Cre17.g713900.t1.2) are

conserved[21, 23]. Selective chemical inhibition of TOR kinase, has been shown to induce TAG accumulation[8] and phosphoproteomics revealed 258 significantly modulated phosphosites on both TOR signaling-related proteins and numerous sites not previously known to be TOR-regulated, including a role in carotenoid biosynthesis[24].

Inositol pyrophosphates are signaling molecules critically important in eukaryotes that play a role in stress response[25-28] and function in diverse cellular processes such as energy sensing, telomere maintenance, homeostasis, and storage[9, 29]. In yeast and animal systems, two distinct families of enzymes are capable of producing pyrophosphorylated inositols, IP6K/KCS1[9] and VIP[30-32]. VIP proteins belong to a class of enzymes known as diphosphate kinases in animals[33] that are conserved in plants[9, 32] and capable of synthesizing polyphosphate inositols. Plants have been shown to have large amounts of $InsP_6$, the precursor to signaling molecules containing diphosphate or triphosphate chains attached to the inositol ring[34-35]. Molecules synthesized by $InsP_6$, such as $InsP_7$ and $InsP_8$, contain high energy pyrophosphate bonds that may store energy in the cell[36] however due to their low amounts and high turnover rates, it has been suggested that they serve as more than simply energy storage molecules[37-38].

A direct link between the Chlamydomonas TOR and InsP pathways was revealed by characterization of a mutant, vip1-1, that conferred hypersensitivity to the TOR inhibitor rapamycin. This loss-of-function mutation in the VIP1 gene was identified in an insertional mutagenesis screen for rapamycin-hypersensitive Chlamydomonas[11]. Vip1-1 is predicted to encode a conserved inositol hexakisphosphate kinase from the VIP family that pyrophosphorylates phytic acid, $InsP_6$. This mutant has defects in $InsP_7$ and $InsP_8$ accumulation with $InsP_7$ and $InsP_8$ levels at 20 to 30% of wild-type levels but $InsP_6$ levels maintaining approximately 70% wild-type levels[11].

The discovery of interplay between the TOR and InsP signaling systems allows for the opportunity to investigate the effects of TOR inhibition on the phosphoproteome of a rapamycin-hypersensitive mutant, vip1-1. Rapamycin-treated cultures revealed similarities with the sites modulated in the wild-type study (Chapter 4) and contained a subset of phosphosites not previously identified as TOR regulated. Cluster and motif analysis was used to identify significant trends among the phosphosites changing.

5.2 Materials and Methods

5.2.1 Cell Culturing and Rapamycin Treatment.

Strain CC-1690 mt+ (Sager 21 gr) (Sager, 1955) was used as the parental strain to generate vip1-1 for the rapamycin-hypersensitive strain. Insertional mutagenesis[39] with a hygromycin resistance gene, *aph7"*[40] was used to generate mutants and transformation was performed as previously described[11]. Rapamycin-hypersensitive mutants were identified by comparing growth on TAP (Tris Acetate Phosphate) agar plates to TAP + 500 nM rapamycin plates.

For phosphoproteomic studies, all cultures were maintained on TAP agar plates and grown in 350-mL TAP liquid cultures at 25ºC as previously described[11]. Experiments were done using five replicate cultures grown to exponential phase (1-2x10^6 cells/mL) for control and rapamycin-treated samples and quenched with 40% methanol prior to harvesting by centrifuging at 4000 *g* for 5 min and discarding supernatant as previously described[24]. Cell pellets were then flash frozen using liquid nitrogen and stored at -80ºC until use. For rapamycin-treated cultures, drug was added to a final concentration of 500 nM for rapamycin (LC Laboratories) from 1mM stocks in DMSO for 15 min prior to harvesting. For control replicates, drug vehicle (DMSO) without rapamycin was added to each replicate culture for 15 min prior to harvesting.

5.2.2 Protein Extraction.

Cell pellets were resuspended in lysis buffer containing 100 mM Tris, pH 8.0 with 1x concentrations of cOmplete protease inhibitor and phosSTOP phosphatase inhibitor cocktails (Roche, Indianapolis, IN, USA). Cells were lysed via sonication using an E220 focused ultrasonicator (Covaris, Woburn, MA, USA) for 120 s at 200 cycles/burst, 100 W power and 13% duty cycle. Following ultrasonication, the supernatant was collected from cellular debris by centrifugation for 10 min at 15,000 *g* at 4ºC and proteins were precipitated using 5 volumes of cold 100 mM ammonium acetate in methanol. Following 3 hr incubation at -80ºC, protein was pelleted by centrifugation for 5 min at 2,000 *g* followed by two washes with fresh 100 mM ammonium acetate in methanol and a final wash with 70% ethanol. Cell pellets were resuspended in 8M urea and protein concentration was determined using the CB-X assay (G-Biosciences, St. Louis, MO, USA).

5.2.3 Protein Digestion and Reduction.

Each 2 mg protein sample replicate at approximately 1mg/mL concentration was reduced using 10 mM dithiothreitol for 30 min at RT and subsequently alkylated with 40 mM iodoacetamide for 45 min in darkness at RT. Following reduction and alkylation, samples were diluted 5-fold in 100 mM Tris to reduce urea concentration to 1.6M for effective trypsin digestion performed at 25°C for 16 h with Trypsin Gold (Promega) at a protease:protein ratio of 1:50.

5.2.4 Solid-Phase Extraction.

After digestion, samples were acidified to pH<3.0 with trifluoroacetic acid (TFA). Pelleted, undigested protein was cleared from the supernatant by centrifugation for 5 min at 5,000 *g* prior to solid-phase extraction. Desalting was performed using C18 50 mg Sep-Pak cartridges

(Waters). Columns were prepared by washing with acetonitrile (MeCN) followed by 80% MeCN/20%H_2O/0.1% TFA and 0.1% TFA. Digested protein lysates were applied to the columns and reloaded twice before being washed with 0.1% TFA and eluted using 80% MeCN/20% H_2O/0.1% TFA.

5.2.5 Phosphopeptide Enrichment and Clean-Up.

Following protein digestion and solid-phase extraction, replicates were dried down using vacuum centrifugation and phosphopeptide enrichment was performed on 2 mg aliquots of each sample using 3 mg Titansphere Phos-TiO_2 kit spin columns (GL Sciences) as previously described[24, 41]. After enrichment, samples were dried down and resuspended in 15 µL of 1% formic acid and 2% MeCN prior to desalting using ZipTips (Millipore). Briefly, ZipTip sample clean-up involved equilibrating tip-based columns 3x with 10 µL of 100% MeCN followed by 3x with 10 µL of 0.1% formic acid. Peptides were then loaded on the ZipTip by passing the lysate through 10x. After loading peptides onto the column, ZipTips were washed 6x with 10 µL of 0.1% formic acid and eluted using 5 µL of 60% MeCN/0.1% formic acid repeatedly pipetting the ZipTip up and down 10x.

5.2.6 LC-MS/MS Acquisition and Data Processing

Following ZipTip clean-up, peptides were dried down and resuspended in 20 µL of 0.1% TFA, 5% MeCN with 25% of total sample loaded onto the column for LC-MS/MS analysis. Separation using a C18 column (NanoAcquity UPLC 1.8 µm HSS T3, 75 µm × 250 mm) was performed via a 90-min linear gradient from 95% H_2O/5% MeCN/0.1% formic acid (FA) to 65% H_2O/35% MeCN/0.1% FA via a NanoAcquity UPLC (Waters). Each sample was loaded onto a trap column (NanoAcquity UPLC 2G-W/M Trap 5 µm Symmetry C18, 180 µm × 20 mm) at a flow rate of 5 µL min^{-1} for 5 min. Peptides were separated using a C18 column (NanoAcquity

UPLC 1.8 μm HSS T3, 75 μm × 250 mm) at a flow rate of 300 nL min^{-1}. A TripleTOF 5600 (AB Sciex) Q-TOF was operated in positive-ionization nanoelectrospray and high-sensitivity mode for data acquisition as previously described[42]. The MS survey spectrum was accumulated from a mass range of 350 to 1250 *m/z* in 250 ms. For MS/MS experiments, the first 20 features above 150 counts threshold and having a charge state of +2 to +5 were fragmented using rolling collision energy ±5%, with 87.5 ms spectra accumulation/experiment.

Acquired spectra (*.wiff) files were imported into Progenesis QI for proteomics (v2.0, Nonlinear Dynamics) as previously described[41] with peptide sequence determination and protein inference done by Mascot (v.2.5.1; Matrix Science) using the *C. reinhardtii* Phytozome v.11 database (www.phytozome.net/; accessed May 2015) appended with the NCBI chloroplast and mitochondrial databases (19,603 entries) and sequences for common laboratory contaminants (http://thegpm.org/cRAP/; 116 entries). For database searching, trypsin protease specificity with up to two missed cleavages, peptide/fragment mass tolerances of 20 ppm/0.1 Da, a fixed modification of carbamidomethylation at cysteine, and variable modifications of acetylation at the protein N-terminus, oxidation at methionine, deamidation at asparagine or glutamine, phosphorylation at serine or threonine and phosphorylation at tyrosine were used. Peptide false discovery rates (FDR) were adjusted to ≤1% using the Mascot Percolator algorithm[43] and only peptides with a Mascot ion score over 13 were considered.

Custom scripts written in Python were implemented to parse results following data normalization and quantification in Progenesis QI for proteomics as previously described[24, 41]. Shared peptides between proteins were grouped together to satisfy the principle of parsimony and represented in Table S1 by the protein accession with the highest amount of unique peptides, otherwise the largest confidence score assigned by Progenesis QI for proteomics. Additionally,

the script appended site localization of variable modifications using an implementation of the Mascot Delta Score[44] to the peptide measurements (*.csv) export from Progenesis QI for proteomics with confident site localization considered a Mascot Delta score >90%. Following scoring, only peptides with phosphorylation at serine, threonine, or tyrosine were considered for further processing and analysis. Additionally, a coefficient of variation filter to remove highly variable sites that were remaining was performed removing sites with >25% coefficient of variation in both control and rapamycin-treated subsets prior to statistical testing.

Supporting Information tables and raw mass spectrometry data have been deposited to the ProteomeXChange Consortium via PRIDE partner repository[45] identifier PXD009163.

5.2.7 Downstream Bioinformatic Analysis.

Missing value imputation was performed on logarithmized normalized abundances in Perseus v1.6.0.0[46-47] requiring at least three of the five replicates in rapamycin-treated and control to be nonzero to continue through the workflow. Missing values were replaced by random numbers drawn from a normal distribution on log-transformed normalized abundances[46, 48]. This was performed using default parameters in the statistical software Perseus v1.6.0.0 optimized to mimic the circumstance that typically missing values represent low abundance measurements[49]. For two sample Student's T-test analyses, replicates were grouped and the statistical tests were performed with fold change ±2 and $p \leq 0.05$ significance threshold to compare control and rapamycin-treated replicates. KEGG pathway annotation[50], Gene Ontology (GO)[51] term annotation, hierarchical clustering, and motif analysis were performed following statistical testing to glean biological insight on modulated sites found in the study. For hierarchical clustering, visualization was performed in Perseus v1.6.0.0. Following data normalization and missing value imputation, intensity values were z-score normalized and grouped using k-means

clustering with default parameters for hierarchical clustering. For motif analysis, sites ±7 around the phosphosites in each cluster were visualized using pLOGO. Positions with significant residue presence are depicted as amino acid letters sized above the red line[52].

5.3 Results and Discussion

5.3.1 Experimental Design

Vip1-1 mutant cells were treated with a saturating dose of rapamycin (500 μM)[7, 11] for 15 minutes to study early phosphorylation changes. The concentration for rapamycin treatment was based on the concentration used to characterize the vip1-1 mutant line previously[11] and the 15-minute time point was based on the time point used in TOR inhibition phosphoproteomic studies in Chlamydomonas[24] and other organisms[53-55].

5.3.2 Quantitative Coverage of the TOR-Inhibited Phosphoproteome in vip1-1 Mutant

Five replicates of vip1-1 mutant cells treated with rapamycin were compared to five control replicates treated with drug vehicle (DMSO) to study the TOR-inhibited phosphoproteome using a label-free quantitative approach. Quantitative coverage on 2,699 phosphosites inferred to 1,442 phosphoproteins (Table S1) was obtained. The majority of sites were found on serine with 82.4% (pS), 16.2% of sites phosphorylated on threonine (pT), and 1.4% phosphorylated on tyrosine (pY) (Figure 5.1A). The majority, 90.8%, of phosphopeptides quantified, were singly phosphorylated with 8.2% doubly phosphorylated, and 1% multiply phosphorylated (Figure 5.1B), similar to what has been found in previous investigations[24, 41, 56].

Inhibition of TOR in the Vip1-1 rapamycin-hypersensitive mutant revealed 316 phosphosites from 281 phosphopeptides significantly changing with at least a two-fold change and a p-value ≤ 0.05 (Figure 5.2, Table S2). These sites are comprised of previously identified phosphosites that

are known to be TOR-regulated and highlighted in Table 5.1 in addition to novel sites that are significantly changing in the vip1-1 mutant but not previously in wild-type studies[24].

5.3.3 Cluster Analysis and Phosphosite Motif Identification.

To identify significant trends among the phosphosites changing following TOR inhibition, hierarchical k-means clustering was performed resulting in 2 clusters for increasing and decreasing sites (Figure 5.3 A,B). Each cluster was examined for significant motifs surrounding phosphosites (Figure 5.3 C) since amino acid residues immediately surrounding phosphorylation sites on substrates can dictate kinase specificity[57]. Cluster 1, which is composed of sites increasing in abundance following rapamycin treatment, had significant enrichment for an aspartic acid residue in the +2 position and glutamic acids in the +3 and +4 positions with respect to the phosphorylation site (position 0). These sites indicate an overall acidic motif on the C-terminal side of the phosphorylation sites. An acidic motif comprised of an enrichment for an aspartic acid in the +3 position was identified in the sites increasing in the wild-type study[24] but additional sites in the +2 and +4 positions were only identified in the vip1-1 strain. This enhanced acidic motif may be connected to inositol polyphosphate signaling in Chlamydomonas, as acidic residues C-terminal to phosphoserines in yeast have been shown to be critical for inositol pyrophosphate signaling and is presumed to be required for binding to magnesium[58]. In cluster 2, which is composed of sites decreasing in abundance following rapamycin treatment, there was significant enrichment for a proline in the +1 position indicating substrates for proline-directed kinases. This common motif was also identified in decreasing sites in the wild-type. However, common rapamycin-sensitive motifs such as RXRXXS/T and RXXS/T seen in wild-type and previous mammalian cell line studies[55] were not identified in either cluster 1 or 2 in vip1-1.

5.3.4 Phosphosites Modulated by TORC1 Inhibition in vip1-1 Strain– Known and Putative Substrates

To begin to understand TOR signaling in vip1-1, proteins that are known TOR targets or associated with the pathway, based on homology to other systems[21] and from previous TOR studies in Chlamydomonas[7, 24, 59-60], were evaluated (Table 5.1). Sites on two proteins conserved in the CrTORC1 complex, TOR and RAPTOR, were identified in this study. Two phosphosites on CrTOR (Cre09.g400553.t1.1), S770/773:NL and S2598, were identified in addition to one phosphosite on RAPTOR (Cre08.g371957.t1.1), S782/S783:NL. Site S770/773:NL on CrTOR significantly decreased 2.86-fold in abundance following rapamycin treatment. Overall, 28 sites on 14 proteins were identified (Table 5.1) and 18 of the 28 sites (64%) were also identified in the wild-type study while 10 were unique, including protein kinases related to signal transduction regulating carbon metabolism in plants[61].

A phosphosite on a protein kinase related to energy sensing, CrSNF1 (T189/S190/S193:NL, Cre04.g211600.t1.1), was identified in this study as increasing by 1.73-fold following TOR inhibition. T189/S190/S193:NL is potentially the conserved site to T198 in Arabidopsis and T210 in yeast and is contained in the activation loop. This phosphorylation site regulates the catalytic activity of the kinase domain in Arabidopsis[62-63] and yeast[64] with rapamycin shown to induce an increase in phosphorylation at T210 in yeast[65-66] with similar functionality possible in Chlamydomonas based on our vip1-1 findings. A site on another protein kinase, CrPDPK1 (Cre11.g467568.t1.1), increased in phosphorylation following TOR inhibition. S403 on CrPDPK1, a site C-terminal to the kinase catalytic domain (Accession: cl21453), increased by 2.56-fold and reports in mammalian studies have shown regulation of PDPK1 by inositol phosphates or pyrophosphates[67].

5.3.5 Comparison of vip1-1 Mutant Study to Wild-Type TOR Inhibited Phosphoproteome Study

To compare the phosphorylation sites modulated by TOR inhibition in this study to the wild-type, fold-changes for differential sites were compared to wild-type fold-changes following TOR inhibition[24]. Of the 281 phosphopeptides changing, 97 (35%) of them overlap with sites identified in the previous wild-type work. This suggests most sites experimentally identified as TOR-regulated in the vip1-1 mutant were not detected in the wild-type study.

For those that do overlap, Table 5.1 shows the fold-change comparison for TOR-associated proteins in Chlamydomonas and Table S2 provides this information on all differential sites. For TOR-associated sites, similar modulation following rapamycin treatment was observed across strains as demonstrated by S817 on LARP1 decreasing phosphorylation by 6.66-fold and 7.69-fold in the vip1-1 mutant and wild-type strains, respectively. Additionally, heightened fold-changes were observed in CrPRKAB which increased in phosphorylation abundance by 4.28-fold in the vip1-1 mutant as compared to 2.27-fold in wild-type. This non-catalytic subunit of AMPK with a conserved 5'-AMP-activated protein kinase beta subunit, interaction domain (pfam: PF04739) serves as an energy sensor protein and the regulatory subunit monitoring cellular energy status activated under cellular metabolic stresses. Because of this, a larger modulation was observed in the rapamycin hypersensitive vip1-1 mutant. Other sites with heightened fold-changes include S155/157:NL on carnosine synthase protein (Cre13.g582800.t1.2), a protein with a conserved ATP-grasp domain (pfam: PF02655), that decreased 17.9-fold in vip1-1 mutant and 7.2-fold in wild type.

Interestingly, numerous sites on phosphoproteins were identified with opposite trends in the mutant strain than were detected in wild-type (Table 5.2) such as Ser23/25:NL on pfkB-like

carbohydrate kinase protein (Cre06.g250500.t1.2). This protein has a conserved carbohydrate domain (pfam: PF01256) and ADP-dependent NAD(P)H-hydrate dehydratase activity based on gene ontology (GO:0052855). This site had a 1.78-fold increase following rapamycin treatment but in the mutant line, had a 2.56-fold *decrease*. Similarly, Ser481 of NAD(P)-binding Rossmann-fold superfamily protein (Cre06.g269050.t1.2), which has a conserved NAD(P)H-binding domain conserved (pfam: PF13460), had a 2.38-fold decrease in wild-type but increased by 4.79-fold in the vip1-1 mutant. These sites, in addition to sites uniformly changing across cell lines, could help to increase the understanding between how the two kinase signaling pathways interact in Chlamydomonas. In combination with the previous work suggesting that InsPs play an essential role in cell growth through the discovery of interplay between these two pathways[11], this work aims to better understand the relationship between TOR and InsPs through delineating overlapping targets and targets unique to both studies.

5.3.6 Additional Proteins with Phosphosites Altered by TORC1 Inhibition

Many of the sites changing from this study are from phosphoproteins not previously identified as TOR-regulated, including some phosphoproteins with numerous unique sites changing. For example, two proteins related to MAPK signaling, NPK1-related protein kinase 2 (Cre10.g464100.t1.2) and a MAPKK-related protein (Cre06.g310100.t1.2), had two phosphosites each decreasing in phosphorylation (Table S2). Another protein, a rhodanese/cell cycle control phosphatase superfamily protein (Cre01.g003550.t1.1), had two sites, S763 and T764, increasing by 3.56- and 4.30- fold, respectively. While their function has not been explored in Chlamydomonas, cell cycle regulatory phosphatases are known to be critical as cell-cycle checkpoint controls[68].

The doubly phosphorylated phosphopeptide S1078-S1081 on the glycine-rich protein Cre12.g549150.t1.1 had the most significant fold change decrease of 55-fold following TOR inhibition. Additionally, two other phosphopeptides from this protein, the doubly phosphorylated S988-S991 and a monophosphorylated S1078, were also significantly decreasing, both by 4-fold. Glycine-rich proteins have been indicated in stress response in other plant species[69] but there is limited site conservation to Chlamydomonas based on BLASTP analysis. While that limits the ability to infer biological significance on this finding, a previous phosphoproteomic study in Chlamydomonas identified S1078 as significantly decreasing following 72 hours of nitrogen depletion[70], indicating that this site is potentially important for energy metabolism from both of these findings.

5.3.7 Glycolysis-Related Enzymes Modulated by TOR Inhibition

Key enzymes in the glycolytic pathway in Chlamydomonas have been reported to be under protein phosphorylation control[71]. A comprehensive study found seven of the ten enzymes of the late glycolytic pathway required for the conversion of fructose 1,6-bisphosphate to pyruvate to be phosphorylated[56]. In this study, we identified numerous sites on these enzymes and other proteins involved in glycolysis that were modulated following TOR inhibition including three pyruvate kinase family proteins (Cre03.g144847.t1.1 T34/36:NL, T88/S90:NL, T663/S665:NL, Cre05.g234700.t1.1 T63/S64:NL, Cre06.g280950.t1.2 S463/S466:NL) which are important regulatory enzymes since they perform irreversible steps in the pathway. Other phosphoproteins that had sites modulated include enolase (Cre12.g513200.t1.2 S417/T420:NL), an E1 component alpha subunit of the pyruvate dehydrogenase complex (Cre07.g337650.t1.2 S294/S296:NL), pyruvate orthophosphate dikinase (Cre17.g734548.t1.1 T535/S536:NL), and a phosphofructokinase (Cre06.g262900.t1.2 S81) that increased by 1.6-fold. Overall, these sites

were increasing following inhibition (Table S2) except T63/S64:NL on Cre05.g234700.t1.1, a pyruvate kinase family protein that decreased by 4-fold. Inositol pyrophosphates have been shown to participate in the control of intracellular ATP concentrations in yeast with mutants devoid of inositol pyrophosphates having increased glycolysis[72]. In this study, coverage on phosphosites that were not detected in the wild-type study on enzymes involved in glycolysis was obtained. The increases in phosphorylation following rapamycin treatment suggest a similar role of enhanced glycolysis and decreased ATP-consuming metabolic processes such as biosynthesis of macromolecules following TOR inhibition.

5.4 Conclusion/Summary

The objective of this study was to characterize the effect of TOR inhibition on the vip1-1 Chlamydomonas mutant. The rapamycin-hypersensitive strain showed similarities with the sites modulated in the wild-type study while also providing other distinct groups of phosphosites not previously interrogated or without coverage in wild-type such as numerous sites on phosphoproteins related to glycolysis and energy metabolism. Common rapamycin-sensitive motifs such as RXRXXS/T and RXXS/T were not identified. A more pronounced acidic motif, S/TXEDE, was found in the mutant line over the wild-type, with implications to similar function to the critical sequence motifs found in inositol pyrophosphate signaling in yeast. This could relate to the large subset of novel sites modulated just in the vip1-1 mutant study, however future work is required to continue to investigate the interplay between these pathways.

5.5 Tables

Table 5.1 TOR targets identified with fold change values for rapamycin vs. control in the vip1-1 mutant study compared to wild-type values from the study performed in wild-type[24]. Fold change values shaded red indicate a statistically signficant increase in phosphopeptide abundance for rapamycin versus control. Fold change values shaded blue indicate a statistically significant decrease in phosphopeptide abundance for rapamycin versus control. Sites that do not have a corresponding fold-change in the wild-type study because they were not identified are denoted with "n/a". Level of p-value statistical significance is denoted by p-value ≤ 0.05 (*) and ≤ 0.01 (**).

Accession	Common Name	Sites	vip1-1 rap:control	WT rap:control
CrTORC1 proteins				
Cre09.g400553.t1.1	TOR	S2598	1.29	1.12
		S770/S773:NL	0.35**	n/a
Cre08.g371957.t1.1	RAPTOR	S782/S783:NL	0.77	1.54
homologs of known substrates				
Cre13.g579200.t1.2	RPS6KB	T771/S773/T777:NL	1.44	1.05
Cre09.g400650.t1.2	RPS6	T78	0.88	n/a
		T127	1.23	0.61*
homologs of TOR pathway-associated proteins				
Cre10.g441200.t1.2	LARP1	T668/S670:NL	0.92	1.96*
		S737/738:NL	0.70*	0.99
		T809/S810:NL	0.64	0.81
		S817	0.15**	0.13**
Cre17.g721850.t1.2	EEF2K	T195/S196:NL	1.78	n/a
		S306	0.97	0.58
		S853/S857:NL	1.00	1.69
Cre12.g511850.t1.2	GSK3B	Y323	0.89	n/a
Cre09.g391245.t1.1	ATG1	S513	1.00	n/a
		T802/S803:NL	1.11	1.53
Cre10.g457500.t1.1	PRKAB	S25	4.28**	2.27**
		S25, S29:NL	1.09	n/a
Cre02.g100300.t1.1	PI-3K/PI-4-like	T80	0.95	n/a
		T149/S150:NL	1.00	0.92
Cre05.g245550.t1.1	PI3KA	S794	0.96	1.51
Cre02.g076900.t1.1	PRKG1	S71	0.74	1.59**
		S78	0.66*	1.41
		T857/T859:NL	0.62*	0.98
		T857/T859:NL	0.55**	0.92
Cre02.g076350.t1.2	ATP6B, ATPase	S7/S8:NL	1.45	2.09**
Cre11.g468550.t1.2	ATP synthase subunit G2	S7	1.02	2.33
		S77	0.95	1.33
		S65/T66:NL	1.29	n/a
Cre04.g211600.t1.1	SNF1 kinase homolog 10	S190/S193:NL	1.73*	n/a
Cre11.g467568.t1.1	PDPK1	S403	2.56**	n/a

*p-value ≤ 0.05 **p-value ≤ 0.01 Up- Down-

Table 5.2 TOR inhibited sites in vip1-1 mutant with opposite trends from sites identified in the rapamycin study performed in the wild-type[24]. Fold change values shaded red indicate a statistically signficant increase in phosphopeptide abundance for rapamycin versus control. Fold change values shaded blue indicate a statistically significant decrease in phosphopeptide abundance for rapamycin versus control. Level of p-value statistical significance is denoted by p-value ≤ 0.05 (*) and ≤ 0.01 (**).

Accession	Sites	Description	vip1-1 rap:control	WT rap:control
Cre06.g250500.t1.2	S23/S25:NL	pfkB-like carbohydrate kinase family protein	0.39**	1.78*
Cre07.g340200.t1.1	S50	PGR5-like B	2.14*	0.50
Cre02.g081250.t1.2	T511	plastid transcriptionally active 16	2.80**	0.74*
Cre06.g280950.t1.2	S463/S466	Pyruvate kinase family protein	3.04*	0.21**
Cre06.g269050.t1.2	S481	NAD(P)-binding Rossmann-fold superfamily protein	4.79**	0.42**
Cre12.g532450.t1.2	S506	UDP-glucose 6-dehydrogenase family protein	5.19**	0.59
Cre07.g337650.t1.2	S294/S296:NL	Thiamin diphosphate-binding fold (THDP-binding) superfamily protein	34.09**	0.09**

*p-value ≤ 0.05 **p-value ≤ 0.01 Up- Down-

5.6 Figures

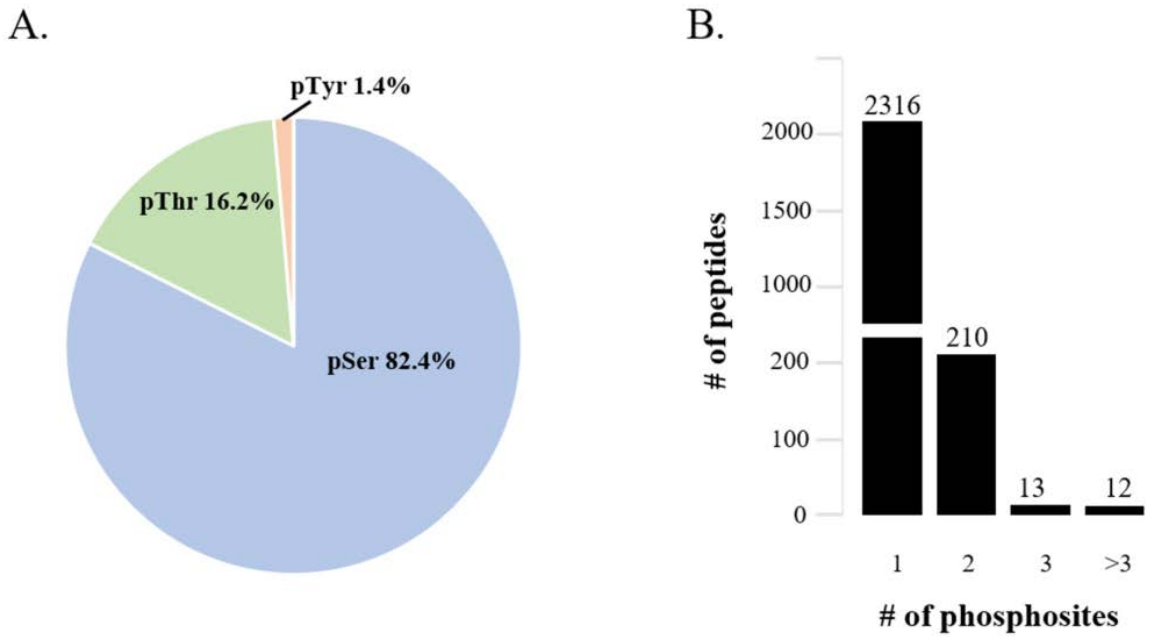

Figure 5.1 Quantitative coverage of the phosphoproteome of Chlamydomonas vip1-1 mutant following TOR inhibition. A pie chart showing the ratio of sites phosphorylated in this study with 82.4% pSer, 16.2% pThr, and 1.4% pY (A). From the sites detected in this study, a bar chart with the amount of phosphorylation events detected per peptide with >90% of phosphopeptides detected singly phosphorylated (B).

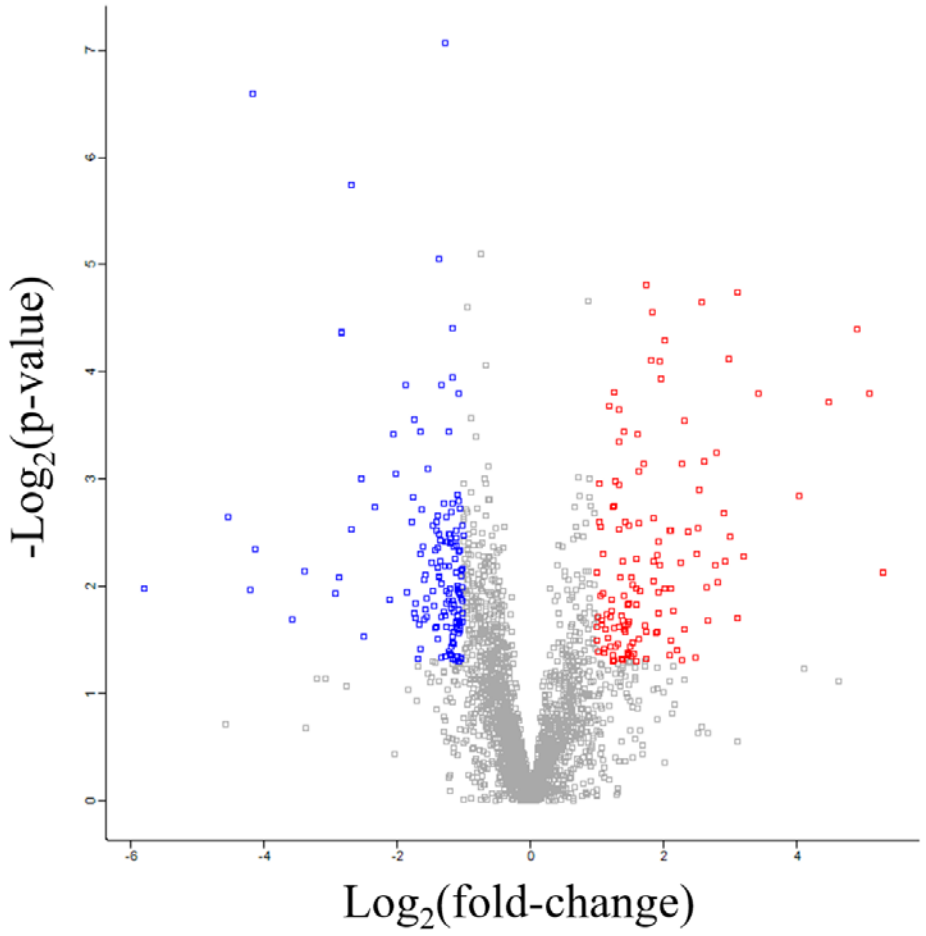

Figure 5.2 Volcano plot of phosphosites modulated by TOR inhibition in a vip1-1 Chlamydomonas mutant. 149 sites significantly decreasing are shaded blue and 132 sites significantly increasing are shaded red. Differentially changing sites were determined using a two-sample t-test with p-value ≤ 0.05 threshold and fold-change ± 2.

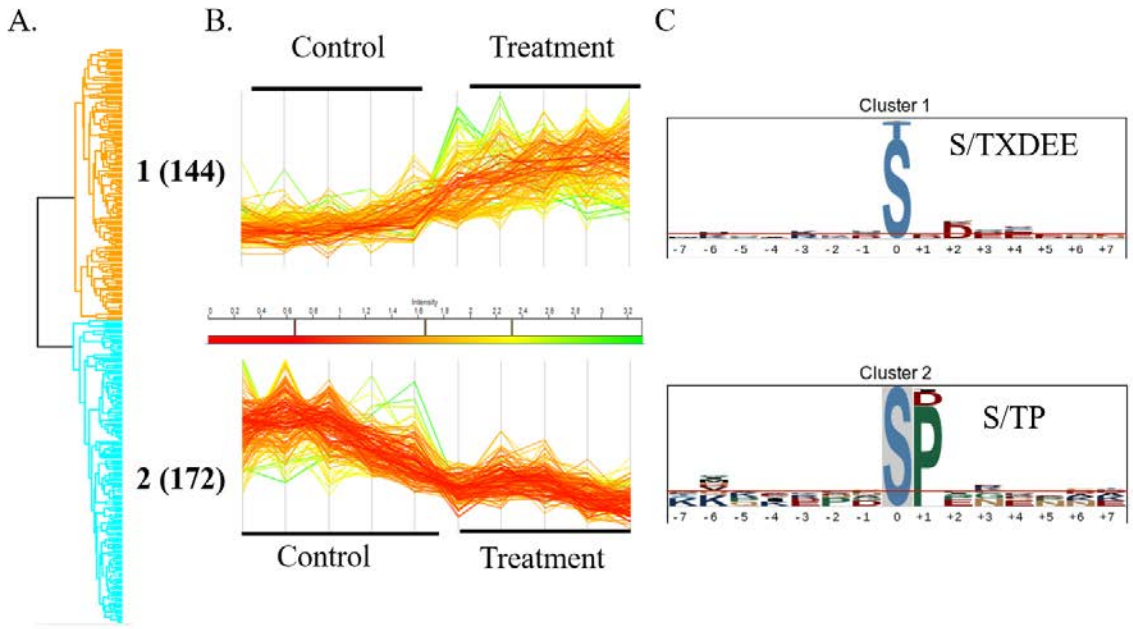

Figure 5.3 Hierarchical clustering of differentially changing sites into 2 clusters (A). Visualization was performed in Perseus v1.6.0.0. Following data normalization and missing value imputation, intensity values were z-score normalized and grouped using k-means clustering with default parameters. Overall trends in site intensity were graphed and colored based on intensity (B). For each of the two clusters, motif analysis was performed (C): motif analysis on clusters 1 and 2 from hierarchical clustering. Sequence logo visualizations were performed using pLOGO with serine or threonine residues fixed at position 0. Positions with significant residue presence are depicted as amino acid letters sized above the red line. For cluster 1, there was significant enrichment for S/TXDEE motif with a significant amount of C-terminal acidic residues in the +2, +3, and +4 positions. For cluster 2, there was significant enrichment for a proline in the +1 position.

REFERENCES

1. Merchant, S. S.; Kropat, J.; Liu, B.; Shaw, J.; Warakanont, J., TAG, you're it! Chlamydomonas as a reference organism for understanding algal triacylglycerol accumulation. *Curr Opin Biotechnol* **2012,** *23* (3), 352-363.

2. Park, J. J.; Wang, H.; Gargouri, M.; Deshpande, R. R.; Skepper, J. N.; Holguin, F. O.; Juergens, M. T.; Shachar-Hill, Y.; Hicks, L. M.; Gang, D. R., The response of Chlamydomonas reinhardtii to nitrogen deprivation: a systems biology analysis. *The Plant Journal* **2015,** *81* (4), 611-624.

3. Imamura, S.; Kawase, Y.; Kobayashi, I.; Shimojima, M.; Ohta, H.; Tanaka, K., TOR (target of rapamycin) is a key regulator of triacylglycerol accumulation in microalgae. *Plant signaling & behavior* **2016,** *11* (3), e1149285.

4. Hu, Q.; Sommerfeld, M.; Jarvis, E.; Ghirardi, M.; Posewitz, M.; Seibert, M.; Darzins, A., Microalgal triacylglycerols as feedstocks for biofuel production: perspectives and advances. *Plant J* **2008,** *54* (4), 621-639.

5. Blaby, I. K.; Glaesener, A. G.; Mettler, T.; Fitz-Gibbon, S. T.; Gallaher, S. D.; Liu, B.; Boyle, N. R.; Kropat, J.; Stitt, M.; Johnson, S.; Benning, C.; Pellegrini, M.; Casero, D.; Merchant, S. S., Systems-level analysis of nitrogen starvation-induced modifications of carbon metabolism in a Chlamydomonas reinhardtii starchless mutant. *Plant Cell* **2013,** *25* (11), 4305-4323.

6. Goodenough, U.; Blaby, I.; Casero, D.; Gallaher, S. D.; Goodson, C.; Johnson, S.; Lee, J. H.; Merchant, S. S.; Pellegrini, M.; Roth, R.; Rusch, J.; Singh, M.; Umen, J. G.; Weiss, T. L.; Wulan, T., The path to triacylglyceride obesity in the sta6 strain of Chlamydomonas reinhardtii. *Eukaryot Cell* **2014,** *13* (5), 591-613.

7. Crespo, J. L.; Diaz-Troya, S.; Florencio, F. J., Inhibition of target of rapamycin signaling by rapamycin in the unicellular green alga Chlamydomonas reinhardtii. *Plant Physiol* **2005,** *139* (4), 1736-1749.

8. Rodrigues, S. P.; Alvarez, S.; Werth, E. G.; Slade, W. O.; Gau, B.; Cahoon, E. B.; Hicks, L. M., Multiplexing strategy for simultaneous detection of redox-, phospho- and total proteome – understanding TOR regulating pathways in Chlamydomonas reinhardtii. *Anal. Methods* **2015,** *7* (17), 7336-7344.

9. Desai, M.; Rangarajan, P.; Donahue, J. L.; Williams, S. P.; Land, E. S.; Mandal, M. K.; Phillippy, B. Q.; Perera, I. Y.; Raboy, V.; Gillaspy, G. E., Two inositol hexakisphosphate kinases drive inositol pyrophosphate synthesis in plants. *The Plant Journal* **2014,** *80* (4), 642-653.

10. Williams, S. P.; Gillaspy, G. E.; Perera, I. Y., Biosynthesis and possible functions of inositol pyrophosphates in plants. *Frontiers in plant science* **2015,** *6*, 67.

11. Couso, I.; Evans, B. S.; Li, J.; Liu, Y.; Ma, F.; Diamond, S.; Allen, D. K.; Umen, J. G., Synergism between Inositol Polyphosphates and TOR Kinase Signaling in Nutrient Sensing, Growth Control, and Lipid Metabolism in Chlamydomonas. *The Plant Cell* **2016,** *28* (9), 2026-2042.

12. Chakraborty, A.; Koldobskiy, M. A.; Bello, N. T.; Maxwell, M.; Potter, J. J.; Juluri, K. R.; Maag, D.; Kim, S.; Huang, A. S.; Dailey, M. J., Inositol pyrophosphates inhibit Akt signaling, thereby regulating insulin sensitivity and weight gain. *Cell* **2010,** *143* (6), 897-910.

13. Kim, J.; Guan, K.-L., Amino acid signaling in TOR activation. *Annual review of biochemistry* **2011,** *80*, 1001-1032.

14. Loewith, R.; Hall, M. N., Target of rapamycin (TOR) in nutrient signaling and growth control. *Genetics* **2011,** *189* (4), 1177-1201.

15. Wullschleger, S.; Loewith, R.; Hall, M. N., TOR signaling in growth and metabolism. *Cell* **2006,** *124* (3), 471-484.

16. Dobrenel, T.; Caldana, C.; Hanson, J.; Robaglia, C.; Vincentz, M.; Veit, B.; Meyer, C., TOR Signaling and Nutrient Sensing. *Annual review of plant biology* **2016,** *67*, 261-285.

17. Pérez-Pérez, M. E.; Couso, I.; Crespo, J. L., The TOR Signaling Network in the Model Unicellular Green Alga Chlamydomonas reinhardtii. *Biomolecules* **2017,** *7* (3), 54.

18. González, A.; Hall, M. N., Nutrient sensing and TOR signaling in yeast and mammals. *The EMBO journal* **2017**, e201696010.

19. Raught, B.; Gingras, A. C.; Sonenberg, N., The target of rapamycin (TOR) proteins. *Proc Natl Acad Sci U S A* **2001,** *98* (13), 7037-7044.

20. Heitman, J.; Movva, N. R.; Hall, M. N., Targets for cell cycle arrest by the immunosuppressant rapamycin in yeast. *Science* **1991,** *253* (5022), 905-909.

21. van Dam, T. J.; Zwartkruis, F. J.; Bos, J. L.; Snel, B., Evolution of the TOR pathway. *J Mol Evol* **2011,** *73* (3-4), 209-220.

22. Crespo, J. L., BiP links TOR signaling to ER stress in Chlamydomonas. *Plant Signal Behav* **2012,** *7* (2), 273-275.

23. Diaz-Troya, S.; Florencio, F. J.; Crespo, J. L., Target of rapamycin and LST8 proteins associate with membranes from the endoplasmic reticulum in the unicellular green alga Chlamydomonas reinhardtii. *Eukaryot Cell* **2008,** *7* (2), 212-222.

24. Werth, E. G.; McConnell, E. W.; Couso, I.; Perrine, Z.; Crespo, J. L.; Umen, J. G.; Hicks, L. M., Investigating the effect of Target of Rapamycin kinase inhibition on the Chlamydomonas reinhardtii phosphoproteome: from known homologs to new targets. *Submitted.* **2018**.

25. Shears, S. B.; Ganapathi, S. B.; Gokhale, N. A.; Schenk, T. M.; Wang, H.; Weaver, J. D.; Zaremba, A.; Zhou, Y., Defining signal transduction by inositol phosphates. In *Phosphoinositides II: The Diverse Biological Functions*, Springer: **2012**; pp 389-412.

26. Laussmann, T.; Reddy, K. M.; Reddy, K. K.; Falck, J.; Vogel, G., Diphospho-myo-inositol phosphates from Dictyostelium identified as D-6-diphospho-myo-inositol pentakisphosphate and D-5, 6-bisdiphospho-myo-inositol tetrakisphosphate. *Biochemical Journal* **1997,** *322* (Pt 1), 31-33.

27. Atteia, A.; Adrait, A.; Brugière, S.; Tardif, M.; Van Lis, R.; Deusch, O.; Dagan, T.; Kuhn, L.; Gontero, B.; Martin, W., A proteomic survey of Chlamydomonas reinhardtii mitochondria sheds new light on the metabolic plasticity of the organelle and on the nature of the α-proteobacterial mitochondrial ancestor. *Molecular Biology and Evolution* **2009,** *26* (7), 1533-1548.

28. Draškovič, P.; Saiardi, A.; Bhandari, R.; Burton, A.; Ilc, G.; Kovačevič, M.; Snyder, S. H.; Podobnik, M., Inositol hexakisphosphate kinase products contain diphosphate and triphosphate groups. *Chemistry & biology* **2008,** *15* (3), 274-286.

29. Gillaspy, G. E., The role of phosphoinositides and inositol phosphates in plant cell signaling. In *Lipid-mediated protein signaling*, Springer: **2013**; pp 141-157.

30. Choi, J. H.; Williams, J.; Cho, J.; Falck, J.; Shears, S. B., Purification, sequencing, and molecular identification of a mammalian PP-InsP5 kinase that is activated when cells are exposed to hyperosmotic stress. *Journal of Biological Chemistry* **2007,** *282* (42), 30763-30775.

31. Fridy, P. C.; Otto, J. C.; Dollins, D. E.; York, J. D., Cloning and characterization of two human VIP1-like inositol hexakisphosphate and diphosphoinositol pentakisphosphate kinases. *Journal of Biological Chemistry* **2007,** *282* (42), 30754-30762.

32. Mulugu, S.; Bai, W.; Fridy, P. C.; Bastidas, R. J.; Otto, J. C.; Dollins, D. E.; Haystead, T. A.; Ribeiro, A. A.; York, J. D., A conserved family of enzymes that phosphorylate inositol hexakisphosphate. *Science* **2007,** *316* (5821), 106-109.

33. Shears, S. B.; Weaver, J. D.; Wang, H., Structural insight into inositol pyrophosphate turnover. *Advances in biological regulation* **2013,** *53* (1), 19-27.

34. Raboy, V., myo-Inositol-1, 2, 3, 4, 5, 6-hexakisphosphate. *Phytochemistry* **2003,** *64* (6), 1033-1043.

35. Munnik, T.; Vermeer, J. E., Osmotic stress-induced phosphoinositide and inositol phosphate signalling in plants. *Plant, cell & environment* **2010,** *33* (4), 655-669.

36. Stephens, L.; Radenberg, T.; Thiel, U.; Vogel, G.; Khoo, K.-H.; Dell, A.; Jackson, T.; Hawkins, P.; Mayr, G., The detection, purification, structural characterization, and metabolism of diphosphoinositol pentakisphosphate (s) and bisdiphosphoinositol tetrakisphosphate (s). *Journal of Biological Chemistry* **1993,** *268* (6), 4009-4015.

37. Glennon, M. C.; Shears, S. B., Turnover of inositol pentakisphosphates, inositol hexakisphosphate and diphosphoinositol polyphosphates in primary cultured hepatocytes. *Biochemical Journal* **1993,** *293* (Pt 2), 583-590.

38. Menniti, F.; Miller, R.; Putney, J.; Shears, S., Turnover of inositol polyphosphate pyrophosphates in pancreatoma cells. *Journal of Biological Chemistry* **1993,** *268* (6), 3850-3856.

39. Galvan, A.; Gonzalez-Ballester, D.; Fernandez, E., Insertional mutagenesis as a tool to study genes/functions in Chlamydomonas. In *Transgenic microalgae as green cell factories*, Springer: **2007**; pp 77-89.

40. Berthold, P.; Schmitt, R.; Mages, W., An engineered Streptomyces hygroscopicus aph 7 ″gene mediates dominant resistance against hygromycin B in Chlamydomonas reinhardtii. *Protist* **2002,** *153* (4), 401-412.

41. Werth, E. G.; McConnell, E. W.; Gilbert, T. S. K.; Couso Lianez, I.; Perez, C. A.; Manley, C. K.; Graves, L. M.; Umen, J. G.; Hicks, L. M., Probing the global kinome and phosphoproteome in Chlamydomonas reinhardtii via sequential enrichment and quantitative proteomics. *The Plant Journal* **2017,** *89* (2), 416-426.

42. Slade, W. O.; Werth, E. G.; McConnell, E. W.; Alvarez, S.; Hicks, L. M., Quantifying reversible oxidation of protein thiols in photosynthetic organisms. *J Am Soc Mass Spectrom* **2015,** *26* (4), 631-640.

43. Käll, L.; Canterbury, J. D.; Weston, J.; Noble, W. S.; MacCoss, M. J., Semi-supervised learning for peptide identification from shotgun proteomics datasets. *Nature methods* **2007,** *4* (11), 923-925.

44. Savitski, M. M.; Lemeer, S.; Boesche, M.; Lang, M.; Mathieson, T.; Bantscheff, M.; Kuster, B., Confident phosphorylation site localization using the Mascot Delta Score. *Molecular & Cellular Proteomics* **2011,** *10* (2), M110. 003830.

45. Vizcaíno, J. A.; Côté, R. G.; Csordas, A.; Dianes, J. A.; Fabregat, A.; Foster, J. M.; Griss, J.; Alpi, E.; Birim, M.; Contell, J., The PRoteomics IDEntifications (PRIDE) database and associated tools: status in 2013. *Nucleic acids research* **2013,** *41* (D1), D1063-D1069.

46. Tyanova, S.; Temu, T.; Sinitcyn, P.; Carlson, A.; Hein, M. Y.; Geiger, T.; Mann, M.; Cox, J., The Perseus computational platform for comprehensive analysis of (prote) omics data. *Nature methods* **2016,** *13* (9), 731-740.

47. Cox, J.; Mann, M., 1D and 2D annotation enrichment: a statistical method integrating quantitative proteomics with complementary high-throughput data. *BMC bioinformatics* **2012,** *13* (16), S12.

48. Cox, J.; Mann, M., MaxQuant enables high peptide identification rates, individualized ppb-range mass accuracies and proteome-wide protein quantification. *Nature biotechnology* **2008,** *26* (12), 1367-1372.

49. Deeb, S. J.; D'Souza, R. C.; Cox, J.; Schmidt-Supprian, M.; Mann, M., Super-SILAC allows classification of diffuse large B-cell lymphoma subtypes by their protein expression profiles. *Molecular & Cellular Proteomics* **2012,** *11* (5), 77-89.

50. Kanehisa, M.; Goto, S., KEGG: kyoto encyclopedia of genes and genomes. *Nucleic acids research* **2000,** *28* (1), 27-30.

51. Ashburner, M.; Ball, C. A.; Blake, J. A.; Botstein, D.; Butler, H.; Cherry, J. M.; Davis, A. P.; Dolinski, K.; Dwight, S. S.; Eppig, J. T., Gene Ontology: tool for the unification of biology. *Nature genetics* **2000,** *25* (1), 25-29.

52. O'shea, J. P.; Chou, M. F.; Quader, S. A.; Ryan, J. K.; Church, G. M.; Schwartz, D., pLogo: a probabilistic approach to visualizing sequence motifs. *Nature methods* **2013,** *10* (12), 1211-1212.

53. Demirkan, G.; Yu, K.; Boylan, J. M.; Salomon, A. R.; Gruppuso, P. A., Phosphoproteomic profiling of in vivo signaling in liver by the mammalian target of rapamycin complex 1 (mTORC1). *PLoS One* **2011,** *6* (6), e21729.

54. Harder, L. M.; Bunkenborg, J.; Andersen, J. S., Inducing autophagy: a comparative phosphoproteomic study of the cellular response to ammonia and rapamycin. *Autophagy* **2014,** *10* (2), 339-355.

55. Rigbolt, K. T.; Zarei, M.; Sprenger, A.; Becker, A. C.; Diedrich, B.; Huang, X.; Eiselein, S.; Kristensen, A. R.; Gretzmeier, C.; Andersen, J. S.; Zi, Z.; Dengjel, J., Characterization of early autophagy signaling by quantitative phosphoproteomics. *Autophagy* **2014,** *10* (2), 356-371.

56. Wang, H.; Gau, B.; Slade, W. O.; Juergens, M.; Li, P.; Hicks, L. M., The global phosphoproteome of Chlamydomonas reinhardtii reveals complex organellar phosphorylation in the flagella and thylakoid membrane. *Molecular & Cellular Proteomics* **2014,** *13* (9), 2337-2353.

57. Chou, M. F.; Schwartz, D., Biological sequence motif discovery using motif-x. *Current Protocols in Bioinformatics* **2011**, 13.15.1-13.15.24.

58. Saiardi, A.; Bhandari, R.; Resnick, A. C.; Snowman, A. M.; Snyder, S. H., Phosphorylation of proteins by inositol pyrophosphates. *Science* **2004,** *306* (5704), 2101-2105.

59. Perez-Perez, M. E.; Florencio, F. J.; Crespo, J. L., Inhibition of target of rapamycin signaling and stress activate autophagy in Chlamydomonas reinhardtii. *Plant Physiol* **2010,** *152* (4), 1874-1888.

60. Diaz-Troya, S.; Perez-Perez, M. E.; Perez-Martin, M.; Moes, S.; Jeno, P.; Florencio, F. J.; Crespo, J. L., Inhibition of protein synthesis by TOR inactivation revealed a conserved regulatory mechanism of the BiP chaperone in Chlamydomonas. *Plant Physiol* **2011,** *157* (2), 730-741.

61. Halford, N. G.; Hardie, D. G., SNF1-related protein kinases: global regulators of carbon metabolism in plants? *Plant molecular biology* **1998,** *37* (5), 735-748.

62. Shen, W.; Reyes, M. I.; Hanley-Bowdoin, L., Arabidopsis protein kinases GRIK1 and GRIK2 specifically activate SnRK1 by phosphorylating its activation loop. *Plant physiology* **2009,** *150* (2), 996-1005.

63. Sugden, C.; Crawford, R. M.; Halford, N. G.; Hardie, D. G., Regulation of spinach SNF1-related (SnRK1) kinases by protein kinases and phosphatases is associated with phosphorylation of the T loop and is regulated by 5′-AMP. *The Plant Journal* **1999,** *19* (4), 433-439.

64. Mitchelhill, K. I.; Stapleton, D.; Gao, G.; House, C.; Michell, B.; Katsis, F.; Witters, L. A.; Kemp, B. E., Mammalian AMP-activated protein kinase shares structural and functional homology with the catalytic domain of yeast Snf1 protein kinase. *Journal of Biological Chemistry* **1994,** *269* (4), 2361-2364.

65. Orlova, M.; Kanter, E.; Krakovich, D.; Kuchin, S., Nitrogen availability and TOR regulate the Snf1 protein kinase in Saccharomyces cerevisiae. *Eukaryotic cell* **2006,** *5* (11), 1831-1837.

66. Hindupur, S. K.; González, A.; Hall, M. N., The opposing actions of target of rapamycin and AMP-activated protein kinase in cell growth control. *Cold Spring Harbor perspectives in biology* **2015,** *7* (8), a019141.

67. Komander, D.; Fairservice, A.; Deak, M.; Kular, G. S.; Prescott, A. R.; Downes, C. P.; Safrany, S. T.; Alessi, D. R.; van Aalten, D. M., Structural insights into the regulation of PDK1 by phosphoinositides and inositol phosphates. *The EMBO journal* **2004,** *23* (20), 3918-3928.

68. Cross, F. R.; Umen, J. G., The Chlamydomonas cell cycle. *Plant J* **2015,** *82* (3), 370-392.

69. Mangeon, A.; Junqueira, R. M.; Sachetto-Martins, G., Functional diversity of the plant glycine-rich proteins superfamily. *Plant signaling & behavior* **2010,** *5* (2), 99-104.

70. Roustan, V.; Bakhtiari, S.; Roustan, P.-J.; Weckwerth, W., Quantitative in vivo phosphoproteomics reveals reversible signaling processes during nitrogen starvation and recovery in the biofuel model organism Chlamydomonas reinhardtii. *Biotechnology for biofuels* **2017,** *10* (1), 280.

71. Pilkis, S.; Claus, T.; El-Maghrabi, M. R., The role of cyclic AMP in rapid and long-term regulation of gluconeogenesis and glycolysis. *Advances in second messenger and phosphoprotein research* **1988,** *22*, 175-191.

72. Szijgyarto, Z.; Garedew, A.; Azevedo, C.; Saiardi, A., Influence of inositol pyrophosphates on cellular energy dynamics. *Science* **2011,** *334* (6057), 802-805.

CHAPTER 6: Conclusions and Future Directions

6.1 Conclusions

The overall goal of this work was to develop and implement label-free quantitative workflows to study the kinome and phosphoproteome in Chlamydomonas. This effort was derived from the limited understanding of the regulatory role post-translational modifications play in cellular signaling as it applies to kinase signaling pathways, specifically Target of Rapamycin kinase signaling, in Chlamydomonas. Prior to this work, a quantitative strategy to effectively probe dynamic protein phosphorylation following chemical inhibition in Chlamydomonas was limited, especially on the global scale.

Phosphorylated protein detection in photosynthetic organisms has a history of almost three decades[1]. The ability to employ quantitative phosphoproteomic approaches using mass spectrometry, however, is relatively new, and at first traditionally focused on gel-based methods[2]. As advances in mass spectrometry continued to improve throughout the past few decades for proteomic applications[3-4], detection of thousands of peptides or phosphopeptides in a single run became feasible. With this came the opportunity to solve complex biological questions requiring quantitative workflows. Efforts to employ quantitative phosphoproteomics in model mammalian systems benefitted extensively from this, creating workflows focused on improving human health. From this, high-quality, comprehensive, and freely accessible platforms for sharing functional information amongst the scientific community were furthered and continue to improve. During this time, significant advancements in the bioinformatic toolkit for studying plant-specific networks were also ongoing and helped push forward the significance behind

"omic" studies in plants as well. The extensive effort to integrate annotations from multiple protein analysis tools and protein homology across organisms, in addition to the advances in high-mass accuracy and high-resolving power instrumentation, allow for biological inference required to make sense of large-scale proteomic and phosphoproteomic data. While this process is constantly improving, the advancements in instrumentation and annotations into protein's functionalities that are available permit quantitative label-free workflows such as the one developed in this work to exist.

One of the primary advantages to using this label-free quantitative approach developed for investigating the kinome and phosphoproteome in Chlamydomonas is the ability to implement the platform on a wide array of potential experimental designs. In this workflow, >2,500 phosphosites per experiment are consistently quantified with special attention focused on reproducibility both at the lab bench and in the data analysis processing post-acquisition. Development and implementation of this discovery-based method have led to a better understanding of TOR signaling in Chlamydomonas with new insights into the role of LARP1 in TOR signaling on downstream protein synthesis, evidence that carotenoid production is under TOR control, and further exploration into the interplay with inositol pyrophosphate signaling. Additionally, this work has guided follow-up efforts to continue to investigate the phosphorylation networks governed by the TOR kinase pathway in Chlamydomonas. This includes raising anti-phospho antibodies for site validation on targets of interest and follow-up affinity purification-mass spectrometry (AP-MS) experiments prioritized by tagging promising targets from this work to examine their interactome in Chlamydomonas through protein-protein interactions.

This workflow has been shown to successfully identify TOR-modulated phosphosites that play fundamental roles in TOR signaling in Chlamydomonas. Since this platform is discovery-based and capable of optimization for a wide array of plant starting materials, future work in other kinase signaling networks in Chlamydomonas and in other photosynthetic organisms is possible moving forward. Through collaborative efforts, investigation into various other signal transduction pathways in Chlamydomonas and Arabidopsis are ongoing and while technology and informatics continue to improve, the ability to learn more from discovery-based methods will as well.

REFERENCES

1. Michel, H.; Griffin, P.; Shabanowitz, J.; Hunt, D.; Bennett, J., Tandem mass spectrometry identifies sites of three post-translational modifications of spinach light-harvesting chlorophyll protein II. Proteolytic cleavage, acetylation, and phosphorylation. *Journal of Biological Chemistry* **1991,** *266* (26), 17584-17591.

2. Slade, W. O.; Werth, E. G.; Chao, A.; Hicks, L. M., Phosphoproteomics in photosynthetic organisms. *Electrophoresis* **2014,** *35* (24), 3441-3451.

3. Aebersold, R.; Mann, M., Mass spectrometry-based proteomics. *Nature* **2003,** *422* (6928), 198-207.

4. Sharma, K.; D'Souza, R. C.; Tyanova, S.; Schaab, C.; Wiśniewski, J. R.; Cox, J.; Mann, M., Ultradeep human phosphoproteome reveals a distinct regulatory nature of Tyr and Ser/Thr-based signaling. *Cell reports* **2014,** *8* (5), 1583-1594.